Cold atoms for deterministic quantum computation with one qubit

Thesis

Cold Atoms for Deterministic Quantum Computation with One Qubit

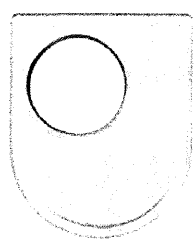

Christopher William Mansell

Department of Physical Sciences

The Open University

A thesis submitted for the degree of

Doctor of Philosophy

August 2014

Date of Submission: 4 August 2014
Date of Award: 23 October 2014

Abstract

In this thesis, I describe a proposal for experiments with dense ensembles of ultracold Rubidium atoms optically excited to high-lying electronic states known as Rydberg states. The proposed experiment is designed to implement a model of quantum computation known as deterministic quantum computation with one qubit (DQC1). My proposal is novel among other proposals for Rydberg atoms because it employs mixed states and could provide insights into the source of the enhancements of quantum technology over classical technology. I demonstrate that ultracold atoms and Rydberg interactions offer new perspectives for exploring the DQC1 model. This is mainly due to the large strength, long range and controllability of Rydberg interactions.

My specific contributions include: a proposal that solves one of the main issues with implementing quantum logic gates between ensembles of atoms; numerical simulations of the proposed cold atom implementation of a DQC1 protocol; and the design and laboratory implementation of a high-performance optical system for imaging ultracold atoms. These contributions bring the experimental exploration of the DQC1 model closer to realisation.

List of Publications

BETEROV, I.I., SAFFMAN, M., YAKSHINA, E.A., ZHUKOV, V.P., TRETYAKOV, D.B., ENTIN, V.M., RYABTSEV, I.I., MANSELL, C.W., MACCORMICK, C., BERGAMINI, S. & FEDORUK, M.P. Quantum gates in mesoscopic atomic ensembles based on adiabatic passage and Rydberg blockade. *Phys. Rev. A*, **88**, 010303 (2013).

MANSELL, C.W. & BERGAMINI, S.
A cold-atoms based processor for deterministic quantum computation with one qubit in intractably large Hilbert spaces. *New Journal of Physics*, **16**, 053045 (2014).

BETEROV, I.I., SAFFMAN, M., ZHUKOV, V.P., TRETYAKOV, D.B., ENTIN, V.M., YAKSHINA, E.A., RYABSTEV, I.I., MANSELL, C.W., MACCORMICK, C., BERGAMINI, S. & FEDORUK, M.P. Coherent control of mesoscopic atomic ensembles for quantum information. *Laser Physics*, **24**, 074013 (2014).

Acknowledgements

I would like to thank the members of the Cold Atoms research group at The Open University, especially Dr Silvia Bergamini, for their contributions to this work. I would also like to thank our collaborators, particularly our long-term collaborator, Dr. Ilya Beterov.

Contents

List of Abbreviations

4LS	Four level system
AOM	Acousto-optic modulator
ARP	Adiabatic rapid passage
AT	Autler-Townes
BEC	Bose Einstein Condensate
BFL	Back focal length
CNOT	Controlled NOT
CZ	Controlled Z
DQC1	Deterministic quantum computation with one qubit
EIT	Electromagnetically induced transparency
HCP	Half cycle pulse
ICCD	Intensified charge-coupled device
MAG	Magnification
MFT	Modulation Transfer Function
MOT	Magneto-optical trap
N.A.	Numerical aperture
QIP	Quantum information processing
STIRAP	Stimulated Raman adiabatic passage
TBR	Three body recombination

List of Figures

Chapter 1

Introduction

The development of quantum technology is an important research topic in modern physics [Nielsen & Chuang, 2010] [Stolze & Suter, 2008]. It encompasses many subfields, including quantum computation [Galindo & Martín-Delgado, 2002], quantum simulation [Buluta & Nori, 2009] [Georgescu *et al.*, 2014], quantum communication [Kimble, 2008] and quantum metrology [Giovannetti *et al.*, 2011]. The overarching goal is to surpass what can be achieved with classical technology [Preskill, 2011]. The research presented in this thesis consists of work towards this regime of "quantum supremacy."

A quantum computer can be defined as a "machine that would exploit the full complexity of a many-particle quantum wavefunction to solve a computational problem [Ladd *et al.*, 2010]." There is a wide range of quantum systems that may be up to performing this task. These include photons, cold atoms, trapped ions, nuclear spins in molecules, quantum dots, dopants in solids and superconductors. The details of the task and the success of these different platforms are discussed in the introductory chapters of this thesis.

Focus is then brought onto quantum computation with cold atoms. The state of the art for this platform employs Rydberg states for the performance of logic operations. Rydberg states are highly excited electronic states. Atoms in such states have properties that considerably differ from atoms in ground

states. After introducing the physics of Rydberg states, I present original work showing how a phenomenon known as stimulated Raman adiabatic passage (STIRAP) can be used to perform quantum logic operations between ensembles of atoms.

Details of a specific model of quantum computation known as deterministic quantum computation with one qubit (DQC1) are then given. This model was originally conceived with nuclear magnetic resonance systems in mind [Knill & Laflamme, 1998] but subsequent experimental demonstrations have been performed in optical set-ups [Lanyon *et al.*, 2008]. The key insight presented in this thesis is that an implementation with cold Rydberg atoms could dramatically supersede these earlier implementations. The main body of the thesis is dedicated to paving the way for such an implementation.

In the core chapter, the stages of the Rydberg implementation of the DQC1 model - the initialisation, processing and read-out stages - are outlined. Results of some modelling are presented and the finer points are discussed.

An introduction to the laboratory set-up is set-up is then given. I describe a high-performance optical system that I designed to dipole-trap and image the atoms. The design of the optical system constituted an important stage of the work towards the laboratory implementation of DQC1 model.

Finally, some conclusions are drawn. The overall conclusion is that *large-scale* implementations of the DQC1 model are possible in the technologically feasible, highly versatile cold atom set-up herein described:

- Standard laser cooling and trapping techniques [Metcalf & van der Straten, 2002] can be applied to load the neutral atoms into dipole traps.

- These atoms can be prepared in the states required for DQC1 using a scheme that I devised with inspiration from an ion trap experiment [Barreiro *et al.*, 2010].

- Various Rydberg-based logic gates [Saffman *et al.*, 2010] (including one

devised by myself and colleagues [Beterov *et al.*, 2013] [Beterov *et al.*, 2014]) can be employed to implement non-trivial unitary processes.

- Fluorescent light from the atoms can be collected by a high-performance optical system in order to determine the outcome of a DQC1 protocol.

Chapter 2

Background: Quantum Computation with Cold Atoms

Quantum mechanics is mankind's most precise theory, agreeing with experimental values to many significant figures [Aoyama *et al.*, 2012]. It is the basis of our understanding of the microscopic world and directly led to invention of both the laser [Townes *et al.*, 1964] and the transistor [Shockley *et al.*, 1956].

Information theory is required knowledge for all computer scientists and communication engineers. Pioneered by Turing [Turing, 1936] and Shannon [Shannon, 1948] in 1930s and 40s, it shapes our thoughts on how information can be transmitted and manipulated. Its assumptions, however, are decidedly classical. Exploring the implications of changing these assumptions to make them agree with quantum mechanics [Deutsch, 1985] has lead to fresh insights into the foundations of physics [Briggs *et al.*, 2013] and has spurred developments in many areas of advanced technology, including communication, computation, simulation and metrology.

The technological aim of quantum computation is to outperform ordinary, classical computation by taking advantage of physical superpositions (and by further making use of phenomena such as entanglement or quantum interference of complex amplitudes). Indeed, certain quantum mechanical algorithms have

been successfully devised to give speed-ups compared to the best known classical algorithms [Deutsch & Jozsa, 1992] [Shor, 1994] [Grover, 1996] [Harrow *et al.*, 2009] and devices have been built that implement small-scale versions of these algorithms [Ladd *et al.*, 2010].

I begin by explaining the main concepts of quantum computers before discussing the goal of using a physical set-up to perform quantum computation. I detail the requirements that any such set-up has to meet and briefly survey the current state-of-the-art set-ups.

The rest of the chapter focuses on cold atoms as a platform for quantum computation. I explain the key ideas of cold atom quantum computers and then describe their current level of success and prospects for further improvements. Finally, I compare cold atoms to the other set-ups.

2.1 Main Concepts of Quantum Computing

A brief introduction to the main concepts of the quantum computing is now given.

2.1.1 Qubits

In an ordinary, classical computer, the data are represented by binary digits, known as bits. One bit can either take the value "0" or the value "1". Crucially, these bits have to be encoded in a physical system. For example, "0" could be encoded by an uncharged capacitor and "1" could be encoded by a charged capacitor.

Physical systems that can exist in a superposition of two different states can be used to encode quantum bits, known as qubits. The two different states of the qubit can be represented in Dirac notation by $|0\rangle$ and $|1\rangle$. They can also be represented by vectors in a complex vector space, known as Hilbert space,

where:

$$|0\rangle = \begin{pmatrix} 1 \\ 0 \end{pmatrix}; \qquad |1\rangle = \begin{pmatrix} 0 \\ 1 \end{pmatrix}. \tag{2.1}$$

The general state, $|\Psi\rangle_1$, of a single qubit is:

$$|\Psi\rangle_1 = c_0|0\rangle + c_1|1\rangle \tag{2.2}$$

$$= \begin{pmatrix} c_0 \\ c_1 \end{pmatrix}, \tag{2.3}$$

where c_0 and c_1 are complex numbers known as amplitudes. When the qubit is measured in the computational basis, the superposition state collapses into one of the two basis states, $|0\rangle$ or $|1\rangle$, with probabilities given by the square of the modulus of the complex amplitudes (so to conserve probability, the complex amplitudes fulfil the normalisation condition $|c_0|^2 + |c_1|^2 = 1$). However, before the superposition state is measured, the qubit, by being in a physical superposition of two different basis states, represents a superposition of two different values.

N bits can represent any of 2^N values (from 00...00 to 11...11). The wavefunction of N qubits is, in general,

$$|\Psi\rangle_N = c_{00...00}|00...00\rangle + c_{00...01}|00...01\rangle + c_{00...10}|00...10\rangle + ... + c_{11...11}|11...11\rangle. \tag{2.4}$$

Thus, in comparison to N classical bits that can only represent a *single* one of 2^N possible values, N qubits can represent a superposition of *all* these values.

2.1.2 Gates

In classical computing, bits can be physically manipulated in accordance with the rules of logic, in such a way that a useful task, known as an algorithm, is performed. This physical manipulation of bits according to fixed rules can be broken down into basic operations called logic gates. An example of a classical logic gate is the NOT gate, which, when supplied with a "0," converts it into a "1," and when supplied with a "1," converts it into a "0".

Similarly, it is also possible to physically manipulate qubits according to fixed rules. When considering quantum mechanical logic gates, it can be helpful to put to the side of one's mind that the *measurement* of quantum states is probabilistic, and instead focus on the result that the *evolution* of quantum states is deterministic[1]. Thus, by avoiding measuring the states of qubits, and by choosing the Hamiltonian that governs the evolution of the qubits, it is possible to physically manipulate the states of the qubits according fixed rules. That is, it is possible to perform "quantum logic gates" on the qubits.

The effect of a logic gate is to change the complex amplitudes of the input qubit states. Since the states of qubits can be written either in Dirac notation or as vectors, quantum logic gates can either be written as operators in Dirac notation, or as matrices.

An example of a single-qubit quantum logic gate is the Hadamard gate, which is commonly drawn in "circuit diagrams" as 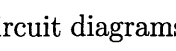 . As a matrix, it is written as:

$$H = \frac{1}{\sqrt{2}} \begin{pmatrix} 1 & 1 \\ 1 & -1 \end{pmatrix}. \tag{2.5}$$

When a single qubit in the state $|\Psi\rangle_1 = c_0|0\rangle + c_1|1\rangle$ is acted on by a Hadamard

[1]The evolution of quantum states can be described by a unitary operator, U, that is given by $U = e^{-i\mathcal{H}t/\hbar}$, where $\mathcal{H}$ is the Hamiltonian of the system, t is time and $\hbar$ is Planck's constant.

gate, its state is changed to:

$$H|\Psi\rangle_1 = \frac{1}{\sqrt{2}} \begin{pmatrix} c_0 + c_1 \\ c_0 - c_1 \end{pmatrix}. \tag{2.6}$$

Quantum logic gates can act on multiple qubits. An example of a two-qubit quantum logic gate is the controlled-Z logic gate. It is commonly abbreviated to CZ. It is depicted in Figure 2.1(a) and its matrix represenation is:

$$\mathrm{CZ} = \begin{pmatrix} 1 & 0 & 0 & 0 \\ 0 & 1 & 0 & 0 \\ 0 & 0 & 1 & 0 \\ 0 & 0 & 0 & -1 \end{pmatrix}. \tag{2.7}$$

When two qubits in the state $|\Psi\rangle_2 = c_{00}|00\rangle + c_{01}|01\rangle + c_{10}|10\rangle + c_{11}|11\rangle$ are acted on by a CZ gate, their state is changed to:

$$\mathrm{CZ}|\Psi\rangle_2 = \frac{1}{\sqrt{2}} \begin{pmatrix} c_{00} \\ c_{01} \\ c_{10} \\ -c_{11} \end{pmatrix}. \tag{2.8}$$

Another example of two-qubit quantum logic gates is the controlled-NOT, or CNOT, logic gate. As a matrix, it is written as

$$\mathrm{CNOT} = \begin{pmatrix} 1 & 0 & 0 & 0 \\ 0 & 1 & 0 & 0 \\ 0 & 0 & 0 & 1 \\ 0 & 0 & 1 & 0 \end{pmatrix} \tag{2.9}$$

and its circuit diagram is shown in Figure 2.1(b) and (c).

By working through the matrix multiplication, one can show that a Hadamard

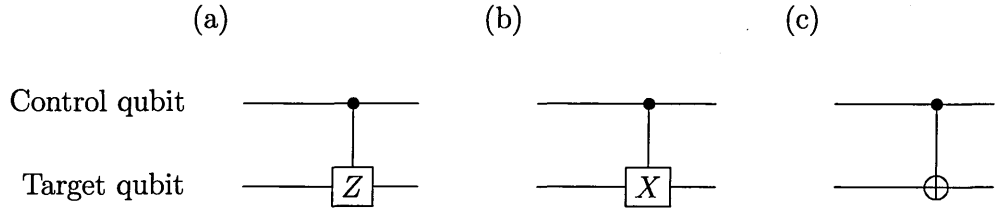

Figure 2.1: Controlled logic gates. (a) is a controlled-Z gate. (b) and (c) are two different ways of representing a controlled-NOT gate.

gate, followed by a CZ gate, followed by another Hadamard gate, is equivalent to a CNOT gate. As we will see in the following section, it is crucial for a physical system to be able to implement these sorts of quantum logic gates.

2.2 Implementation of a Quantum Computer

Physics and information theory were once separate disciplines. However, with the emergence of the field of quantum computation came a growing recognition of the physical nature of information [Nielsen & Chuang, 2010] [Lloyd, 2000] [Landauer, 1996] [Landouer, 1991].

In short, information is said to be physical because:

- it must be encoded in a physical system (e.g. in marks on a piece paper).

- it can only be altered by manipulating the physical system in which it is encoded (e.g. rearranging the marks on the paper).

In this section, I discuss the ability of physical systems to use quantum mechanical phenomena to encode and manipulate information. I begin with the requirements that a physical system must fulfil in order to successfully implement quantum computation. I then briefly discuss the achievements and prospects of the various physical platforms that are currently being investigated and developed for this purpose.

2.2.1 Requirements for an Implementation

In order to compare the ability of different physical systems to perform quantum computation, David DiVincenzo identified seven criteria that a physical system would have to successfully fulfil to be of use as a quantum computer [DiVincenzo, 2000]. These "DiVincenzo criteria" were highly influential in the field of quantum computation. They allowed researchers to identify what aspects of their physical system were in most need of improvement and also facilitated comparisons between different physical systems.

The DiVincenzo criteria can be recalled according to the acronym SILURIT:

- The physical system needs to be "**S**calable" with well-defined qubits.
- One needs to be able to "**I**nitialise" the system to a certain state from which the computation can then begin.
- The system needs to have a "**L**ong" decoherence time compared to the time it takes to perform logic gates.
- The system needs to be able to perform a "**U**niversal" set of logic gates (i.e. a set of gates that enables any quantum algorithm to be performed).
- One needs to be able to "**R**ead Out" the state of the qubits at the various stages, but particularly the end, of the computation.
- One needs to be able to "**I**nterconvert" the state of a moveable qubit with the state of a immobile qubit.
- Finally, one needs to be able to coherently "**T**ransmit," or move, the moveable qubits between specified locations.

The first five criteria are related to a single quantum system being able to compute. The last two criteria are related to the ability to link together, or network, spatially separated quantum systems (where moveable, or "flying," qubits are often, but not always, photons).

With the development of different models of quantum computation other than the original circuit model[1] came different sets of criteria for each model [Pérez-Delgado & Kok, 2011]. For example, adiabatic quantum computation and measurement based quantum computation (MBQC) do not require logic gates. The former requires that the Hamilitonian of the system can be slowly varied whilst the latter requires that a resource state can be prepared.

In a recent review paper, Ladd *et al.* [2010] gave four model-independent criteria for universal quantum computation:

- The 'closed box' criterion: internal operation of a quantum computer, while under the control of a programmer, must otherwise be isolated form the rest of the universe.

- The scalability criterion: The computer must operate in a Hilbert space whose dimensions can grow exponentially without an exponential cost in resources (such as time, space or energy).

- The universal logic criterion: The large Hilbert space must be accessible using a finite set of control operations; the resources for this set must also not grow exponentially.

- The correctability criterion: It must be possible to extract the entropy of the computer to maintain the computer's quantum state.

Ladd explains the core challenge of quantum computation extremely succinctly: "Quantum computation is difficult because the [...] criteria we have discussed appear to be in conflict. For example, those parts of the system in place to achieve rapid measurement must be turned strongly 'on' for error-correction and read-out, but must be turned strongly 'off' to preserve the

[1]These models include: global control (also known as quantum cellular automata) [Lloyd, 1993]; topological quantum computation [Kitaev, 2003] [Kitaev, 1997]; DQC1 (non-universal) [Knill & Laflamme, 1998]; instantaneous quantum computation (non-universal) [Shepherd & Bremner, 2009]; adiabatic quantum computation [Farhi *et al.*, 2001]; measurement based quantum computation [Raussendorf & Briegel, 2001]; ancilla-driven quantum computation [Anders *et al.*, 2010]; and boson sampling (non-universal) [Aaronson & Arkhipov, 2011].

coherences in the large Hilbert space. Generally, neither the 'on' state nor the 'off' state is as difficult to implement as the ability to switch between the two!" As is shown in Figure 2.2, Rydberg atoms interact many orders of magnitude more strongly than ground state atoms. Hence, cold atoms can be turned on (i.e. made to interact strongly with each other) by laser-exciting them to Rydberg states and turned off (i.e. made to interact weakly with their surroundings) by de-exciting them with another laser pulse. Designs for quantum logic gates based on Rydberg states (and their strong, long-range, controllable interactions) is the topic of Chapter 3.

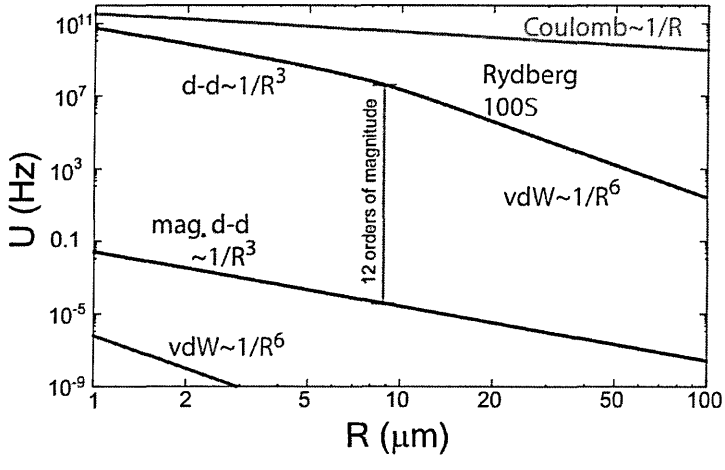

Figure 2.2: The two-body interaction strengths for various physical systems: ground state Rb atoms, interacting by van der Waals interactions (purple line) and magnetic dipole-dipole interactions (blue line); Rb atoms excited to the 100S Rydberg level (red line); and ions, interacting by the Coulomb interaction (brass line). Note that the interaction strength for ground state atoms and for Rydberg atoms can differ by about 12 orders of magnitude. The Figure is taken from Saffman *et al.* [2010].

2.2.2 Different Implementations

In this subsection, I discuss the state-of-the-art implementations of quantum computation. These implementations include photons, trapped ions, NMR, quantum dots, dopants in solids and superconductors. It is beyond the scope of my work for this survey to be comprehensive. I begin with photons.

Photons meet the closed box requirement since they are relatively free of decoherence. Photonic quantum computers are close to reaching the scalabiltiy criterion: Varnava *et al.* [2006] found that under some assumptions, scalability can be achieved if the product of source and detector efficiency is $> 2/3$. Lita *et al.* [2008] developed a single-photon detector with 95% efficiency; and Claudon *et al.* [2010] developed a single-photon source with 72% efficiency[1]. Universal logic can be performed in photonic systems using the scheme of Knill, Laflamme and Milburn [Knill *et al.*, 2001b]. The correctability requirement is fairly well met due to the low decoherence of photons. Loss of photons is a significant challenge but, like decoherence, loss can be handled by quantum error correction techniques [O'Brien, 2007] [Varnava *et al.*, 2006].

Trapped ions are another important platform for quantum computation. They meet the closed box criterion very well, having coherence times of seconds or longer [Langer *et al.*, 2005]. Trapped ion systems are not yet scalable. This is largely because the scaling of trapped-ion Coulomb gates becomes difficult when large numbers of ions participate in the collective motion of the trap. Segmented traps, where there are only a small number of ions per segment and the ions can be shuttled from one segment to another, may be able to overcome this limitation [Home *et al.*, 2009]. Universal logic can be performed in ion traps using the scheme of Cirac & Zoller [1995] or Mølmer and Sørenson [Sørensen & Mølmer, 1999] [Mølmer & Sørensen, 1999]. The correctability requirement is well-met by employing optical pumping.

Liquid-state NMR systems meet the closed box requirement very well. The coherence times are several seconds [Ryan *et al.*, 2009]. However, NMR is difficult to scale because it operates with pseudo-pure states. Universal logic can be performed in NMR systems and algorithms have been performed [Vandersypen *et al.*, 2001]. Furthermore, quantum error correction has been

[1]Considerable effort is being focused on further improving the efficiencies of single-photon detectors [Migdall & Dowling, 2004] [Hadfield, 2009] and single-photon sources [Grangier *et al.*, 2004].

performed [Cory *et al.*, 1998] [Leung *et al.*, 1999] [Knill *et al.*, 2001a].

Quantum dots and dopants in solids come in many different forms, some of which have excellent coherence times (e.g. silicon-28 [Saeedi *et al.*, 2013]). For the scalability requirement to be met, improvements to the fabrication are needed. Universal logic and quantum error correction both still need to be experimentally implemented.

Superconductors do not meet the closed box requirements, having short coherence times. They can be fabricated with small variation in qubit parameters and thus meet the scalability requirement. Universal logic gates can be performed with very high fidelity [Barends *et al.*, 2014]. For models of quantum computation where logic gates implement both the computational steps and the error-correcting steps, there is a threshold fidelity below which errors increase with the number of steps and above which errors decrease with the number of steps. The fidelity of superconducting quantum logic gates is at this threshold value, known as the fault tolerance threshold.

2.3 Cold Atoms

Cold neutral atoms have two main characteristics that are advantageous for quantum information processing (QIP) [Buluta *et al.*, 2011] [Negretti *et al.*, 2011]:

- They meet the closed box requirement by being relatively weakly coupled to the environment [Schrader *et al.*, 2004] [Treutlein *et al.*, 2004] [Yavuz *et al.*, 2006] [Deutsch *et al.*, 2010].

- Their quantum mechanical degrees of freedom can be well-controlled [Miroshnychenko *et al.*, 2006] [Beugnon *et al.*, 2007].

The quantum mechanical degrees of freedom that are best suited to encoding the qubit states are the internal states of the atom [Negretti *et al.*, 2011]. Due

to their high level of stability, the states most commonly used as qubit states are the long-lived (electronic) ground state hyperfine levels of the atoms. For example, the ground state hyperfine levels of Rubidium-87 are the $5S_{1/2}$ $F = 1$ and $F = 2$ levels. These are shown in Figure 8.2 of the appendix.

The atoms are prepared using standard laser cooling and trapping techniques (see sections 6.1 and 6.2). They are initially confined in a magneto-optical trap (MOT) from which they can be loaded into traps that better suited for the implementation of quantum computation. A discussion of these traps is now given. Focus is then brought onto the mechanisms by which quantum logic gates can be performed with the trapped atoms.

2.3.1 Traps

A variety of traps of have been developed for confining cold, neutral atoms. The nature of the traps affects how the various requirements of quantum computation can be fulfilled: how the qubit states can be encoded in the states of the atoms; how conveniently the atoms can be spatially positioned; etc. As an example, consider magnetic traps that rely on the force exerted on an atom by an inhomogeneous magnetic field. This force is dependent upon the magnetic moment of the internal state of the atom, which means that states with zero magnetic moment cannot be trapped and therefore cannot be used as qubit states.

The three main types of traps for neutral atoms are magnetic traps, optical lattices and optical dipole traps. Their state-of-the-art realisations are discussed below.

2.3.1.1 Magnetic Traps

Magnetic fields can be used to trap neutral atoms tens of micrometres above a solid substrate [Reichel, 2002] [Folman *et al.*, 2002] [Fortágh & Zimmermann,

2007]. The set-ups can be made light, compact and robust, in which case they are known as microtraps or atom chips [Westbrook, 2009]. Bose-Einstein condensates (BECs) [Ott *et al.*, 2001] [Hänsel *et al.*, 2001] and degenerate Fermi gases [Aubin *et al.*, 2006] can be loaded into these traps. Once loaded, they can be intricately manipulated (see, for example, Schumm *et al.* [2005]).

Magnetic traps for neutral atoms can be created by superconducting thin film structures [Müller *et al.*, 2010] [Bernon *et al.*, 2013]. Such a superconductor - cold atom hybrid device could combine the different strengths of these two platforms for quantum computation. The considerable prospects of this combination are currently being explored (see, for example, Patton & Fischer [2013] and Pritchard *et al.* [2014]).

2.3.1.2 Optical Lattices

Optical lattices are periodic arrays of optical traps generated by lasers in a standing wave configuration (see Figure 2.3).

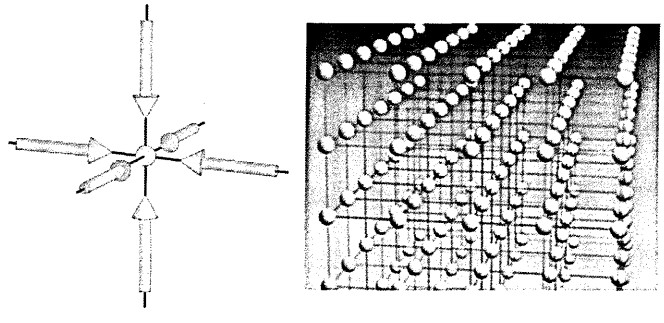

Figure 2.3: A schematic drawing of a three-dimensional optical lattice. It is formed by the interference pattern of three pairs of counter-propagating lasers (left). Atoms are confined in the resulting periodic array of traps (right). The Figure is taken from Bloch [2005].

Optical lattices can trap millions of atoms, making them highly suitable for simulating many-body physics [Jaksch & Zoller, 2005][Bloch, 2008] [Jrdens *et al.*, 2008] [Schneider *et al.*, 2008] [Ernst *et al.*, 2009]. The large number of atoms that they can trap is also helpful for creating stable clocks [Derevianko & Katori, 2011] and for fulfilling the scalability requirement of quantum computation

[Klein, 2007] [Beals *et al.*, 2008] [Saffman & Mølmer, 2008a] (see section 2.4.1 for a discussion).

2.3.1.3 Optical Dipole Traps

Optical dipole traps rely on the electric dipole interaction between an atom and an inhomogeneous field of far-detuned light [Grimm *et al.*, 2000][1]. State-of-the-art experiments have demonstrated that single atoms trapped in optical dipole traps can be cooled to their vibrational ground state [Thompson *et al.*, 2013b] [Kaufman *et al.*, 2012]. This provides an extremely suitable environment for manipulating the internal states of the atoms for quantum computation purposes.

The light incident on the atoms can be red- or blue-detuned from the atomic transition used for the trapping[2]. For the case of red-detuned light, the atom experiences a force pushing it towards the region of highest intensity. Consequently, the simplest example of an optical dipole trap is the focus of red-detuned laser [Ashkin, 1978]. Several adjacent traps can be simply created using several focussed, red-detuned beams. This can be achieved either by arrays of microlenses [Dumke *et al.*, 2002] or by holographic techniques [Bergamini *et al.*, 2004][3]. Recently, it has been demonstrated that optimisation techniques can ensure that the depths of the traps in the array are highly uniform [Nogrette *et al.*, 2014].

For the case of blue-detuned light, the atom experiences a force pushing it towards the region of lowest intensity. Blue-detuned traps are useful for quantum computation because the lower light intensity in the region where the atoms are confined, the lower the decoherence rate of the atoms. However,

[1]For details on the physics of optical dipole traps, see section 6.2.2.

[2]When a photon of light has less energy than the energy difference between the two states involved in the transition, it is said to be red-detuned. When it has more energy, it is said to be blue-detuned.

[3]Another possibility is to create time-averaged potentials by rapidly varying the position of a focussed beam [Henderson *et al.*, 2009].

in comparison to red-detuned traps, more elaborate arrangements of lasers are required (e.g. blue bottle traps [Isenhower *et al.*, 2009]). Nevertheless, a recent experiment [Piotrowicz *et al.*, 2013] has succeed in creating arrays of blue-detuned optical dipole traps.

2.3.2 Gates

For neutral atoms, there are two types of operation that can be used to perform quantum logic gates: controlled collisions and Rydberg interactions.

A controlled collision is the process of bringing trapped atoms into close spatial proximity. For atoms trapped in an optical lattice, this is a massively parallel operation (see Figure 2.4).

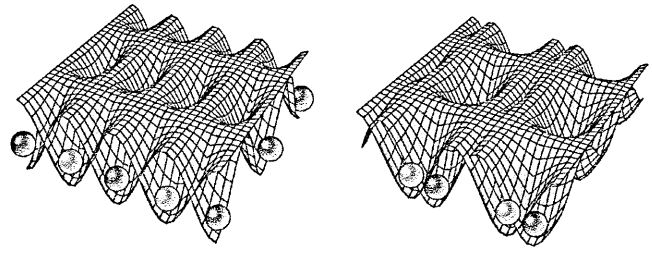

Figure 2.4: Controlled collisions between atoms in an optical lattice. Atoms in a certain internal state are depicted in blue and atoms in another internal state are depicted in red. The atoms begin the operation in their default positions (left). The optical lattice is manipulated so as to bring atoms of differing internal states into close spatial proximity (right). The Figure is taken from Monroe [2002].

Jaksch *et al.* [1999] devised a scheme to use controlled collisions between atoms in different internal states to perform quantum logic gates. The scheme relies on short-range, "contact" interactions.

Quantum logic gates can also be performed by exploiting the exchange symmetry of the wavefunction. This was initially proposed by Loss & DiVincenzo [1998] for quantum dot systems and then by Hayes *et al.* [2007] for neutral atoms.

Performing massively parallel entangling operations on atoms in optical lat-

tices is an enticing prospect because it could be used to create the resource state for MBQC [Briegel *et al.*, 2009]. However, to date, experimental demonstrations have proved challenging. Anderlini *et al.* [2007] performed the exchange symmetry logic gate in an optical lattice and achieved a fidelity of around 0.6.

Quantum logic gates can be performed, typically on a microsecond timescale, by exciting atoms to Rydberg states [Saffman *et al.*, 2010]. Chapter 3 is devoted to Rydberg-based quantum logic gates.

2.4 Cold Atoms as a Platform for Quantum Computation

In this section, I discuss how well cold atoms meet the DiVincenzo criteria and how they compare to other physical platforms.

2.4.1 Criterion 1: Scalability

The first of the criteria is scalability. Three dimensional optical lattices can be loaded with millions of atoms from a BEC [Bloch, 2008]. Typically, optical lattices are deepest in the centre and shallower with increasing radial distance. When the system is in the Mott insulator state, this results in the number of atoms per site increasing in integer steps with distance from the centre [Fölling *et al.*, 2006] [Campbell *et al.*, 2006]. For sufficiently deep lattices, each and every lattice site in the central region of the lattice contains exactly one atom [Klein, 2007].

Individually addressing the atoms in each of these lattice sites can be challenging because the separation between them is typically hundreds of nanometres, which is the same order of magnitude as the wavelength of the laser light that is intended to address the atoms. This challenge has been tackled in a variety of ways.

Nelson *et al.* [2007] worked around this challenge by interfering their trapping lasers at a small angle (10°) to create a lattice with the much larger spacing of 4.9 μm. Unfortunately, when atoms are separated by such distances, the interactions between them may not be sufficiently strong to allow high fidelity logic gates to be performed.

More closely spaced atoms have been imaged by Gericke *et al.* [2008] using electron microscopy. Unfortunately, their technique is not state-selective, which is crucial for quantum computation.

A highly successful way of tackling the issue of resolving closely spaced atoms is to employ the solid immersion effect [Mansfield & Kino, 1990]. For example, Bakr *et al.* [2009] use this effect to increases the numerical aperture of their objective lens from 0.55 to 0.8. This allows atoms to be individually addressed with none of the issues plaguing the other techniques.

2.4.2 Criterion 2: Initialisation

The second criterion is the ability to initialise the system to a certain state from which the computation can begin. Optical pumping initialises cold atom qubits with low error probabilities. Optical pumping schemes take advantage of the selection rules of photon absorption and emission in such a way that over many cycles of absorption and emission, the atoms have a high probability of being in the desired final state. For example, the vibrational motion of trapped atoms can be cooled using Raman sideband cooling [Kasevich & Chu, 1992].

2.4.3 Criterion 3: Long decoherence times compared to the time it take to perform a quantum logic gate

The third criterion is long decoherence times compared to the time it take to perform a quantum logic gate. The internal, hyperfine qubit states have long coherence times (up to a few minutes). Trap lifetimes are, however, shorter

(approaching one minute for optical dipole traps [Frese *et al.*, 2000]) due to collisions with background gases. Using pulsed lasers [Huber *et al.*, 2011], logic gates based on Rydberg interactions could be as short as a few nanoseconds, so in principle, it may be possible to implement quantum algorithms that require billions of quantum gates. However, technical constraints such as stray fields and laser beam instabilities also decrease coherence times, meaning fewer gate operations will be possible in practice [Saffman & Walker, 2005a].

2.4.4 Criterion 4: Universal Gates

The fourth criterion is the ability to perform universal gates. For a physical system to be sufficiently versatile to perform any quantum algorithm, one needs to be able to implement logic gates that act on one qubit at a time and logic gates that can generate entanglement between two qubits. Single-atom quantum logic gates can be performed using two-photon Raman pulses. Entangling two-atom quantum logic gates can be performed by utilising the Rydberg blockade phenomenon, as first proposed in Jaksch *et al.* [2000]. A CNOT gate has recently been experimentally implemented in this way [Isenhower *et al.*, 2010] [Wilk *et al.*, 2010]. The atoms were trapped in optical dipole traps and laser excitation pulses were applied in an appropriate sequence.

2.4.5 Criterion 5: Read-out

The fifth criterion is read-out. A weak laser beam can be used to produce a strong fluorescence signal dependent upon the initial state of the atom [Saffman & Walker, 2005a]. However, despite the low errors associated with this technique, it typically involves heating of the trapped atom, measurement times a few orders of magnitude longer than Rydberg-based gate operation times and thus, possible loss of the atom from the trap. Lossless high fidelity read-out is possible with a cavity [Bochmann *et al.*, 2010]. Employing such cavity-assisted read-out

in conjunction with deterministic, coherent atom transport in optical dipole traps (as experimentally demonstrated by Miroshnychenko *et al.* [2006]), could provide a viable means to fulfilling this criterion, especially since this read-out scheme does not require the coupling between the atom and the cavity to be in the strong regime of cavity QED.

2.4.6 Criterion 6: Inter-converting between stationary and flying qubits

The sixth criterion is inter-converting between stationary and flying qubits. An ensemble of neutral atoms has a higher cross-section for absorbing a photon than a single atom does. Using the phenomenon of Rydberg blockade (see section 3.1), it is possible to ensure that an ensemble of ground state atoms do not accidentally get transferred in states with multiple excitations [Saffman & Walker, 2002]. This aids the task of faithfully transferring the state of a photon to the state of an atomic ensemble [Dudin & Kuzmich, 2012] [Dudin *et al.*, 2012] [Li *et al.*, 2013].

2.4.7 Criterion 7: Transmitting the flying qubits

The seventh criterion is transmitting the flying qubits. By choosing the wave vectors of the photons that excite an ensemble of atoms, one can achieve directed emission of a single photon (i.e. one can specify the wave vector of the photon that is spontaneously emitted when the ensemble returns to the ground state) [Saffman & Walker, 2002] [Saffman & Walker, 2005b] [Brekke *et al.*, 2008].

2.5 Cold Atoms Compared to the Other Platforms

Cold atoms perform very well on several of the criteria (namely scalability, initialisation and long decoherence times) and have good prospects for fulfilling the others. An important step forwards for cold atoms would be to improve the fidelity of the two-qubit logic gates to ~ 0.99 as this would put them on par with the platforms that currently have greater success in meeting DiVincenzo's 'universal gates' criterion. Recent analyses of the sources of errors in Rydberg-based gates have found that this is a feasible goal [Zhang *et al.*, 2012] [Müller *et al.*, 2014].

Unlike some of the aformentioned systems, cold atom systems have not yet been used to perform any quantum algorithms. However, they have been widely used in quantum simulation experiments (see section VI. A. of Georgescu *et al.* [2014]) and are one of the main systems that could be used in creating a network of quantum computers [Sangouard *et al.*, 2011]. Overall, cold atoms are extremely well-placed to move the field of quantum computation forwards.

2.6 Summary

In this chapter, I provided the relevant background for understanding the circuit model of quantum computation. I also described the criteria a physical system needs to fulfil in order to perform this model. I mentioned that other models of quantum computation have different criteria to the circuit model. This will become relevant because after Chapter 3 on quantum logic gates with Rydberg atoms and Chapter 4 on the DQC1 model, I will demonstrate how the properties of these gates make them extremely well suited to implementing the DQC1 model. In particular, they allow for very large-scale implementations of the model.

I briefly surveyed various state-of-the-art platforms for quantum computation before finishing the chapter by focussing in detail on the cold atom platform.

Chapter 3

Quantum Gates With Rydberg Atoms

In this chapter, I give an introduction to the physics of Rydberg atoms. I discuss their extraordinary properties and the phenomena to which they lead.

I then describe the two original proposals for quantum logic gates based on Rydberg interactions [Jaksch *et al.*, 2000] [Lukin *et al.*, 2001]. The former proposal is for a CZ gate between single atoms, whilst the latter is for a controlled-Z rotation between ensembles of atoms. Working with ensembles has a number of advantages over working with single atoms (see section 3.2.2). However, the logic gate between ensembles of atoms only works with high fidelity when one can accurately and precisely estimate the number of atoms in the ensembles. This is an experimentally challenging situation that requires either randomly loading the traps with very high atom numbers ($\gtrsim 10^4$) or creating a BEC in order to uniformly load the traps.

I briefly survey the further work, both experimental and theoretical, that the two orignal proposals for Rydberg-based logic gates inspired. I continue by focussing on a recent proposal for a CNOT gate between a single atom and an ensemble of atoms [Müller *et al.*, 2009]. The proposal is based on Rydberg interactions and electromagnetically induced transparency (EIT). This proposed

gate compares well to the original one for ensembles because the number of atoms in the ensemble does not need to be accurately estimated. Later in the thesis (in Chapter 5), this gate (or rather, a very small modification of it) is modelled as part of the modelling of a Rydberg-based DQC1 protocol.

I then present the work of myself and colleagues [Beterov *et al.*, 2013] [Beterov *et al.*, 2014]. We first propose methods to perform single qubit gates on an ensemble of atoms. We then propose a Rydberg-based logic gate between *two* ensembles with *different, random* numbers of atoms. The gate relies on adiabatic passage techniques. Like EIT, these techniques are insensitive to atom-number. The key advantage over the EIT-based gate is that one is not required to work with both single atoms and ensembles, a scenario that would increase the complexity of the experimental sequence. Rather, one can load the traps with random numbers of atoms and proceed to the subsequent experimental stages straight away.

3.1 Rydberg Atoms

Rydberg states are highly excited electronic states. They have played an prominent in the history of atomic physics[1]. Nowadays, they are involved in phenomena ranging from many-body physics, quantum chaos and metrology (see section 3.1.3) to macrodimers, quantum optical effects and ultracold plasmas (see 8.3 of the appendix).

The energy levels of atoms in Rydberg states are accurately described by

$$E_{nlj} = \frac{-R_y}{(n - \delta_{lj}(n))^2}, \tag{3.1}$$

where $R_y = 109737.315685\ \text{cm}^{-1}$ is the Rydberg constant, named after the

[1]For example, they were considered in great depth by Bohr [1913] in the early days of atomic physics and later on, they helped with understanding the vacuum field in cavity quantum electrodynamics [Walther *et al.*, 2006].

Property	Dependence
Binding energy	$(n^*)^{-2}$
Energy between adjacent states	$(n^*)^{-3}$
Orbital radius	$(n^*)^2$
Geometric cross section	$(n^*)^4$
Dipole moment $\langle nd\|er\|nf\rangle$	$(n^*)^2$
Polarisability	$(n^*)^7$
Radiative lifetime	$(n^*)^3$
Fine-structure interval	$(n^*)^{-3}$

Table 3.1: Properties of Rydberg atoms and their dependence on the effective principal quantum number, n^*. The scaling with n^* is taken from Gallagher [1988].

physicist Johannes Rydberg. $\delta_{lj}(n)$ is the quantum defect, which is a slowly varying function of the principal quantum number, n. For a monovalent atom, it takes into account the extent to which the wavefunction of the valence electron penetrates the core electrons (that have mean positions closer to the nucleus than the valence electron does).

The low orbital angular momentum states have larger quantum defects since they are typically found closer to the nucleus and so experience a greater Coulomb attraction towards it. The effective principal quantum number, n^*, is given by $n^* = n - \delta_{lj}(n)$. As shown in Table 3.1, the important properties of atoms depend crucially on the value of the effective principal quantum number.

3.1.1 Strong Interactions and Blockade

In the absence of applied, external fields, Rydberg atoms have no permanent dipole moment and instead interact with one another via time-varying, or fluctuating dipole moments, either by the van der Waals interaction or by the Förster interaction. The van der Waals interaction is isotropic and scales as n^{11}/R^6, where R is the spatial separation between the nuclei of the interacting Rydberg atoms. The Förster interaction is a resonant, anisotropic interaction that scales as n^4/R^3. It occurs when a pair of atoms in Rydberg states $|r_1, r_2\rangle$ couple to, and exchange internal energy with, other, energetically-nearby

Rydberg states, $|r_1', r_2'\rangle$ [Comparat & Pillet, 2010][1].

The strength of the interactions between Rydberg atoms gives rise to an interesting phenomenon known as blockade. This is when the excitation of one atom to a Rydberg state suppresses, or 'blocks', any further laser-excitation of nearby atoms to Rydberg states. Due to the interaction strength decreasing with increasing atomic separations, atoms far from the excited Rydberg atom can still be excited. We can define a "blockade radius" as shown in Figure 3.1. The blockade shift, B, is the difference between the energies of the single-atom Rydberg state $|r\rangle$ and the two-atom Rydberg state $|r\rangle|r\rangle$. The scaling of the blockade shift with the inter-nuclei separation depends on the the type of interaction between the Rydberg atoms (i.e. $B(R) \sim R^{-6}$ for van der Waals interactions and $\sim R^{-3}$ for Förster interactions). Crucially, the blockade radius, R_b, is defined relative to the linewidth, $\Delta\omega$, of the exciting laser such that $B(R_b) = \Delta\omega$. When R is less than R_b, the two-atom Rydberg state $|r\rangle|r\rangle$ is far off resonance with the exciting laser and is only populated with a small probability, whilst when R is greater than R_b, the two-atom Rydberg state $|r\rangle|r\rangle$ is close to resonance with the exciting laser and is populated with a high probability.

3.1.2 Sensitivity To External Fields

Rydberg atoms are very sensitive to external fields. Electric fields polarise Rydberg atoms. They can cause the Rydberg states of an atom to mix, resulting in the atom acquiring a permanent electric dipole moment. When external electric fields are well controlled, they can be used to tune Rydberg states into a Förster resonances (leading to strong, anisotropic blockade shifts). Uncontrolled electric fields, on the other hand, may inhomogeneously broaden Rydberg energy levels and hinder successful demonstrations of protocols involving Rydberg

[1]The Förster interaction strength is maximal when the energies of the states, $E(|\cdot\rangle)$, fulfil $E(|r_1\rangle) + E(|r_2\rangle) = E(|r_1'\rangle) + E(|r_2'\rangle)$ [Safinya *et al.*, 1981].

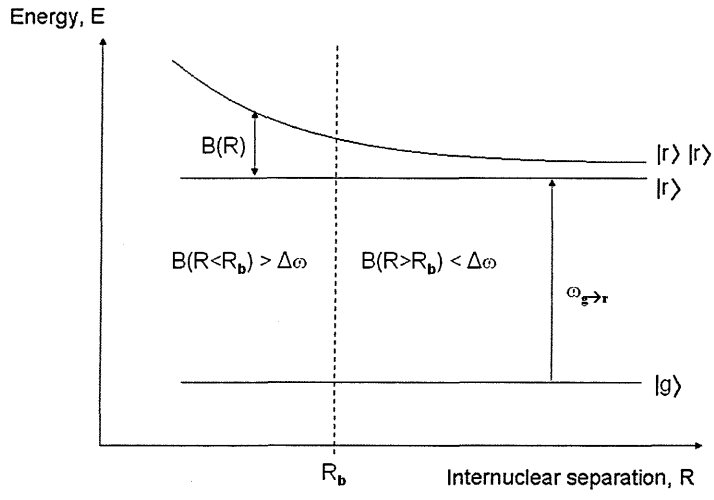

Figure 3.1: Schematic plot of how the blockade radius, R_b, is defined. See text for further details.

atoms.

Magnetic fields break the Zeeman degeneracy that produces Rydberg-Rydberg Förster interactions. Depending on the angle between the applied magnetic field and the interatomic axis and on the laser coupling to the Rydberg-Rydberg state, magnetic fields can be used to increase or decrease interaction strengths.

3.1.3 Notable Rydberg Phenomena

The phenomena related to the work presented in this thesis includes many-body physics, quantum chaos and metrology[1].

Cold Rydberg atoms are suitable for investigating many-body physics because they have lifetimes on the microsecond timescale and during such time periods, Rydberg atoms tend to move only a few percent of their interatomic spacing [Anderson *et al.*, 1998] [Mourachko *et al.*, 1998]. Thus, Rydberg atoms are often referred to as being "frozen in place" on timescales of interest. The

[1]In section 8.3 of the appendix, I mention some other key Rydberg phenomena: macrodimers; quantum optical effects; ultracold plasmas. I do this partly for the sake of completeness and partly because there may be connections between my work and these phenomena that I have not spotted.

limited kinetic energy of the atoms allows one to cleanly study the energy of the atomic interactions. The long range nature of Rydberg-Rydberg interactions means that a given Rydberg atom simultaneously interacts with many others. Such many-body interactions occur in a wide variety of interesting systems [Jaksch & Zoller, 2005] [Balents, 2010] [Olmos *et al.*, 2010][1].

Rydberg atoms are very good systems for studying quantum chaos ([Burke & Mitchell, 2009] and references therein). A wavefunction representing a coherent superposition of quantum states that is localised in phase space is often called a wave packet and experiments have found cases where the spatial position coordinate of the Rydberg electron wave packet approximates a classical orbit, known as a Kepler orbit [Yeazell *et al.*, 1989]. The phase space of Rydberg atoms contains a large area, the "chaotic sea," in which the wave packet of the Rydberg electron is dispersive and small areas, "stable islands," in which it is non-dispersive. Pulsed, unidirectional electric fields of duration much less than the Kepler period are termed half cycle pulses (HCPs). They change the angular momentum of the Rydberg atoms (which, in this situation, can be called kicked tops). The HCPs can be used to accurately control the position of the Rydberg wave packet in phase space [Zhao *et al.*, 2006] [Yoshida *et al.*, 2008], placing it in the chaotic sea, near the centre of a stable island or even on the "shore" (i.e. on the periphery of a stable island)[2].

Rydberg atoms have been employed in metrology, the science of measurement. Due their high sensitivity to fields, Rydberg atoms can be employed to make precise and reliable measurements of electric fields [Osterwalder & Merkt, 1999] [Sedlacek *et al.*, 2012] [Sedlacek *et al.*, 2013] and magnetic fields [Schwindt *et al.*, 2004][3].

[1] I return to the topic of many-body physics in section 5.5.2.

[2] The work in this thesis has implications for investigations of chaos in Rydberg systems. See section 4.4.1.

[3] Quantum metrology, the science of quantum-enhanced measurements, is described in section 4.4.3.

3.2 Original Proposals for Rydberg Quantum Logic Gates

In this section, I discuss the proposals of Jaksch *et al.* [2000] and Lukin *et al.* [2001].

3.2.1 Proposal with Single Atoms

The aim of single atom proposal [Jaksch *et al.*, 2000] was to design a fast two-qubit gate, the CZ gate. The authors began by identifying Rydberg states as being able to provide a strong and controllable interaction between two neutral atoms. However, large interactions can be associated with strong mechanical forces. If this were the case, then the internal states of the atoms (i.e. the qubit states) would become entangled with their motional degrees of freedom, which would serve as a dephasing mechanism for the atoms. The proposal can be implemented in either of two regimes related to the blockade shift, B (c.f. section 3.1 and Figure 3.1), and Rabi coupling, Ω. The first regime is where $B \ll \Omega$ and the second regime is where $B \gg \Omega$.

In the regime where $B \ll \Omega$, the gate operation does not require the two atoms to be individually addressable. The procedure to perform the gate involves applying a Rydberg-excitation π-pulse (i.e. a pulse that causes the atoms to perform half a Rabi cycle between the ground state and the Rydberg state) to the atoms, waiting a time $\Delta t = \varphi/E$ and then applying a final π-pulse to return any excited atoms back to the ground state (see Figure 3.2). Between the two pulses of this procedure, the components of the wavefunction where the atoms are in Rydberg states pick up a phase $\varphi = E\Delta t$, which equals π for the case of the CZ gate but could have a different value if one preferred to implement a more general controlled-Z rotation. (The Rydberg-Rydberg state has an energy shift B, so the unitary evolution of this state, $e^{-i(E+B)t/\hbar}$,

proceeds slightly faster and this component of the wavefunction picks up a small additional phase. However, since $B \ll E$, this unwanted additional phase is negligible.)

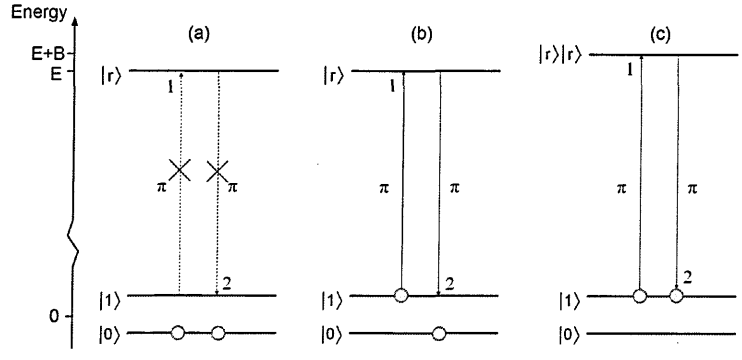

Figure 3.2: Gate operation in the regime $B \ll \Omega$: a laser, applied to both atoms, excites from the $|1\rangle$ state to the Rydberg state $|r\rangle$; no lasers are applied for a time $\Delta t = \varphi/E$, where φ is the desired phase rotation; finally, a laser, applied to both atoms, de-excites from the $|r\rangle$ to the $|1\rangle$ state. In (a), the atoms are initially in the state $|00\rangle$ and so are not excited and pick up no phase. The red crosses indicate that the laser pulse does not transfer any population. In (b), the atoms are initially in the state $|01\rangle$ or $|10\rangle$. One of the atoms is excited, picks up a phase φ and is then returned to the ground state. In (c), the atoms are initially in the state $|11\rangle$. The atoms are both excited (to the state $|rr\rangle$). A phase $\simeq \varphi$ is picked up and then both atoms are returned to the ground state.

One downside to operating in this regime is that when both atoms are in the Rydberg-Rydberg state, they experience an attractive or repulsive force. This creates unwanted entanglement between the qubit states and the motional degrees of freedom, which leads to dephasing.

In the regime where $B \gg \Omega$, the gate operation requires the atoms to be individually addressable. The procedure, shown in Figure 3.3, involves applying a π-pulse to the first atom, a 2π-pulse to the $|1\rangle$-$|r\rangle$ transition of the second atom and then finally a π-pulse to the first atom. If the first atom begins the procedure in qubit state $|1\rangle$ and the second atom in state $|1\rangle$, as shown in Figure 3.3(a), then the first atom is excited into the Rydberg state and the 2π-pulse on the second atom has no effect, since the large value of B ensures that the blockade phenomenon occurs and only one atom populates the

Rydberg state at a time. If the first atom begins the procedure in qubit state $|0\rangle$ and the second atom in state $|1\rangle$, as shown in Figure 3.3(b), then the first atom is not excited to the Rydberg state and the 2π-pulse results in the second atom acquiring a π phase shift relative to the first atom. The final pulse has no effect on the first atom since it never left the $|0\rangle$ state. For the cases where the second atom starts in state $|0\rangle$, no phase is picked up. In this way, a CZ gate is performed.

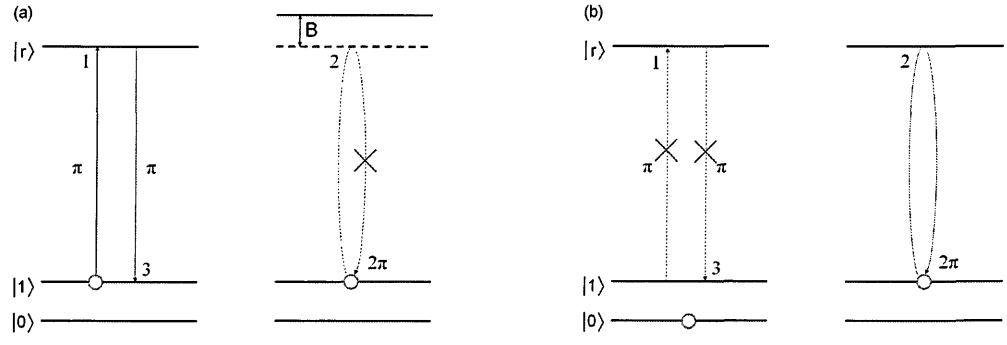

Figure 3.3: Gate operation in the regime $B \gg \Omega$ (for the cases where the second qubit, on the right, starts in the state $|1\rangle$). In case (a) the first qubit, on the left, starts in state $|1\rangle$ and the second qubit, on the right, acquires no phase. The red crosses indicate that the laser pulse does not transfer any population. In case (b), the first qubit, on the left, starts in state $|0\rangle$ and the second qubit, on the right, acquires a π phase shift. The sequence of laser pulses is the same in both cases.

Operating in the $B \gg \Omega$ regime has the following advantages: the gate is not sensitive to the precise value of B because the only requirement on B is that it is sufficiently large for the blockade effect to occur; and the gate no longer involves a stage where the atoms simultaneously populate the Rydberg state and experience dephasing, mechanical forces.

3.2.1.1 Recent Developments

Recent work has focussed on the in the $B \gg \Omega$ regime. On the experimental side, a Rydberg-based CNOT gate has been experimentally implemented by two independent research groups, Wilk *et al.* [2010] and [Isenhower *et al.*,

2010]. These groups proceeded to employ their Rydberg CNOT gates to generate entanglement between the control and target atoms [Zhang *et al.*, 2010] [Gatan *et al.*, 2010]. The gates suffered from considerable errors (of several tens of percent), including loss of atoms from the traps during the gate operation. However, most of the sources were of a technical nature, so considerable improvements could be envisaged.

On the theoretical side, detailed error analyses of the gate operation have been performed [Zhang *et al.*, 2012] [Müller *et al.*, 2014]. These analyses showed that with various technical improvements, the errors could be as low as a percent or a few tenths of a percent[1].

3.2.2 Proposal with Ensembles of Atoms

An ensemble of atoms is a group of identical atoms in a single trap. Lukin *et al.* [2001] extended the usefulness of Rydberg blockade from the implementation of logic gates on qubits encoded in single-atom states to qubits encoded in the collective states of ensembles. This is possible because the excitation of a single atom to an appropriate Rydberg state can prevent *all* the nearby atoms from being excited to this state.

After outlining the proposal of Lukin *et al.* [2001] for a quantum logic gate with ensembles of atoms, the advantages of using ensembles for quantum protocols are discussed. The main obstacle to using ensembles for high fidelity logic gates is given and, finally, some recent developments are briefly reviewed.

Let the number of atoms in a single ensemble be denoted by N. Let each atom have two stable ground states, $|0\rangle$ and $|1\rangle$, and a Rydberg state $|r\rangle$. Before defining the logical states of the collective encoding, consider the following, informative case. All the atoms are initially in the state $|0\rangle$ and a laser tuned to

[1]Circular Rydberg states, where the valence electron has a large value for its orbital angular momentum quantum number, have longer radiative lifetimes than low angular momentum Rydberg states. Gates based on circular Rydberg states are expected to have errors as a low as one thousandth of a percent [Xia *et al.*, 2013].

the $|0\rangle - |r\rangle$ transition illuminates all N atoms with equal intensity. Due to the Rydberg blockade effect, the resulting state contains only a single, collectively shared Rydberg excitation. This can be written as $|\underline{r}\rangle = \frac{1}{\sqrt{N}}\Sigma_i|0_1...r_i...0_N\rangle$. A laser tuned to the $|r\rangle - |1\rangle$ transition can convert the collectively shared excitation of the Rydberg state into a collectively shared excitation of the (stable) $|1\rangle$ state.

The logical states, $|\underline{0}\rangle$ and $|\underline{1}\rangle$ of the collective encoding are therefore sensibly chosen to be:

$$|\underline{0}\rangle = |0_1...0_N\rangle \tag{3.2}$$

$$|\underline{1}\rangle = \frac{1}{\sqrt{N}}\Sigma_i|0_1...1_i...0_N\rangle. \tag{3.3}$$

These logical states are depicted in Figure 3.4. Single qubit operations are performed with two-photon transitions via the Rydberg level, $|r\rangle$. Crucially, the Rydberg-Rydberg blockade shift, B, prevents the doubly-excited Rydberg state being excited, which, in turn, prevents the ensemble atoms from leaving the computational Hilbert space.

The proposal of Lukin *et al.* [2001] to perform two-qubit gates between ensemble qubits is entirely analogous to the gate for single atoms in the $B \gg \Omega$ regime: the blockade effect means that only one Rydberg excitation can be present in the two-ensemble system; the excitation of the control ensemble is dependent upon its logical state; whether the target ensemble picks up a phase shift or does not depends upon the excitation state of the control ensemble; and finally, the control atom is returned to its initial logical state.

Lukin *et al.* [2001] identified a few advantages of working with ensembles. The main advantage is that compared to single atoms, the blockade effect can be employed to enhance the coupling between ensembles and the radiation field. This enhancement is derived below.

For a laser coupling the states $|a\rangle$ and $|b\rangle$, the Rabi frequency, Ω, of the

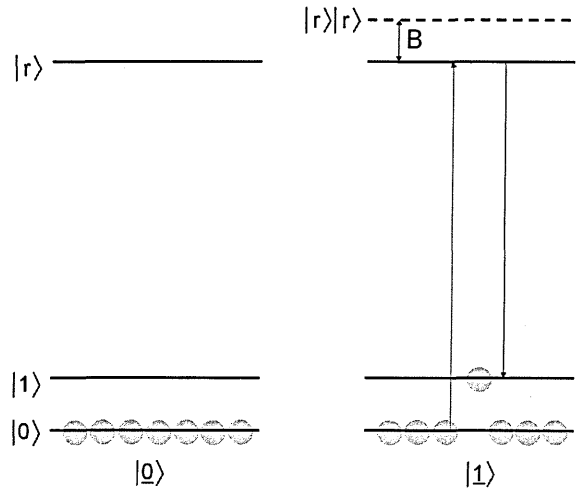

Figure 3.4: Collective qubit encoding in N-atom ensembles. The state depicted on the left is the logical state $|\underline{0}\rangle = |0_1...0_N\rangle$. The state depicted on the right is the (symmetrical) logical state $|\underline{1}\rangle = \frac{1}{\sqrt{N}}\Sigma_i|0_1...1_i...0_N\rangle$. As described in the main text, single qubit operations are performed by making straightforward use of the blockade effect.

transition is defined as:

$$\Omega = \langle a|\frac{-e\hat{\mathbf{r}}}{\hbar}|b\rangle E_0, \tag{3.4}$$

where $-e$ is the charge of an electron, $\hat{\mathbf{r}}$ is the position operator of the atom and E_0 is the electric field amplitude of the laser radiation.

For a single atom, the Rabi frequency of laser coupling the states $|0\rangle$ and $|r\rangle$ is $\Omega_1 = \langle 0|(-e\hat{\mathbf{r}}/\hbar)|r\rangle E_0$. For N atoms, the Rabi frequency of a laser coupling the states $|\underline{0}\rangle$ and $|\underline{r}\rangle$ is

$$\Omega_N = \langle \underline{0}|\frac{-e\hat{\mathbf{r}}}{\hbar}|\underline{r}\rangle E_0 \tag{3.5}$$

$$= \langle \underline{0}|\frac{-e\hat{\mathbf{r}}}{\hbar}\frac{1}{\sqrt{N}}\Sigma_i|0_1...r_i...0_N\rangle E_0 \tag{3.6}$$

$$= \sqrt{N}\Omega_1. \tag{3.7}$$

Thus, the collective Rabi frequency, Ω_N, is larger than the single-atom Rabi frequncy, Ω_1, by a factor of $\sqrt{N}$.

This enhanced coupling is important for the sixth and seventh DiVincezo criteria that are related to quantum networking (cf. sections 2.2, 2.4.6 and 2.4.6). It can also be employed to aid in the manipulation of photon states [Lukin, 2003] [Hammerer *et al.*, 2010]. One may expect that the decoherence rates would also be enhanced. However, shortly before Lukin's proposal, it was shown in Dür *et al.* [2000] that the proposed symmetric, entangled states are very robust to perturbations. They are even robust to the particles in this entangled state being lost in some way[1].

Some further advantages of ensembles were identified after the work of Lukin *et al.* [2001]. Ironically, one of the first of these was a technique to use ensembles as a starting point for single-atom loading [Saffman & Walker, 2002]. The technique, illustrated in Figure 3.5, begins with an ensemble where all the atoms populate the same ground state. The blockade effect is employed to create a single, collectively shared Rydberg excitation. De-excitation of this state moves precisely one atom into a different ground state. A strong light pulse is then used to remove all the atoms that have remained in the initial ground state. At the end of the sequence, only a single atom remains in the trap.

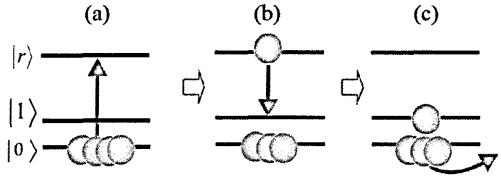

Figure 3.5: Using collective states for single-atom loading. (a) All the atoms are in the same ground state. A single Rydberg excitation is created. (b) The single Rydberg excitation is de-excited into a different ground state. (c) All the atoms that have remained in the initial ground state are removed from the trap, leaving it containing only a single atom.

Another advantage that was found was a method to encode several qubits per ensemble [Brion *et al.*, 2007] [Saffman & Mølmer, 2008a]. This method

[1] In our case, this could correspond to the a small number of atoms in the ensemble being lost from the trap.

could provide route to achieving larger registers of qubits whilst working with fewer ensemble but requires a high degree of control of the internal states of atoms with multiple ground states.

The main obstacle to using ensembles for high fidelity logic gates is the difficulty of preparing the ensembles in states with *exactly* one collectively shared Rydberg excitation. This difficulty stems from equation 3.5, according to which a collective Rydberg excitation can be created by:

- estimating the number of atoms, N, in the ensemble
- and then applying a pulse of duration $\tau_N = \pi/(\Omega_1\sqrt{N})$

This, however, relies on the estimate of N being correct. Since ensembles are most conveniently loaded in a random fashion[1], N cannot be precisely estimated.

For randomly loaded traps, the N follows a Poissonian distribution and so, for an average atom-number $\overline{N}$, the standard deviation in the atom-number is $\sqrt{\overline{N}}$. Lukin *et al.* [2001] point out that the relative error in an atom-number estimate can be small in the regime where $\sqrt{\overline{N}} \ll \overline{N}$. However, for reliable quantum computation, errors must be of the order 10^{-3} or lower, meaning that $\overline{N}$ would have to be of the order of 10^6. The impracticality of traps with such a high number of atoms is a significant obstacle to using ensembles for Rydberg-based quantum logic gates.

3.2.2.1 Recent Developments

The seminal proposal of Lukin *et al.* [2001] came a few years after the study of cold Rydberg atoms in MOTs had begun [Anderson *et al.*, 1998] and [Mourachko *et al.*, 1998]. Spurred on by the prospect of quantum information applications, suppression of Rydberg excitation was observed in many experimental works

[1]Even though one can employ BECs to load a (small) constant number of atoms per site [Fölling *et al.*, 2006] [Campbell *et al.*, 2006], such experiments are complex and time-consuming.

[Tong *et al.*, 2004] [Singer *et al.*, 2004] [Liebisch *et al.*, 2005] [Vogt *et al.*, 2006] [Vogt *et al.*, 2007] [Heidemann *et al.*, 2007][1].

The goal of studying a system where the blockaded region is larger than the sample size proved elusive until the work of the research group of Alex Kuzmich [Dudin & Kuzmich, 2012] [Dudin *et al.*, 2012] [Li *et al.*, 2013]. Whilst the goal of implementing the logic gate of Lukin *et al.* [2001] has still not been reached, this research group is taking important steps in that direction.

3.3 A Logic Gate based on Rydberg Interactions and Electromagnetically Induced Transparency

In this section, I discuss the physics of EIT and then describe the scheme of Müller *et al.* [2009], which employs EIT to implement a Rydberg-based quantum logic gate in ensembles of atoms. In Chapter 5, I report on detailed simulations of this scheme as it forms a key part of my modelling of a Rydberg-based DQC1 protocol.

3.3.1 EIT

The term *electromagnetically induced transparency* was first used in Harris *et al.* [1990] and its experimental oberservation was first reported in Boller *et al.* [1991]. It is a phenomenon where an optically opaque transition is made transparent to laser radiation. It is known as EIT because this transparency is induced by applying electromagnetic radiation [to a different optical transition].

EIT can occur when at least two lasers interact with a system that posses at least three energy levels. One of these levels must be coupled to at least two of the other levels. In Figure 3.6, an example of the simplest case - two lasers

[1]See Gallagher & Pillet [2008] for a review experiments of these experiments.

interacting with a three-level system - is shown[1]. A laser, known as the probe laser, with Rabi frequency Ω_p weakly couples the states $|1\rangle$ and $|2\rangle$, whilst a second laser, known as the coupling laser, with Rabi frequency $\Omega_c \gg \Omega_p$ strongly couples the states $|2\rangle$ and $|3\rangle$.

EIT can be understood in several different ways: (a) in a picture where the excitation pathways of the bare atomic states are seen to interfere; (b) in a dressed state picture, in which one notes the presence of dark states; and finally, (c) by straightforwardly numerically solving the Schrödinger equation.

Each of these ways turns out to be useful: (a) provides the most conceptually simple introduction to the phenomena; (b) is convenient for understanding why the high-fidelity mesoscopic logic gate falls short of having perfect fidelity; and (c) is central to my modelling of a Rydberg-based DQC1 protocol.

Let us consider the picture of EIT, based on the interference of different excitation pathways, given in Fleischhauer *et al.* [2005]. The relevant pathways for transferring population from state $|1\rangle$ to state $|2\rangle$ are:

- a *direct* pathway, $|1\rangle \rightarrow |2\rangle$
- an *indirect* pathway, $|1\rangle \rightarrow |2\rangle \rightarrow |3\rangle \rightarrow |2\rangle$

Since the coupling provided by the aptly named coupling laser is so much stronger than that provided by the probe laser, the indirect pathway has an amplitude that is equal in magnitude to the direct pathway. It turns out, however, that when the lasers are on resonance, the two amplitudes have opposite sign and the destructive interference of the pathways results in no population being transferred out of state $|1\rangle$. The presence of the coupling laser has induced the three-level system to be transparent to the probe laser.

As the detuning from resonance increases, the three-level system becomes less transparent to the probe laser. The transparency width caused by EIT

[1]In the mesoscopic gate based on EIT and Rydberg interactions, three lasers interacting with a four-level system will be considered.

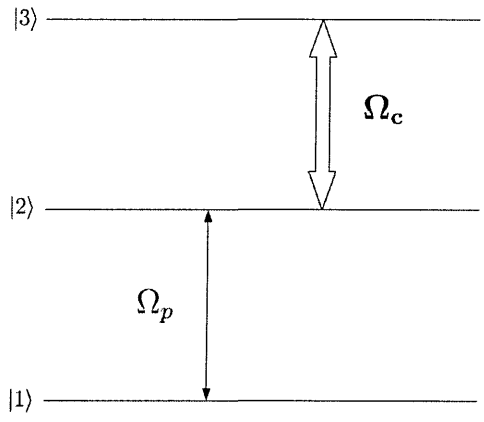

Figure 3.6: A schematic diagram of EIT in a ladder system where states $|1\rangle$ and $|2\rangle$ are weakly coupled and states $|2\rangle$ and $|3\rangle$ are strongly coupled. The laser beam that weakly couples two of the states is commonly known as the probe beam (with Rabi frequency Ω_p). The laser beam that strongly couples two of the states is commonly known as the coupling beam (with Rabi frequency Ω_c). Rabi frequencies must fulfil $\Omega_p \ll \Omega_c$.

can be narrower than the natural linewidth of the probe transition. This has lead to EIT being used used for applications such as giant non-linear responses [Schmidt & Imamoglu, 1996], ultraslow propagation [Hau *et al.*, 1999] and storage of light [Phillips *et al.*, 2001].

3.3.2 Logic Gate Between a Single Atom and an Ensemble

Müller *et al.* [2009] have proposed a two-qubit gate based on EIT and Rydberg interactions. The target qubit is a mesoscopic ensemble of trapped atoms and the control qubit is a single atom[1]. They are confined in two separate, individually addressable traps.

As shown in Figure 3.7, the control atom has three relevant energy levels: two ground states, $|0\rangle$ and $|1\rangle$, and a Rydberg state $|r\rangle$. Only one laser is ever applied to the control atom. This laser couples states $|1\rangle$ and $|r\rangle$. The atoms in

[1]A single atom rather than an ensemble has to be used as the control qubit because at the time of the proposal, no solutions to the difficulty (described in section 3.2) of preparing an ensemble in a state with exactly one collectively shared Rydberg excitation had been found.

the ensemble have four relevant energy levels: two ground states, $|A\rangle$ and $|B\rangle$, an intermediate state, $|P\rangle$, and a Rydberg state $|R\rangle$. Three lasers are shone on the ensemble so that EIT takes place: the coupling laser strongly couples the intermediate state $|P\rangle$ and the Rydberg state $|R\rangle$ whilst the probe laser is actually pair of lasers set up in a Raman configuration.

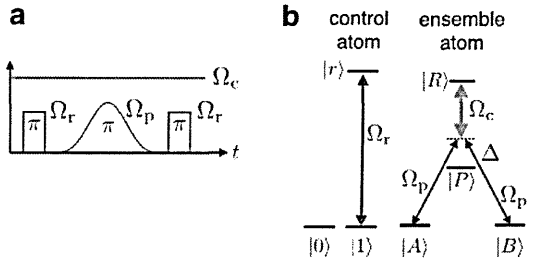

Figure 3.7: This figure is taken from Müller *et al.* [2009]. (a) A schematic diagram of the sequence of laser pulses. (b) is a schematic diagram of the relevant energy levels of the control and ensemble atoms and the applied laser fields. For the control atom, the ground state $|1\rangle$ and the (control) Rydberg state $|r\rangle$ are coupled on resonance. For the target atoms, there are two weak probe lasers, both with Rabi frequency Ω_p. One of these couples state $|A\rangle$ to $|P\rangle$ with a detuning Δ and the other couples state $|B\rangle$ to $|P\rangle$ with an equal detuning. In this way, states $|A\rangle$ and $|B\rangle$ are coupled in a Raman configuration. A strong coupling laser, with Rabi frequency $\Omega_c \gg \Omega_p$, is applied to the ensemble. It couples the (ensemble) Rydberg level $|R\rangle$ to $|P\rangle$ in such a way that $|R\rangle$ is in two-photon resonance with $|A\rangle$ and $|B\rangle$.

As is typical for controlled gates based on Rydberg interactions, the control atom is conditionally laser-excited to a Rydberg state dependent on its internal state. If the control *is* excited, there are strong Rydberg-Rydberg interactions between the control atom and the ensemble and a different physical process takes place to the case when the control atom is *not* excited. We now briefly consider each physical process in turn.

As shown in Fig. 3.8 (a), when the control atom is *not* in the state that gets excited to the Rydberg state, no Rydberg-Rydberg interactions are present and the ensemble atoms remains transparent to the probe Raman lasers for the entire gate operation. The EIT is said to 'block' the Raman transfer.

As shown in Fig. 3.8 (b), when the control atom *is* excited to the Rydberg

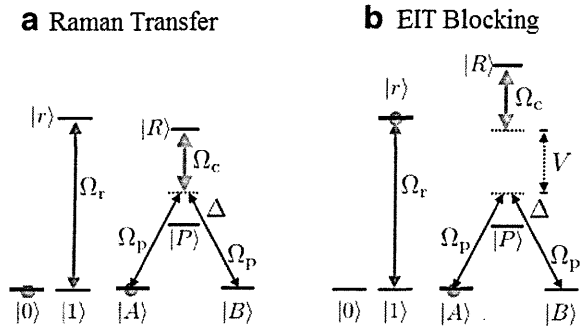

Figure 3.8: This figure is taken from Müller *et al.* [2009]. In (a), the control atom is not excited to the (control) Rydberg state $|r\rangle$. The phenomenon of EIT means that the ground states of the target atoms are transparent to the probe laser. The Raman transfer from $|A\rangle$ to $|B\rangle$ is said to be "blocked" by the EIT. In (b), the control atom excited is excited to the (control) Rydberg state $|r\rangle$, which shifts the (target) Rydberg energy level $|R\rangle$ by the Rydberg-Rydberg interaction energy, V. This energy shift lifts the two-photon resonance and off-resonant transfer between states $|A\rangle$ and $|B\rangle$ can occur.

state, the resultant Rydberg-Rydberg interactions (between the control atom and the ensemble atoms) shift the Rydberg levels of the ensemble atoms out of resonance with the EIT lasers. This shift destroys the EIT taking place in the ensemble, so that the ensemble atoms are no longer transparent to the probe Raman lasers. Thus, the ensemble atoms undergo an off-resonant Raman transfer process.

Finally, at the end of the gate operation, the control atom is returned to the internal state from which it was originally laser-excited. A controlled mesoscopic gate is thus performed.

We now consider each these two processes - Raman transfer and EIT blocking - in more detail. Specifically, we consider the sources of error.

As clearly explained in [Müller *et al.*, 2009], three factors influence the fidelity of the Raman transfer process. Firstly, in the ensemble, there is radiative decay from the intermediate state, $|P\rangle$, during the Raman transfer. Secondly, there is radiative decay from the control atom Rydberg state, $|r\rangle$. Thirdly, if an ensemble atom gets excited to the Rydberg state then there would be a mechanical force between it and the excited control atom. This

would create unwanted entanglement between the internal and external degrees of freedom of the atoms.

In addition to the inter-trap Rydberg-Rydberg interaction, there will also be interactions between the individual ensemble atoms. One might suspect that these interactions between atoms within the ensemble could reduce the fidelity of the Raman transfer aspect of the gate. However, for judicious choices of the Rydberg states, this is not the case. The Rydberg states can be chosen such that the interactions within the ensemble *add* to the inter-trap interaction shift, V, and so the EIT taking place in the ensemble is still destroyed and the Raman transfer still happens with high fidelity.

A dark state is a superposition (of atomic states) for which the different amplitudes for optical transitions to other states destructively interfere. This isolates the atom from the light field [Liu *et al.*, 2002]. As identified by Müller *et al.* [2009], there are two dark states involved in the EIT blocking. For the k-th ensemble atom, these dark states are:

$$|d_1\rangle_k = |-\rangle_k \tag{3.8}$$

$$|d_2\rangle_k = \frac{1}{\sqrt{1+x^2}}(|+\rangle_k - x|R\rangle_k), \tag{3.9}$$

where $|\pm\rangle = (1/\sqrt{2})(|A\rangle \pm |B\rangle)$ and $x(t) = \sqrt{2}\Omega_p(t)/\Omega_c$. The collective state of the ensemble during the EIT blocking is simply the tensor product of the states of all the ensemble atoms.

During the EIT, the atoms respond to the probe lasers by adiabatically following a superposition of these two dark states[1]. At the start ($t = 0$) and end ($t = t_{\text{end}}$) of the gate, $x = 0$ and the atoms are in an equally weighted superposition of the two dark states. That is, for the k-th ensemble atom, we have $|d\rangle_k(0) = |d\rangle_k(t_{\text{end}}) = (1/\sqrt{2})(|d_1\rangle_k + |d_2\rangle_k) = |A\rangle$.

Even though the interactions between the ensemble atoms do not reduce

[1]The dark states are sufficiently separated in energy from the "non-dark" states that non-adiabatic transitions from the dark states to the non-dark states are suppressed.

the fidelity of the Raman transfer aspect of the gate, it turns out that they do detrimentally affect the EIT blocking aspect. This can be seen as follows. The collective state of the ensembles during the EIT blocking is a superposition of different states: states with no Rydberg excitations (e.g. $|d_1 d_1\rangle$), states with a single Rydberg excitation (e.g. $|d_1 d_2\rangle$) and states with multiple Rydberg excitations (e.g. $|d_2 d_2\rangle$ has the term $x^2|RR\rangle/(1+x^2)$). The interactions between the ensemble atoms cause the components of the collective state with multiple Rydberg excitations to be shifted in energy. Their unitary evolution therefore proceeds at a different rate to the other components of the collective state. By the end of the gate sequence, they have acquired a phase shift[1]. These unwanted phase shifts reduce the fidelity of the EIT blocking aspect of the gate. Müller *et al.* [2009] performed a detailed analysis and conclude that despite this, the fidelity of this aspect of the gate is high ($\sim$0.98) for $x \sim 0.1$.

3.4 Rydberg Interactions with Adiabatic Passage Techniques

In this section, I first describe the phenomomenon of population transfer by adiabatic passage techniques. In particular, I focus on how either Adiabatic Rapid Passage (ARP) or Stimulated Raman Adiabatic Passage (STIRAP) can be used to completely transfer population between a ground state, $|g\rangle$, and a Rydberg state, $|r\rangle$. I then present a proposal that was conceived by myself and colleagues [Beterov *et al.*, 2013] [Beterov *et al.*, 2014] to employ these phenomena in conjunction with Rydberg interactions to perform quantum logic gates on ensembles of atoms.

[1] If the interaction between, say, two excitations of the ensemble Rydberg state $|R\rangle$ causes the energy of the $|RR\rangle$ to be shifted in energy by E_g, then the unitary evolution of this doubly excited state is changed by a factor equal to $\exp(-iE_g t/\hbar)$ and by the end of the gate sequence, it has a acquired a phase shift $\exp(-iE_g t_{\text{end}}/\hbar)$.

3.4.1 Adiabatic Passage Techniques

Adiabatic passage techniques have been extensively studied, both experimentally and theoretically, for a number of decades. Recent reviews include Bergmann *et al.* [1998], Vitanov *et al.* [2001] and Král *et al.* [2007]. The first ARP experiments were performed in nuclear magnetic resonance systems with the first experimental demonstration involving a laser coming in 1974 [Loy, 1974]. STIRAP was developed later on: it was conceived by Oreg and collaborators [Oreg *et al.*, 1984] [Oreg *et al.*, 1985] and was then experimentally implemented by Gaubatz and collaborators [Gaubatz *et al.*, 1988] [Gaubatz *et al.*, 1990].

The central concepts upon which an understanding of adiabatic phenomena rely are the following (see Vitanov *et al.* [2001] for a similar, yet more substantive, account). A constant Hamiltonian (e.g. that of a two-level system) is made to vary with time due to the application of an additional, time-varying Hamiltonian (e.g. that of a pulsed laser). The instantaneous eigenstates of a total Hamiltonian are known as the adiabatic states. According to Landau-Zener theory, the likelihood of the system undergoing transitions between the adiabatic states can be considered negligible when the total Hamiltonian fulfils certain conditions. When this is the case, the amplitudes for the system to be in given adiabatic states remain constant in time and the evolution of the system is said to be adiabatic. In the most commonly encountered scenarios [Comparat, 2009], adiabatic evolution requires the time evolution of the total Hamiltonian to be slow compared to the differences between the eigenfrequencies of the adiabatic states.

Population transfer is considered in terms of the eigenstates of the constant Hamiltonian. These are known as the "bare" eigenstates (e.g. the "bare" energy levels of two-level system). Since the adiabatic states are time-varying and the bare eigenstates are constant in time, it is convenient to express the adiabatic states are time-varying superpositions of the bare eigenstates. Population

transfer from an initial bare state to a final bare state is achieved as follows:

- the time-varying Hamiltonian initially is extremely weak, such that initially populated bare states coincides with an adiabatic state.

- the total Hamiltonian fulfils the conditions required for adiabatic evolution, so that the system remains in this adiabatic state.

- the populated, time-varying adiabatic state finishes its evolution coincident with the desired final bare state.

3.4.1.1 ARP

The technique of ARP involves the application of a chirped pulse to systems with two or more levels. This is shown for the case of a Rydberg ensemble in Figure 3.9. A chirped laser pulse, with single-atom Rabi frequency Ω_0 and detuning $\delta_{\text{ARP}}(t)$, couples a ground state, $|0\rangle$, to a Rydberg state, $|r\rangle$, causing it to undergo (single-photon) ARP[1]. The laser pulse has a Gaussian temporal profile and the detuning is swept linearly across the resonance.

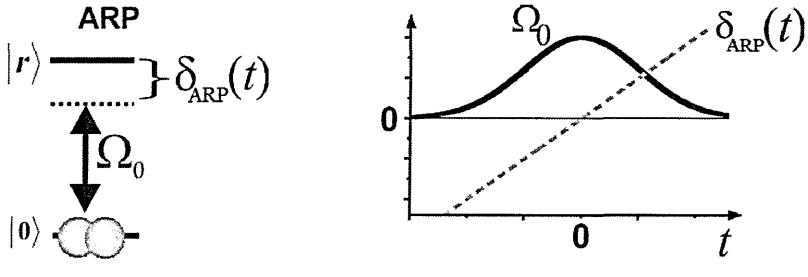

Figure 3.9: The energy levels and laser pulses for ARP.

Mathematically, the electric field of the chirped pulse is given by

$$E(t) = E_0 \exp\left[\frac{-t^2}{2\tau_{\text{ARP}}^2}\right] \cos\left(\omega_0 t + \alpha\frac{t^2}{2}\right), \tag{3.10}$$

[1]The laser system required to directly excite from a ground state to a Rydberg state is technically challenging to implement [Manthey *et al.*, 2014] and two-photon transitions via an intermediate state are more commonly employed.

where E_0 is the peak electric field at $t = 0$, ω_0 is the frequency of the atomic transition, τ_{ARP} is the half-width at $1/e$ amplitude and α is the chirp rate. In order to create such a chirped pulse, one can employ acousto-optic modulators (AOMs).

The adiabatic condition for ARP is that the chirp rate, α, in Equation 3.10 must be small compared to the Rabi frequency. In the case of an ensemble being excited to a collective Rydberg state, the relevant Rabi frequency is the (enhanced) collective Rabi frequency, Ω_N. Quantitatively, the condition is that $|\frac{d\delta_{\mathrm{ARP}}(t)}{dt}| \ll \Omega_N^2$, where $\delta_{\mathrm{ARP}}(t)$ is the detuning shown in Figure 3.10. Since Ω_N is always greater than the (known) single-atom Rabi frequency, Ω_0, we are sure to fulfil the adiabatic condition if $|\frac{d\delta_{\mathrm{ARP}}(t)}{dt}| \ll \Omega_0^2$.

3.4.1.2 STIRAP

STIRAP can only be employed in systems with at least three energy levels. This is shown for the case of a Rydberg ensemble in Figure 3.10. A laser with peak Rabi frequency, Ω_1, is red-detuned by δ from the transition between the ground state $|0\rangle$ and the excited $|e\rangle$. A laser with peak Rabi frequency, Ω_2, is blue-detuned by δ from the transition between the excited state $|e\rangle$ and the Rydberg $|r\rangle$. For STIRAP excitation from $|0\rangle$ to $|r\rangle$, the pulses are applied in a "counterintuitive" order: second-step excitation is applied before the first-step pulse. That is, the Ω_2 pulse is applied before the Ω_1 pulse.

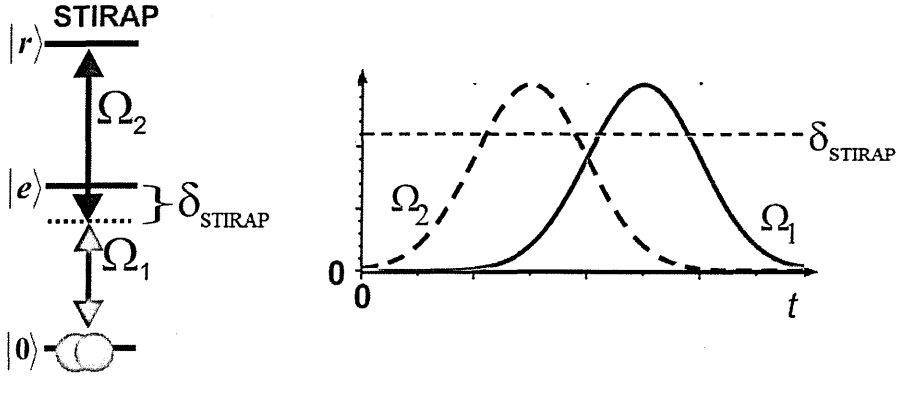

Figure 3.10: The energy levels and laser pulses for STIRAP.

Mathematically, the Rabi frequencies of the two lasers are given by

$$\Omega_j(t) = \Omega_j \ \exp\left[\frac{-(t-t_j)^2}{2\tau^2_{\text{STIRAP}}}\right], \tag{3.11}$$

where $j = 1, 2$ and $t_2 < t_1$.

To apply the general adiabatic condition to off-resonant STIRAP, let us first consider the STIRAP adiabatic condition when there is no detuning from the intermediate state. The condition is that (a) the pulses must be smoothly varying, (b) the pulse areas must be larger than a few π and (c) there must be sufficient overlap of the two pulses. For smoothly varying pulses, we can quantitatively summarise conditions (b) and (c) with $T_{\text{overlap}}\sqrt{\Omega_1^2 + \Omega_2^2} > 10$, where Ω_1 and Ω_2 are shown in Figure 3.10, T_{overlap} is time period for which the two pulses overlap and 10 is obtained from experience with experiments and simulations [Bergmann *et al.*, 1998]. The adiabatic condition for *off*-resonant STIRAP is similar but the non-zero single-photon detuning, $\delta_{\text{STIRAP}} \neq 0$, means that larger pulse areas are required [Vitanov & Stenholm, 1997].

3.4.2 Logic Gate Between Two Ensembles

In work by myself and colleagues [Beterov *et al.*, 2013] [Beterov *et al.*, 2014], we devised Rydberg-based logic gates for ensembles of atoms. Our proposed gates build on earlier work by Beterov *et al.* [2011] that provided two methods to solve the problem of reliably (i.e. deterministically) exciting a randomly loaded ensemble to a state with a single, collectively shared Rydberg excitation[1]. The first method relied on ARP and the second on STIRAP. In our work [Beterov *et al.*, 2013] [Beterov *et al.*, 2014], we extend both of these methods, devising both single-qubit and two-qubit gates.

Notably, in our two-qubit gates, both qubits are encoded in ensembles,

[1]The problem of reliably exciting a randomly loaded ensemble was described in section 3.2.2.

which contrasts with the EIT-based proposal of Müller *et al.* [2009] where the control qubit is a single atom and only the target qubit is an ensemble. This is important from an experimental perspective because randomly loading two adjacent traps is more straightforward than loading one trap with a single atom and an ensemble of atoms.

I begin by describing how we extend the prior work on the deterministic excitation of ensembles [Beterov *et al.*, 2011] to perform deterministic *de*-excitation. I then describe how this can be employed to perform a single-qubit Identity gate. From this foundation, we devise a non-trivial single-qubit gate before finally extending this to two-qubit gates.

3.4.2.1 Deterministic Rydberg Excitation

Beterov *et al.* [2011] provide two methods to deterministically prepare a randomly loaded ensemble in a state with a single Rydberg excitation: ARP and off-resonant STIRAP[1]. These methods are illustrated schematically in Figure 3.11 along with the the probability, P_1, of the ensemble having single Rydberg excitation.

The atoms are initially in the collective ground state (with $P_1 = 0$). P_1 increases with time while the blockade effect ensures that the probability for the ensemble to be in a state with more than one atom Rydberg excitation is negligible. By the end of the procedure, P_1 is greater than 0.99. Crucially, the procedure is insensitive to the number, N, of atoms in the ensemble.

ARP and STIRAP in multi-atom ensembles were described in sections 3.4.1.1 and 3.4.1.2, respectively. In addition to the adiabacity condition, for the methods of Beterov *et al.* [2011] to work, Rydberg blockade needs to be effective. This is not an issue for the off-resonant STIRAP method but as noted by Beterov *et al.* [2011], the frequency chirp in the ARP method broadens the

[1] *On*-resonance STIRAP in a Rydberg-blockaded ensemble has been studied by Møller *et al.* [2008], who showed that it can be used to create entangled states such as Greenberger-Horne-Zeilinger states.

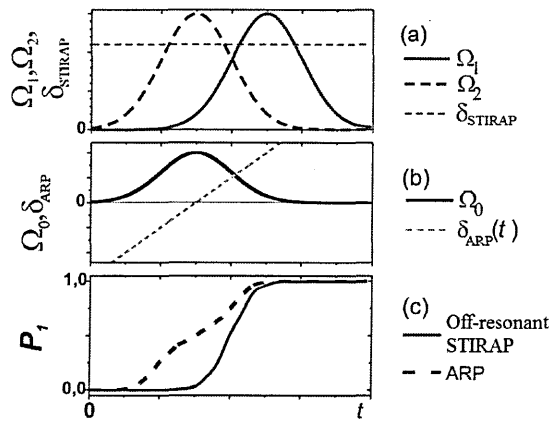

Figure 3.11: Two methods for deterministic Rydberg excitation of a randomly loaded ensemble. (a) The off-resonant STIRAP laser pulses. (b) The ARP laser pulse. (c) The probability of the ensemble having a single Rydberg excitation as a function of time.

linewidth of the excitation laser. The spectral width of the excitation laser is an important parameter in defining the blockade radius. As discussed in section 3.1.1, the blockade radius is defined to be the interatomic separation at which the Rydberg interaction strength equals the linewidth of the excitation laser. Since the Rydberg interaction strength decreases with interatomic separation, a larger linewidth would reduce the blockade radius. However, the numerical simulations performed by Beterov *et al.* [2011][1] showed that the ARP method nevertheless still works well.

3.4.2.2 Deterministic De-excitation and Identity Gate

An ensemble in a collective Rydberg state can be deterministically de-excited by performing the pulse(s) described in Beterov *et al.* [2011] in a time-reversed fashion. For the off-resonance STIRAP method, this corresponds to applying the Ω_1 pulse prior to the Ω_2 pulse. For the ARP method, the single chirped pulse is simply applied as before.

In order to perform an identity procedure (or identity "gate"), more re-

[1]These simulations involved solving the time-dependent Schrödinger equation for the amplitudes of the collective states. They included up to seven atoms interacting via a Förster interaction (which had previously been studied in detail [Ryabtsev *et al.*, 2010a] [Ryabtsev *et al.*, 2010b]) and considered all possible binary interactions between the Rydberg atoms.

quirements need to be met than those involved with performing deterministic excitation and de-excitation. In the latter case, one only requires that the *moduli* of the complex amplitudes for the collective states need to be controlled. Specifically, the modulus of the amplitude for the collective ground state needs to go from one to zero in the excitation process and then back to one in the de-excitation process. However, for an identity gate, both the modulus and the phase of the complex amplitudes need to be controlled. Specifically, the modulus and phase of the amplitude for the collective ground state both need to be returned to their original values at the end of the gate.

In order to consider designs for quantum logic gates, even identity gates, we must now explicitly consider atoms with two hyperfine ground states, $|0\rangle$ and $|1\rangle$ (i.e. we must consider qubits). Figures 3.9 and 3.10 can be amended appropriately.

In Figure 3.12 (a) and (b), it is shown how identity gates can be performed using adiabatic passage techniques. As shown in Figure 3.12 (a), a STIRAP-based identity gate requires that the detuning for the excitation pulses and the detuning for the de-excitation pulses have opposite sign (e.g. δ_{STIRAP} is positive for the excitation pulses and negative for the de-excitation pulses). As shown in Figure 3.12 (b), an ARP-based identity gate requires that the excitation pulse and the de-excitation pulse are 180° out of phase (e.g. the Rabi frequency of the excitation pulse is positive and that of the de-excitation pulse is negative). This can be achieved using AOMs.

Figure 3.13 presents numerical evidence of these requirements. In Figure 3.13(a), the phase of the collective ground state is shown as a function of time for a double STIRAP sequence where the sign of the detuning is *not* switched between the excitation and de-excitation pulses. The phase clearly does not return to its initial value and as such, this pulse sequence does not perform an identity gate. In contrast, Figure 3.13(b) shows how switching the sign of detuning allows the phase to have the same value at the end of the procedure

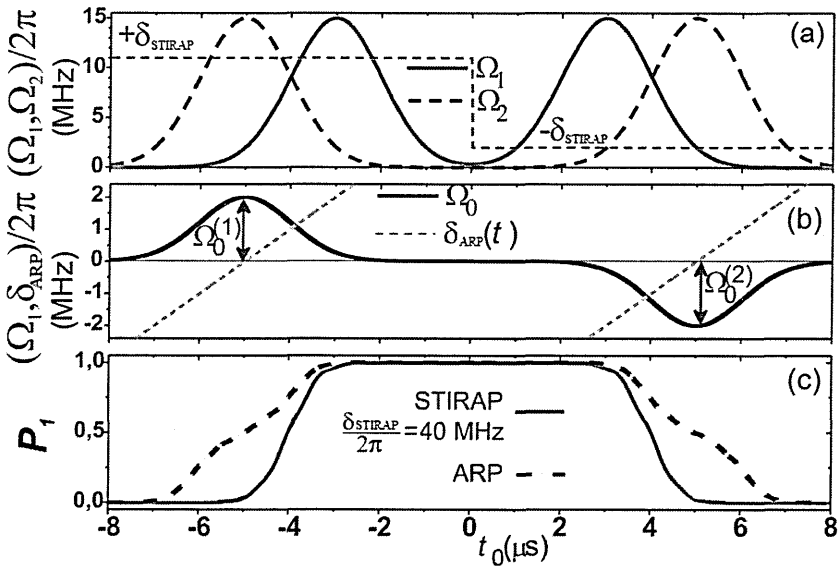

Figure 3.12: (a) The STIRAP laser pulses for the identity gate. (b) The ARP laser pulses for the identity gate. (c) Time dependence of the single-atom excitation probability.

as at the beginning. Therefore, Figure 3.13(a) and (b) show how switching the sign of the detuning is crucial to performing a STIRAP-based identity gate.

In Figure 3.13(c), the phase of the collective ground state is plotted during a double ARP pulse sequence where the excitation and de-excitation pulses are 180° out of phase. Since the phase returns to its original value, an ARP-based identity gate is performed.

For these identity gates to be considered as a stepping stone in the design of other logic gates, one first needs to perform a detailed error analysis. In Figure 3.14(a), the excitation component of the gates is compared to applying a π-pulse when different numbers of atoms are in the ensemble. The application of a π-pulse has errors of the order 10^{-1} for all numbers of atoms except the atom number for which the pulse is optimised. In contrast, ARP and STIRAP excitation have considerably lower errors for a wide range of atom numbers.

Figure 3.14(b) shows the results of numerical simulations of STIRAP excitation when the finite linewidths of the intermediate and Rydberg states are included. It was found that the finite linewidth of the intermediate state means

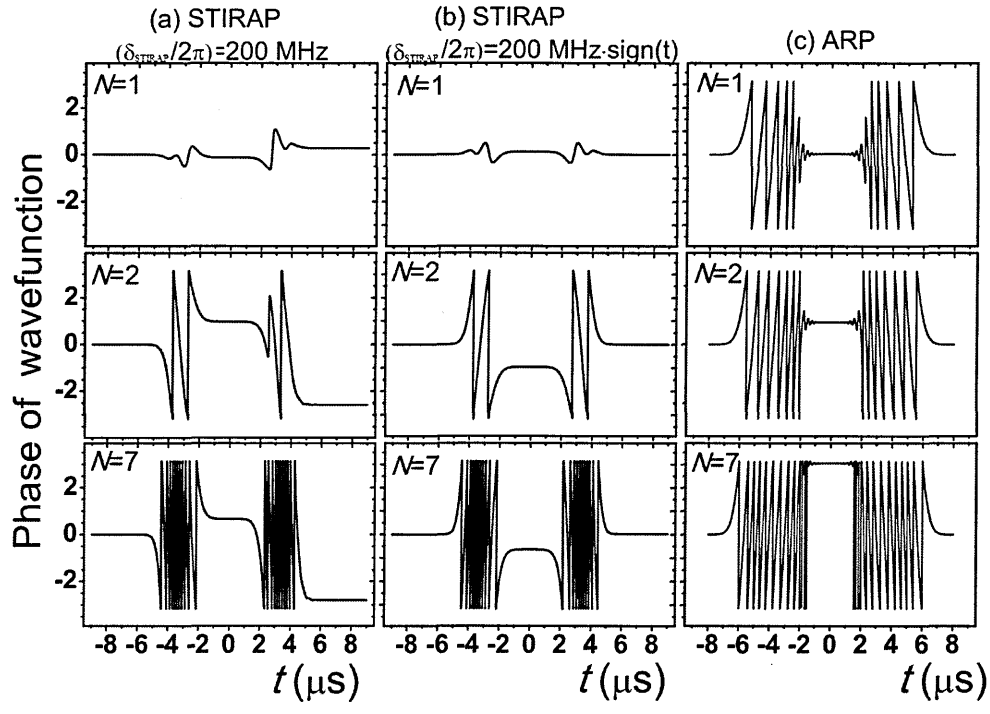

Figure 3.13: The calculated time-dependence of the phase of the collective ground state amplitude for $N = 1, 2, 7$ atoms (top to bottom). (a) and (b) show the double STIRAP sequence. The Rabi frequencies obey equations of the form of Equation 3.11 with peak Rabi frequencies $\Omega_1/2\pi = 30$ MHz and $\Omega_2/2\pi = 40$ MHz and pulse widths $\tau_{\text{STIRAP}} = 1$ μs. For the first pair of STIRAP pulses that perform the excitation, $t_1 = -3.5$ μs and $t_2 = -5.5$ μs. For the second pair of STIRAP pulses that perform the de-excitation, $t_1 = 3.5$ μs and $t_2 = 5.5$ μs. For (a), $\delta_{\text{STIRAP}}/2\pi = 200$MHz (i.e. there is no switching of the sign of the detuning). For (b) $\delta_{\text{STIRAP}}/2\pi = 200$ MHz $\times \text{sign}\,(t)$ (i.e. there is switching of the sign of the detuning). (c) shows a double ARP pulse sequence. The first ARP pulse that performs the excitation obeys $\Omega_0(t) = \Omega_0 e^{-(t-t_{\text{peak}})^2/2\tau_{\text{ARP}}^2}$ with peak, single-atom Rabi frequency $\Omega_0/2\pi = 2$ MHz, pulse width $\tau_{\text{ARP}} = 1$ μs, and linear chirp rate $\alpha/2\pi = (1/2\pi)(d\delta_{\text{ARP}}(t)/dt) = 1$ MHz/μs. The second ARP pulse that performs the de-excitation obeys an equivalent equation with opposite sign for the peak Rabi frequency.

that $\delta_{\text{STIRAP}} \gg \Omega_1, \Omega_2$ is an important requirement for low population error. Similarly, the finite linewidth of the Rydberg states means a short pulse width, τ_{STIRAP}, is conducive to keeping population errors low[1].

With the population errors of the excitation aspect of the gates found to be low enough for quantum information purposes, we now proceed to an

[1]In order for the STIRAP excitation to operate in the correct parameter regime (and thus remain effective) with a shorter pulse width, higher Rabi frequencies, Ω_1, Ω_2, and a larger detuning, δ_{STIRAP}, are all required.

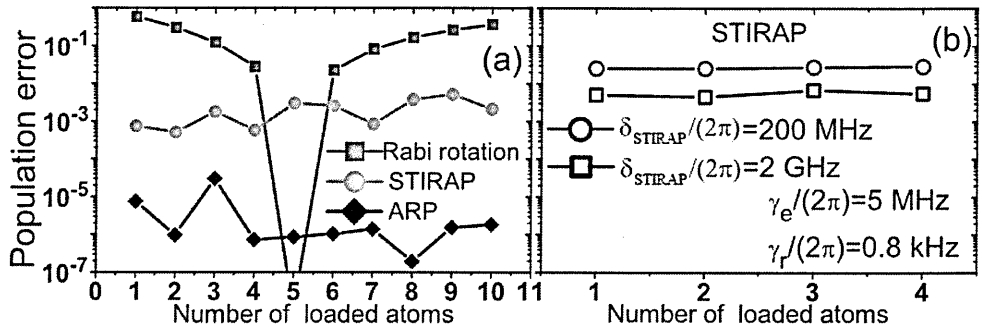

Figure 3.14: (a) A comparison of the population error for exciting a single, collective Rydberg excitation for different numbers of ensemble atoms. Three different methods are compared: a π-pulse that has its area optimised for $N = 5$ atoms ($t = \pi/\sqrt{5}\Omega$); off-resonant STIRAP pulses; and an ARP pulse. All parameters are as in Figure 3.13. Spontaneous emission is not taken into account. (b) The population error for using the off-resonant STIRAP method to create a single, collective Rydberg excitation for different numbers of ensemble atoms. It is calculated taking into account the finite linewidth $\gamma_R/(2\pi) = 0.8$ kHz of the Rydberg state and the finite linewidth $\gamma_e/(2\pi) = 5$ MHz of the intermediate state. The parameters for the blue data points are $\delta_{\text{STIRAP}} = 200$ MHz, $\Omega_1/2\pi = 30$ MHz, $\Omega_2/2\pi = 40$ MHz and $\tau_{\text{STIRAP}} = 1$ μs. The parameters for the black data points are $\delta_{\text{STIRAP}} = 2$ GHz, $\Omega_1/2\pi = \Omega_2/2\pi = 250$ MHz and $\tau_{\text{STIRAP}} = 0.2$ μs.

investigation of the phase errors that accumulate by the end of the identity gates. One source of the phases errors in the identity gates is unwanted differences between the excitation pulses and de-excitation pulses (recall Figure 3.12). In particular, we investigated the effect of unwanted differences between the peak Rabi frequencies of the excitation and de-excitation pulses. In Figure 3.15(a), the phase error of the STIRAP-based identity gate is shown to depend linearly on the ratio $\Omega_1^{(2)}/\Omega_2^{(1)}$. In Figure 3.15(b), the phase error of the ARP-based identity gate is shown to depend linearly on $\Omega_0^{(2)}/\Omega_0^{(1)}$. Experimentally, the peak Rabi frequencies involved in either identity gate are separated by only a few microseconds, which is a timescale over which lasers are typically very stable. This means that the peak Rabi frequencies can have the same value to within 10^{-6} of the absolute values [Wineland *et al.*, 1998]. Consequently, the phase errors in the identity gates are acceptably low.

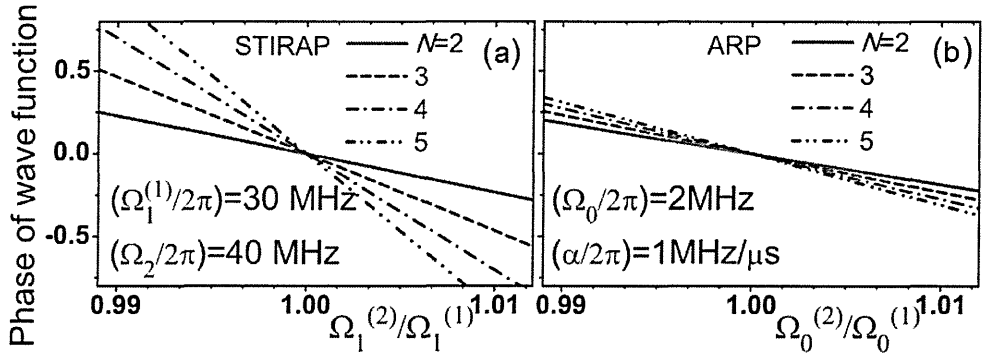

Figure 3.15: (a) and (b) show the dependence of the phase error on the unwanted changes in peak Rabi frequency between excitation and de-excitation pulses for STIRAP-based and ARP-based identity gates, respectively. For the STIRAP-based identity gate in (a), $\delta_{\text{STIRAP}} = 200$ MHz and $\tau_{\text{STRIAP}} = 1$ μs.

3.4.2.3 Single-Qubit Gate

For a single-qubit gate, we require two Rydberg levels, $|r_0\rangle$ and $|r_1\rangle$. As shown in Figure 3.16, the state $|0\rangle$ can be optically coupled to the Rydberg state $|r_0\rangle$ and the state $|1\rangle$ can be optically coupled to the Rydberg state $|r_1\rangle$.

The gate acts on collective states. Consider the states $|\overline{0}\rangle = |000...000\rangle$, $|\overline{1}\rangle' = (1/\sqrt{N})\Sigma_{j=1}^{N}|000...1_j...0\rangle$ and $|\overline{r}\rangle' = (1/\sqrt{N})\Sigma_{j=1}^{N}|000...r_j...0\rangle$. From these states, we can define the logical basis states and the auxiliary Rydberg state as $|\overline{0}\rangle = |000...000\rangle$, $|\overline{1}\rangle = e^{i\chi_N}|\overline{1}\rangle'$, $|\overline{r}_0\rangle = e^{i\chi_N}|\overline{r}_0\rangle'$ and $|\overline{r}_1\rangle = e^{i\chi_N}|\overline{r}_1\rangle'$, where χ_N is the phase produced by a single N atom STIRAP pulse with positive detuning.

Figure 3.16 shows the scheme, consisting of five pulses, to implement a single-qubit gate. The first pulse couples the states $|1\rangle$ and $|r_1\rangle$. The second pulse couples the states $|0\rangle$ and $|r_0\rangle$. The third pulse is a microwave pulse that couples the two Rydberg levels with a detuning Δ. In this case, the off-resonance Rabi frequency is $\Omega_{\text{off}} = \sqrt{\Omega_{\text{on}}^2 + \Delta^2}$, where Ω_{on} denotes the on-resonance Rabi frequency. The rotation angle is about the Rabi vector,

$$\vec{\Omega}' = \Omega\vec{n_x} + \Delta\vec{n_z}, \tag{3.12}$$

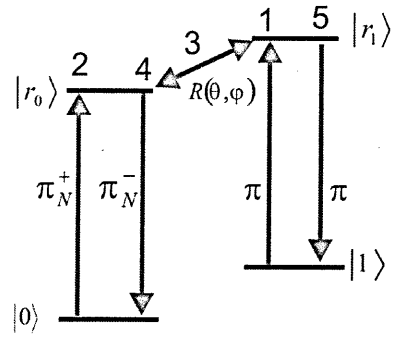

Figure 3.16: Single qubit gate for a mesoscopic qubit with N atoms. Pulses $1-5$ act between the qubit states $|0\rangle, |1\rangle$ and the Rydberg states $|r_0\rangle, |r_1\rangle$. Pulses $1, 2, 4, 5$ are optical transitions and pulse 3 is a microwave frequency transition between Rydberg states. The optical pulses are π-pulses, where the subscript N indicates use of the ARP or STIRAP techniques and no subscript indicates a conventional Rabi pulse. The positive or negative superscript indicates the sign of the detuning for the STIRAP pulses or the sign of the chirp rate for the ARP pulse.

where $\overrightarrow{n_x}$ and $\overrightarrow{n_z}$ are the x and z axes of the Bloch sphere. The fourth pulse couples the states $|r_0\rangle$ and $|0\rangle$. The final pulse couples the states $|r_1\rangle$ and $|1\rangle$.

If the qubit state is initially $|\psi\rangle = a|\overline{0}\rangle + b|\overline{1}\rangle$, the pulses 1 to 5 give the sequence of states:

$$|\psi_1\rangle = a|\overline{0}\rangle + ib|\overline{r}_1\rangle \tag{3.13}$$

$$|\psi_2\rangle = a|\overline{r}_0\rangle + ib|\overline{r}_1\rangle \tag{3.14}$$

$$|\psi_3\rangle = a'|\overline{r}_0\rangle + ib'|\overline{r}_1\rangle \tag{3.15}$$

$$|\psi_4\rangle = a'|\overline{0}\rangle + ib'|\overline{r}_1\rangle \tag{3.16}$$

$$|\psi_5\rangle = a'|\overline{0}\rangle - b'|\overline{1}\rangle \tag{3.17}$$

Thus, the gate can perform single-qubit rotations.

In order to further investigate the properties of the single-qubit gates, we numerically modelled the STIRAP-based gate for $N = 13$ atoms for the following sequence of rotations. The qubit is initially in state $|0\rangle$. It is then rotated by an angle of $\pi/2$ about the $y-$axis of the Bloch sphere to the state $|+\rangle = (|0\rangle + |1\rangle)/\sqrt{2}$ (which lies on the $x-$axis of the Bloch sphere). A rotation

by angle ϕ around the $z-$axis of the Bloch sphere is then performed. The qubit is then, once again, rotated by an angle of $\pi/2$ about the $y-$axis of the Bloch sphere.

This sequence of rotations is a Ramsey sequence [Ramsey, 1950]. Such sequences have played a prominent role in characterising quantum systems (e.g. in the Nobel prize winning work of Haroche & Wineland [2012]). The results of the modelling of the sequence with STIRAP-based gates are plotted in Figure 3.17.

In Figure 3.17(a), the probability, $P_{|1\rangle}$, of finding the ensemble in the state $|1\rangle$ at the end of the sequence of STIRAP-gates is shown for different values of ϕ. It is compared to equivialent sequences of ideal (Rabi) rotations. The STIRAP-based rotations give the values of $P_{|1\rangle}$ that would be expected for ideal operation. This indicates that coherence is maintained throughout the sequence.

In Figure 3.17(b), the probability, $P_{|1\rangle}$, of finding the ensemble in the state $|1\rangle$ at the end of the sequence is shown for the case when the sign of the detuning is not switched between the excitation and de-excitation pulses. The gate is extremely error-prone, which re-emphasises that this switching is crucial to the gate performance.

3.4.2.4 Two-Qubit gate

Figure 3.18 shows the scheme to implement a two-qubit gate between a control qubit with N_c atoms and a target qubit with N_t atoms.

The first pulse couples the states $|0\rangle$ and $|r_0\rangle$ of the control ensemble. The second pulse couples the states $|1\rangle$ and $|r_1\rangle$ of the target ensemble. The third pulse couples the states $|0\rangle$ and $|r_0\rangle$ of the target ensemble. The fourth pulse is a microwave pulse that perform a rotation of both the control ensemble and the target ensemble in the Bloch sphere according to Eq. 3.12. The fifth pulse couples the states $|r_0\rangle$ and $|0\rangle$ of the target ensemble. The sixth pulse couples

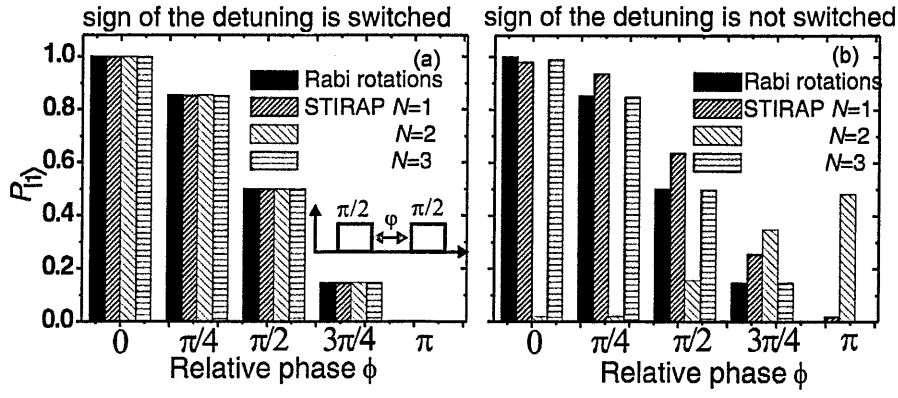

Figure 3.17: A Ramsey-sequence test of the STIRAP-based gate. The population of the qubit state $|1\rangle$ is plotted as a function of the phase difference ϕ between two $\pi/2$ rotations. The STIRAP-based gates are performed with (a) and without (b) switching the sign of the detuning between the STIRAP sequences. For comparison, the population is also plotted after an equivalent sequences of ideal (Rabi) rotations.

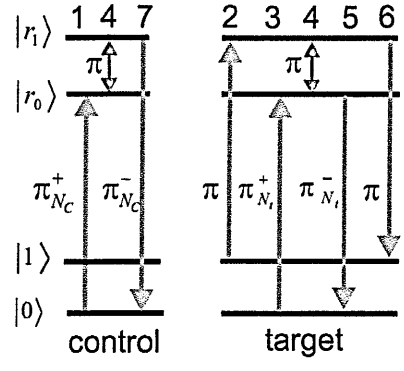

Figure 3.18: CNOT gate between mesoscopic qubits with N_c atoms in the control qubit and N_t atoms in the target qubit.

the states $|r_1\rangle$ and $|1\rangle$ of the target ensemble. The final pulse couples the states $|r_1\rangle$ and $|0\rangle$ of the control ensemble.

If the qubits are initially in the state $|\psi\rangle = a|\overline{00}\rangle + b|\overline{01}\rangle + c|\overline{10}\rangle + d|\overline{11}\rangle$,

the pulses 1 to 7 give the sequence of states:

$$|\psi_1\rangle = a|\overline{r}_0\overline{0}\rangle + b|\overline{r}_0\overline{1}\rangle + c|\overline{10}\rangle + d|\overline{11}\rangle \tag{3.18}$$

$$|\psi_2\rangle = a|\overline{r}_0\overline{0}\rangle + b|\overline{r}_0\overline{1}\rangle + c|\overline{10}\rangle + id|\overline{1}\overline{r}_1\rangle \tag{3.19}$$

$$|\psi_3\rangle = a|\overline{r}_0\overline{0}\rangle + b|\overline{r}_0\overline{1}\rangle + c|\overline{1}\overline{r}_0\rangle + id|\overline{1}\overline{r}_1\rangle \tag{3.20}$$

$$|\psi_4\rangle = ia|\overline{r}_1\overline{0}\rangle + ib|\overline{r}_1\overline{1}\rangle + ic|\overline{1}\overline{r}_1\rangle - d|\overline{1}\overline{r}_0\rangle \tag{3.21}$$

$$|\psi_5\rangle = ia|\overline{r}_1\overline{0}\rangle + ib|\overline{r}_1\overline{1}\rangle + ic|\overline{1}\overline{r}_0\rangle - d|\overline{10}\rangle \tag{3.22}$$

$$|\psi_6\rangle = ia|\overline{r}_1\overline{0}\rangle + ib|\overline{r}_1\overline{1}\rangle - c|\overline{11}\rangle - d|\overline{10}\rangle \tag{3.23}$$

$$|\psi_7\rangle = ia|\overline{00}\rangle + ib|\overline{01}\rangle - c|\overline{11}\rangle - d|\overline{10}\rangle \tag{3.24}$$

Thus, the gate performs the operation

$$U_{\mathrm{CNOT}} = \begin{pmatrix} i & 0 & 0 & 0 \\ 0 & i & 0 & 0 \\ 0 & 0 & 0 & -1 \\ 0 & 0 & -1 & 0 \end{pmatrix}, \tag{3.25}$$

which can be converted into a standard CNOT gate with a single-qubit rotation.

3.5 Comparing the Different Gates

In order to assess the relative merits of the different gates, it is useful to summarise their main characteristics side by side. This is done for the various single-qubit gates in Table 3.2 and for the two-qubit gates in Table 3.3. The key points are the following.

The timescale over which the gates operate should be as short as possible in order to reduce errors arising from spontaneous decay. In this respect, the original proposal based on ensembles [Lukin *et al.*, 2001] was a notable improvement on the original proposal for single-atoms [Jaksch *et al.*, 2000][1].

[1]This reduced operation time is due to the enhanced coupling of ensembles to light fields.

Gate	Timescale	Sensitive to N	Number of pulses	
			Identity	General
ARP	Several μs	No	2	5
STIRAP	Several μs	No	4	7

Table 3.2: Summary of the single-qubit gates. See Fig. 3.12 for the Identity gates and Fig. 3.16 for the general gates. Note that π_N for ARP consists of one pulse for ARP but two pulses for STIRAP.

Gate	Timescale	Individual Addressing	Sensitive to N	Number of pulses
Original single-atom				
Regime $B \ll \Omega$	$\approx 1\ \mu s$	No	Not	2
Regime $B \gg \Omega$	$\approx 1\ \mu s$	Yes	applicable	3
Original ensemble	$< 1\ \mu s$	Yes	Yes	3
EIT	$< 1\ \mu s$	Yes	No*	4
ARP	Several μs	Yes	No	7
STIRAP	Several μs	Yes	No	11

Table 3.3: Summary of the two-qubit gates. * = however, the control atom must be a single atom.

However, the original ensemble-based proposal had a significant weakness in its dependence on the (unknown) number of atoms, N.

The first gate to resolve the N-dependence issue was the EIT-based proposal of Müller *et al.* [2009]. Unfortunately, this came at the expense of having to work with the control qubit as a single atom and the target qubit as an ensemble, which considerably complicates the experimental procedure. Even though the logic gate of myself and colleagues [Beterov *et al.*, 2013] [Beterov *et al.*, 2014] resolves the N-dependence issue without this drawback, it operates over fairly long timescales and requires numerous pulses. Overall, the gate most appropriate for inclusion in a cold atom implementation of the DQC1 model is the EIT gate.

3.6 Summary

In this chapter, I introduced the physics of Rydberg atoms. I discussed the original proposals for Rydberg-based quantum logic gates and the further work they inspired. I then discussed a more recently conceived gate that involves Rydberg interactions and EIT. This gate is important for the work presented in this thesis because in Chapter 5, I present numerical simulations of its operation as part of the modelling of the proposed cold atom implementation of the DQC1 model.

I detailed the work of myself and colleagues [Beterov *et al.*, 2013] [Beterov *et al.*, 2014] which extended the prior work on deterministic excitation of ensembles [Beterov *et al.*, 2011]. We demonstrated that procedures based on adiabatic passage techniques can be used on ensembles to perform deterministic *de*-excitation. We showed such procedures operate with high fidelity for a wide range of atom-numbers.

Furthermore, we demonstrated a practical way to sequentially apply the excitation and de-excitation procedures so as to implement a high-fidelity Identity gate on a qubit encoded in an ensemble. We showed that the performance of this gate is insensitive to the number of atoms in the ensemble. Importantly, this means the gate can be used on randomly loaded ensembles that are far more easily prepared than uniformly loaded ensembles.

Building on our work [Beterov *et al.*, 2013] [Beterov *et al.*, 2014], we devised non-trivial single-qubit and two-qubit gates. We used numerical simulations to check that coherence is maintained throughout the operation and that they perform as intended.

Finally, I compared the strengths and weaknesses of the different Rydberg-based logic gates discussed in this chapter. They are all within reach of current experimental capabilities. The greatest advantage of the gates devised by myself and colleagues is the ease of their implementation. Our gates can operate on

randomly loaded ensembles, which avoids the considerable challenges of either loading the ensembles uniformly or loading some traps with single atoms and other traps with more than atom. Furthermore, work on ensembles is extremely timely because state-of-the-art experiments [Dudin & Kuzmich, 2012] [Dudin *et al.*, 2012] [Li *et al.*, 2013] have recently reached the regime required for logic gates to be performed between ensembles (i.e. the regime where the blockaded region is larger than the sample size). On balance, the EIT-based gate is the one that is most suitable for investigations of the DQC1 model.

Overall, the work presented in this chapter is of great relevance to the central topic of this thesis. As will be explained in the following two chapters, logic gates involving numerous atoms are the key to the cold atom implementation of the DQC1 model being of a vastly larger scale than implementations with other platforms.

3.

Chapter 4

Background: The DQC1 Model, Its Motivations and Protocols

The DQC1 model of quantum computation was conceived by [Knill & Laflamme, 1998]. In this chapter, I focus on a particular protocol that exemplifies this model. A generalisation of this protocol [Datta *et al.*, 2005] is then used to draw attention to a remarkable facet of the DQC1 model.

A key motivation for the study of the DQC1 model is that its theoretical analysis may help with elucidating exactly what it is about quantum physics that allows quantum computers to perform tasks more quickly than classical computers can. The goal of a community of physicists and computer scientists is to conceive a general theory explaining how the various, and often counter-intuitive, aspects of quantum physics lead to these "quantum speed-ups." Current theories typically involve quantitative measures of correlations and pay particular attention to correlations that are nonclassical in some way. I give an introduction to these measures of correlations and then proceed to discuss the roles of these correlation measures as resources for the DQC1 model.

The chapter ends with a survey of the protocols that have been devised within the DQC1 model.

4.1 The DQC1 Model

The DQC1 model was initially formulated by Knill and Laflamme [Knill & Laflamme, 1998]. DQC1 protocols involve only one pure qubit and an ensemble of mixed qubits. The DQC1 is not a universal model of quantum computation but nevertheless, some of the protocols have significant speed-ups compared to the best known classical algorithms. In particular, the DQC1 protocol for normalised trace estimation gives an exponential speed-up. A description of this algorithm is now given.

4.1.1 The DQC1 Protocol for Normalised Trace Estimation

The exemplary protocol in the DQC1 model is the protocol for the estimation of the normalised trace of a unitary matrix. For certain choices of unitaries, the DQC1 circuit can implement the Shor algorithm [Parker & Plenio, 2002]. For an appropriate choice of the unitary, the estimation of the normalised trace can be made equivalent to approximation of the Jones polynomial at the fifth root of unity [Shor & Jordan, 2008]. The Jones polynomial is a knot invariant so its approximation would be useful in knot theory. It would also be useful in statistical mechanics, in quantum field theory and in some formulations of quantum gravity.

Figure 4.1 describes the DQC1 algorithm.

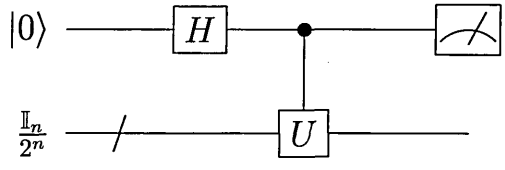

Figure 4.1: Circuit diagram for the DQC1 algorithm (where the slash through the lower horizontal line is conventional circuit diagram notation for indicating more than one qubit).

The input state consists of a single qubit, known as the special qubit, prepared in the state $|0\rangle\langle 0|$ and an ensemble of n qubits prepared in the maximally mixed state $\mathbb{I}_n/2^n$, where $\mathbb{I}_n$ is the identity matrix for n qubits. The initial state of the system is

$$\rho_1 = \tfrac{1}{2}\begin{pmatrix} 1 & 0 \\ 0 & 0 \end{pmatrix} \otimes \tfrac{1}{2^n}\mathbb{I}_n \tag{4.1}$$

$$= \tfrac{1}{2^{n+1}}\begin{pmatrix} \mathbb{I}_n & 0_n \\ 0_n & 0_n \end{pmatrix} \tag{4.2}$$

where 0_n is the n–by–n matrix with every matrix element equal to zero.

A Hadamard gate (introduced in section 2.1.2) is then performed on the special qubit, leaving the system in the state

$$\rho_2 = \frac{1}{2^{n+1}}\begin{pmatrix} \mathbb{I}_n & \mathbb{I}_n \\ \mathbb{I}_n & \mathbb{I}_n \end{pmatrix}. \tag{4.3}$$

A controlled unitary is performed on the n-qubit mixed state. This leaves the system in the state

$$\rho_3 = cU_n\ \rho_2\ cU_n^\dagger \tag{4.4}$$

$$= \frac{1}{2^{n+1}}\begin{pmatrix} \mathbb{I}_n & 0_n \\ 0_n & U_n \end{pmatrix}\begin{pmatrix} \mathbb{I}_n & \mathbb{I}_n \\ \mathbb{I}_n & \mathbb{I}_n \end{pmatrix}\begin{pmatrix} \mathbb{I}_n & 0_n \\ 0_n & U_n^\dagger \end{pmatrix} \tag{4.5}$$

$$= \frac{1}{2^{n+1}}\begin{pmatrix} \mathbb{I}_n & U_n^\dagger \\ U_n & \mathbb{I}_n \end{pmatrix} \tag{4.6}$$

where we have used the defining property of a unitary matrix, namely that a unitary multiplied by its complex conjugate is the identity (i.e. $U_n^\dagger U_n = U_n U_n^\dagger = \mathbb{I}_n$).

The ensemble of n qubits is no longer needed for the rest of the protocol.

We therefore calculate the reduced state of the special qubit to be

$$\rho_{\text{special}} = \frac{1}{2^{n+1}} \sum_{\{|i\rangle\}} \langle i| \begin{pmatrix} \mathbb{I}_n & U_n^\dagger \\ U_n & \mathbb{I}_n \end{pmatrix} |i\rangle \tag{4.7}$$

$$= \frac{1}{2} \begin{pmatrix} 1 & \frac{\text{Tr}[U_n^\dagger]}{2^n} \\ \frac{\text{Tr}[U_n]}{2^n} & 1 \end{pmatrix}, \tag{4.8}$$

where $\{|i\rangle\}$ is a complete basis set for the n ensemble atoms (e.g. $\{|0_1 0_2 ... 0_n\rangle$, $|0_1 0_2 ... 1_n\rangle$,...,$|1_1 1_2 ... 1_n\rangle\}$.

The protocol encodes the normalized trace of the unitary into one of the off-diagonal elements and the normalised trace of the conjugate of the unitary into the other off-diagonal element.

The real part of the normalised trace of the unitary U_n can be determined by finding of the expectation value of the Pauli X measurements of special qubit: $\langle X \rangle = \text{Tr}[\rho_{\text{special}} X] = \text{Re}[\text{Tr}(U_n)]/2^n$. The negative of the imaginary part of the normalised trace of the unitary can be determined by finding the expectation value of Pauli Y measurements of the special qubit: $\langle Y \rangle = \text{Tr}[\rho_{\text{special}} Y] = -\text{Im}[\text{Tr}(U_n)]/2^n$.

According to the central limit theorem, to estimate the expectation value of the real part of the normalised trace such that the probability, P_x, that the estimate is no more than ϵ_x away from the true value, one needs to repeat the experiment with Pauli X measurements $L \sim \ln(1/P_x)/\epsilon_x^2$ times. (An identical error analysis can be done for the Pauli Y measurements.) In other words, the number of repetitions is independent of the number of mixed qubits, n. The best known classical algorithms for determining the normalised trace of a 2^n-by-2^n unitary matrix scale exponentially with n. The DQC1 algorithm therefore provides an exponential speed-up compared to known classical algorithms. This exponential speed-up is remarkable because there is only one qubit of purity in the system implementing the protocol. This has been termed the 'power of one

qubit' [Datta *et al.*, 2005] [Datta *et al.*, 2008].

In Datta *et al.* [2005], the authors consider a generalisation of the DQC1 circuit where the special qubit is no longer completely pure. Instead, it has a polarisation, $0 \leq \alpha \leq 1$. When $\alpha = 1$, the special qubit is completely pure and when $\alpha = 0$, the special qubit is maximally mixed. Thus, α generalises the circuit to account for different levels of special qubit purity (see Figure 4.2).

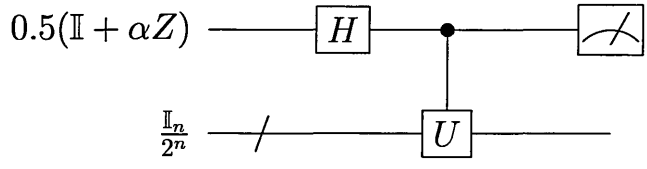

Figure 4.2: Generalised DQC1 circuit.

The reduced state of the special qubit just before the final measurement is now

$$\rho_{\text{special}} = \frac{1}{2}\begin{pmatrix} 1 & \frac{\alpha \text{Tr}[U_n^\dagger]}{2^n} \\ \frac{\alpha \text{Tr}[U_n]}{2^n} & 1 \end{pmatrix}. \tag{4.9}$$

The number of repetitions of the experiment for estimating the real part of the normalised trace is now

$$L \sim \frac{\ln(1/P_x)}{\alpha^2 \epsilon_x^2}. \tag{4.10}$$

This means that the DQC1 protocol retains its exponential speed-up over known classical algorithms for all non-zero α (i.e. for all systems with non-zero purity)[1]. This has been referred to as the 'power of the tiniest fraction of a qubit.' It is an important theoretical result because it sharpens the questions about the source of speed-ups in quantum devices [Datta & Shaji, 2011]. These questions shall be discussed further in the next section.

[1]In practical terms, reducing the purity of the special qubit reduces the contrast in the measurements, meaning that more have to be taken to achieve the same level of precision.

4.2 Motivation

The DQC1 model is one of a few computational models, including instantaneous computation [Bremner *et al.*, 2011] and boson sampling [Aaronson & Arkhipov, 2011], that have more computational power than is possible classically and yet are less powerful than universal models of quantum computation. Theoretical analysis of these 'intermediate' models may help with elucidating exactly what it is about quantum physics that allows quantum technologies to *potentially* outperform classical ones. Experimental implementation of these models is a highly exciting prospect because there has not yet been a clear, uncontroversial demonstration of a quantum computer *actually* outperforming its classical counterpart[1].

At present, no single feature of the quantum world has been identified as the source of the enhancement, efficiency and speed-ups of quantum technology [Vedral, 2010]. Initially, Deutsch [1985] argued that the source was size of the Hilbert space[2]. Steane [2003] argued against this, instead favouring entanglement as a more likely source.

Since these initial debates, a number of results have been made. For example, Poulin *et al.* [2011] found that most states in Hilbert space can only be produced after an exponentially long time. Despite the different results, the question of the source is still open[3].

It is within this context that intermediate models become particularly interesting for they provide a speed-up despite being limited to some extent. DQC1 provides an exponential speed-up despite having extremely limited purity and its analysis has shed light on the role of nonclassical correlations in quantum speed-ups.

[1]The company D-Wave Systems has made claims about manufacturing a quantum computer that can challenge classical computers for certain tasks but to date, limited evidence has been provided to support these claims.

[2]He framed his arguments in the many worlds interpretation of quantum mechanics.

[3]The list of possible sources includes nonclassical correlations, interference, distinguishability and contextuality. See Howard *et al.* [2014] for an important result on contextuality.

4.2.1 Nonclassical Correlations as a Resource

Nonclassical correlations have been an extremely important aspect of quantum mechanics since the 1930s when [Schrödinger, 1935] coined the term "entanglement" and the implications were debated by Einstein *et al.* [1935] and Bohr [1935]. It is now widely recognised as a key resource in quantum technology [Horodecki *et al.*, 2009].

One of the most rigorous demonstrations of the usefulness of entanglement comes from the paper of Jozsa & Linden [2003]. In this paper, the authors consider a quantum system in a pure state where entanglement can be present within a block of no more than p qubits but there is no entanglement between blocks. They show that for any quantum algorithm operating on such a system to exhibit an exponential speed-up compared to classical algorithms, p must grow as the problem size increases. Interestingly, some states are too entangled (as judged by the entanglement measure known as geometric entanglement) to be used as a computational resource [Gross *et al.*, 2009] [Bremner *et al.*, 2009][1].

Research into nonclassical correlations moved beyond the entanglement paradigm when it was recognised that unentangled states still have quantum features. The first step came in 2001 when quantum discord was defined as a measure of quantum correlations by Henderson & Vedral [2001] and, independently, by Ollivier & Zurek [2001]. For several years, it received relatively little attention until it was proposed in 2008 [Datta *et al.*, 2008] as a figure of merit for characterising the resources present in the DQC1 model of quantum computation. Since this seminal theoretical paper, a great deal of work was done to explore whether the non-classical correlations characterised by quantum discord could be harnessed in general QIP settings [Modi *et al.*,

[1]Some results in the same vein inlcude an early result known as the Gottesman-Knill theorem [Gottesman, 1998] [Gottesman, 1999] identified certain quantum circuits as ones that could be efficiently simulated on a classical computer. Mari & Eisert [2012] generalised this and showed that one can efficiently simulate quantum circuits in which the Wigner function, an indicator of non-classicality, is never negative at any stage. Van den Nest [2013] considered a pure-state quantum computer that is restricted to operate within a small environment around the state $|00...00>$ and showed that it has universal computational power.

2012][1].

Other measures of nonclassical correlations have also been proposed [Modi *et al.*, 2012]. The motivation for these further measures was that the calculation of quantum discord requires full knowledge of the state and an optimisation over all possible projective measures of a subsystem[2]. Out of these different measures, the ones most relevant to the DQC1 model (and therefore to this thesis) are geometric quantum discord, D_{G}, and entangling power[3], E_{p}. These shall be considered in the next section.

4.3 Resources in the DQC1 Model

In this section, the question of whether nonclassical correlations can act as a resource in DQC1 protocols is examined. I discuss entanglement and quantum discord in order to set the scene. I then discuss geometric discord and entangling power because these turn out to be experimentally accessible (even if they are not as paradigmatic as entanglement and quantum discord).

4.3.1 Entanglement

In Poulin *et al.* [2004], the authors show the special qubit is unentangled with the maximally mixed qubits for *any* controlled unitary. In other words, there is no entanglement across the bipartite split of the DQC1 circuit that is known as the "natural" split (see Figure 4.3(a)).

In Datta *et al.* [2005], the authors perform a more comprehensive analysis

[1]This question has received some encouraging preliminary answers [Gu *et al.*, 2012] [Madhok & Datta, 2013] [Dakic *et al.*, 2012a]. In particular, quantum discord has been identified as being a resource in the fully quantum Slepian-Wolf protocol [Abeyesinghe *et al.*, 2009] [Madhok & Datta, 2013], which is the parent protocol of all QIP protocols [Abeyesinghe *et al.*, 2009]. The interested reader can see section ?? of the appendix for further details.

[2]Even in the simple case of two qubits, a general closed form of the discord has not been found. Rather, to determine the discord of a two-qubit state, one has to numerically solve a set transcendental equations [Girolami & Adesso, 2011].

[3]Strictly speaking, entangling power is not actually a measure of correlations. Rather, it measures the ability of a unitary to generate correlations.

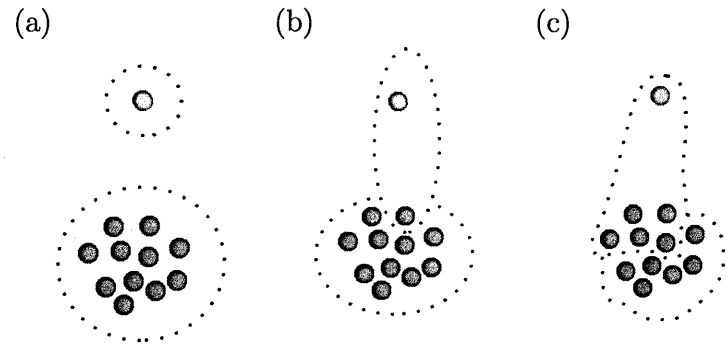

Figure 4.3: Possible bipartite splits in the DQC1 model. The red dot is the special qubit. The blue dots are the maximally mixed qubits. The dashed lines indicate how the qubits are split into two groups. (a) The natural split, where the special qubits is on one side of the split and the maximally mixed qubits are on the other side. (b) and (c) are unnatural splits, where the special qubit and one of the maximally mixed qubits are on one side of the split and all the other maximally mixed qubits are on the other side. In (b) the split is such that the smaller part only contains one maximally mixed qubit and the special qubit. In (c), the split is roughly half: each part contains half of the qubits when $n+1$ is even or just under and just over half of the qubits when $n+1$ is odd.

of the entanglement in the DQC1 model. They examine how the entanglement across the "unnatural" splits, shown in Figure 4.3(b) and (c), varies with the purity, α, of the control qubit. They use multiplicative negativity, $M(\rho)$, as their entanglement measure[1] and obtain the following results:

- The authors construct a family of unitaries such that for $\alpha > 1/2$, the DQC1 system is entangled for all unnatural bipartite divisions. However, for large and roughly equal bipartite divisions, this entanglement is a vanishingly small fraction of the maximum value that the negativity could take.

- They find that for typical unitaries, the DQC1 system has some entanglement across the unnatural splits.

- They show that for *all* unitaries and *all* bipartite divisions, $M(\rho)$ is

[1] A property of this measure that is useful for appreciating the significance of the results is that for a bipartite division where d is the dimension of the smaller part, $1 \leq M(\rho) \leq d$, where the upper bound holds for maximally entangled states.

upper-bounded by a function that is independent of the number, n, of maximally mixed qubits. For large and roughly equal bipartite divisions, the multiplicative negativity therefore becomes a vanishingly small fraction of the maximum possible value it could take.

In none of their work could they find entanglement for $\alpha \leq 1/2$.

Overall, these results suggest that the speed-up of the DQC1 algorithm is not due to the total amount of entanglement in the system. The authors speculate that it may be due to the distribution of entanglement.

4.3.2 Quantum Discord

In order to define quantum discord, consider: a system, S, with density matrix ρ_S; a system, A, with density matrix ρ_A; and the total system with density matrix $\rho_{S,A}$. The quantum discord is defined as the difference between two expressions for the mutual information. The first expression for mutual information of the system is:

$$I(\rho_S : \rho_A) = \mathcal{H}(\rho_S) + \mathcal{H}(\rho_A) - \mathcal{H}(\rho_{S,A}), \tag{4.11}$$

where $\mathcal{H}(\rho)$ is the von Neumann entropy. It is defined as

$$\mathcal{H}(\rho) = \sum_i -\lambda_i \log(\lambda_i), \tag{4.12}$$

where the λ_i are the eigenvalues of ρ and the base of the logarithm is two because this is the convention in information theory.

The second expression for mutual information of the system is with respect to a complete set of projective measurements on A. The complete set is denoted $\{\prod_j^A\}$, where j distinguishes the different outcomes of the measurements. The projective measurement $\prod_j^A$ leaves S in the state $\rho_{S|\prod_j^A}$. The second expression

for the mutual information is:

$$J(S:A)_{\{\prod_j^A\}} = \mathcal{H}(\rho_S) - \mathcal{H}(\rho_{S|\{\prod_j^A\}}), \tag{4.13}$$

where $\mathcal{H}(\rho_{S|\{\prod_j^A\}})$ is the conditional entropy on S given the complete set of projective measurements. It is given by von Neumann information of all the post-measurement states of S weighted by their probabilities, p_j. That is:

$$\mathcal{H}(\rho_{S|\{\prod_j^A\}}) = \sum_j p_j \mathcal{H}(\rho_{S|\prod_j^A}). \tag{4.14}$$

The quantum discord, as defined by Ollivier & Zurek [2001], is the difference between I and J. That is:

$$\delta(S:A)^{O\&Z}_{\{\prod_j^A\}} = I(S:A) - J(S:A)_{\{\prod_j^A\}} \tag{4.15}$$

$$= \mathcal{H}(\rho_A) - \mathcal{H}(\rho_{S,A}) + \mathcal{H}(\rho_{S|\{\prod_j^A\}}). \tag{4.16}$$

This definition depends on both the joint state $\rho_{S,A}$ and on the projectors $\{\prod_j^A\}$. In the definition of discord given by Henderson & Vedral [2001], one minimises the above definition of discord over the projectors and thus arrives at a measure of correlations that is solely dependent on the joint state. Due to the benefits of a measure that depends solely on the joint state, the definition of Henderson & Vedral [2001] is usually assumed unless stated otherwise. Hence, we arrive at:

$$\delta(S:A) = \min_{\{\prod_j^A\}} I(S:A) - J(S:A)_{\{\prod_j^A\}} \tag{4.17}$$

$$= \min_{\{\prod_j^A\}} \mathcal{H}(\rho_A) - \mathcal{H}(\rho_{S,A}) + \mathcal{H}(\rho_{S|\{\prod_j^A\}}). \tag{4.18}$$

With quantum discord defined, we now consider some its properties [Modi *et al.*, 2012]. These include:

- Discord is non-negative. That is, $\delta(S:A) \geq 0$.

- Discord vanishes if and only if one or both of the subsystems is a classical system.

- Discord is generally not symmetric. That is, $\delta(S:A) \neq \delta(A:S)$. This is because conditional entropy is generally not symmetric.

- Discord is invariant under local unitary transformations. That is, it is the same for $\rho_{S,A}$ and for $(U_S \bigotimes U_A)\rho_{S,A}(U_S \bigotimes U_A)^\dagger$, where U_S is a unitary that acts on system S and U_A is a unitary that acts on system A.

In Datta *et al.* [2008], a theoretical analysis of the DQC1 circuit found that for typical unitaries, the circuit generates quantum discord across the natural bipartite split (Figure 4.3). This was an important result since it was the first signature of nonclassical correlations in the DQC1 circuit for $\alpha \leq 1/2$.

4.3.3 Geometric Discord

Geometric discord was conceived by Dakić *et al.* [2010][1]. It was defined in terms of the Hilbert-Schmidt distance. However, using an equivalent definition of geometric discord found by Luo & Fu [2010], Passante *et al.* [2012] worked out how to experimentally measure geometric discord in the output of the DQC1 circuit. They found that

$$D_{\mathrm{G}}(\rho_{\mathrm{DQC1}}) = \frac{\alpha^2}{4}\frac{1}{2^n}(1-\tau_2), \tag{4.19}$$

where $\tau_2 = \frac{1}{2^n}|\mathrm{Tr}\,[U^2]\,|$. Importantly, the value of τ_2 can simply be obtained from the expectation value of measurements on the control qubit when the controlled unitary is applied twice in succession. In Chapter 5 on the cold atom implementation of DQC1 circuits, I use this result to numerically investigate

[1]For a definition of geometric discord and a brief discussion about some of the issues surrounding it, see section 8.4 of the appendix.

how geometric discord varies throughout the protocol for normalised trace estimation.

Geometric discord was not found to play an important role in the DQC1 circuit [Passante *et al.*, 2012] because its maximum value ($= \frac{\alpha^2}{4}\frac{1}{2^n}$) exponentially decreases with n. However, in Tufarelli *et al.* [2013], an "adjusted" version of quantum discord was defined as the geometric discord rescaled by the purity of the system:

$$D_{\mathrm{G}}^{A} = \frac{D_{\mathrm{G}}}{\mathrm{Tr}\left[\rho^2\right]}. \tag{4.20}$$

The purity in the DQC1 model is:

$$\mathrm{Tr}\left[\rho_{\mathrm{DQC1}}^2\right] = \frac{1}{2^{(n+1)}}(1+\alpha^2). \tag{4.21}$$

Hence, one arrives at

$$D_{\mathrm{G}}^{A} = \frac{1}{2(1+\alpha^2)}(1-\tau_2). \tag{4.22}$$

As can be seen, this measure does not become negligible at large n. Importantly, this leaves open the possibility that it plays the role of a resource in the DQC1 model.

4.3.4 Entangling Power

The entangling power, $E_{\mathrm{p}}(U)$, of a unitary operator, U, acting on a bipartite system was initially defined in Zanardi *et al.* [2000] as

$$E_{\mathrm{p}}(U) = \Sigma_{i,j} p(|\psi_{(i)}\rangle_1, |\psi_{(j)}\rangle_2) M\left[U(|\psi_{(i)}\rangle_1 \otimes |\psi_{(j)}\rangle_2)\right] \tag{4.23}$$

where $|\psi\rangle_1$ is a pure state of subsystem 1, $|\psi\rangle_2$ is a pure state of subsystem 2, $p(|\psi\rangle_1, |\psi\rangle_2)$ is a probability distribution over the manifold of product states

and M is an entanglement measure.

The entangling power of the DQC1 circuit was investigated by Yu *et al.* [2013], who found that it can be given by

$$E_{\mathrm{p}} = \alpha\sqrt{1-\tau_2}, \tag{4.24}$$

where (using the same notation as Passante *et al.* [2012]) $\tau_2 = \frac{1}{2^n}|\mathrm{Tr}\left[U^2\right]|$. As discussed in section 4.3.3, this can simply be obtained from the expectation value of measurements on the control qubit when the controlled unitary is applied twice in succession. In Chapter 5, I use this result to numerically investigate how the entangling power varies throughout a cold atom implementation of the protocol for normalised trace estimation.

Yu *et al.* [2013] also find an interpretation for the entangling power of a unitary in the DQC1 protocol. They do this by analysing the protocol not in terms of absolute errors (as in section 4.1.1) but in terms of relative errors. Hence, for a constant relative error, as the normalised trace decreases, the number of repetitions required increases, as does the entangling power.

4.4 Protocols

I finish this chapter by mentioning protocols in the DQC1 model besides the one for normalised trace estimation. These protocols are related to a wide variety of topics: chaos [Poulin *et al.*, 2003] [Poulin *et al.*, 2004]; the differences between quantum states [Yu *et al.*, 2012]; metrology [Modi *et al.*, 2011], thermodyanics [Dorner *et al.*, 2013] [Mazzola *et al.*, 2013]; macrorealism [Souza *et al.*, 2011]; and contextuality [Moussa *et al.*, 2010]. Where possible, I attempt to provide some information about how cold atoms or, more specifically, Rydberg atoms could be relevant to these topics. Detailed consideration of Rydberg-based implementations of these protocols is left for future work.

4.4.1 Chaos

There are two protocols in the DQC1 model that are related to quantum chaos[1]. The first of these, by Poulin *et al.* [2003], determines exhibits whether a system exhibits chaotic or regular motion[2]. The second protocol [Poulin *et al.*, 2004] investigates how sensitive the system is to evolution under different unitaries. High sensitivity is indicative of a chaotic system and low sensitivity is indicative of a regular system.

4.4.2 Overlap

The overlap of two density matrices, ρ_1 and ρ_2, is defined as $\mathrm{Tr}[\rho_1\rho_2]$. This parameter is of interest for several reasons [Filip, 2002] [Brennen, 2003] [Alicki *et al.*, 2008]. Filip [2002] conceived a DQC1 protocol to measure the overlap of two systems[3]. The protocol employs a controlled SWAP gate and so could be implemented with cold atoms using a Rydberg-based controlled SWAP operation [Huai-Zhi *et al.*, 2012].

Yu *et al.* [2012] consider the correlations that arise during the protocol. Interestingly, they show that there are no quantum correlations between the control qubit and the two other quantum systems that aren't captured by entanglement.

4.4.3 Metrology

Cold atoms have been widely used for implementing interferometers [Torii *et al.*, 2000] [Roos *et al.*, 2006], gyroscopes [Cooper *et al.*, 2010], quantum clocks [Swallows *et al.*, 2011] [Martin *et al.*, 2013] [André *et al.*, 2004], magnetic field

[1]The relationship between Rydberg physics and quantum chaos was outlined in section 3.1.3.

[2]The authors discuss their protocol using the example of a kicked top, which is a very relevant example because kicked Rydberg atoms have been studied experimentally. Furthermore, a recent theory paper has explored the relationship between quantum discord and chaos in a quantum kicked top [Madhok *et al.*, 2013].

[3]Ekert *et al.* [2002] independently presented the same protocol. They showed that it can be used to directly estimate both linear and nonlinear functionals of any density operator.

detectors [Simmons *et al.*, 2010] [Ng, 2013] [Wasilewski *et al.*, 2010] [Zhou *et al.*, 2010] and micro-gravity sensors [Zhou *et al.*, 2012] [Müntinga *et al.*, 2013]. The sensitivity of Rydberg atoms to external fields was described in section 3.1.2. The relationship between Rydberg physics and metrology was outlined in section 3.1.3.

The DQC1 protocol can be adapted to perform quantum metrology. Four such schemes were presented and analysed in Modi *et al.* [2011]. The analysis provided evidence that in the case of metrology, a quantum advantage can be attained even with states of low purity and that quantum discord may be responsible for this quantum advantage.

4.4.4 Thermodynamics

Dorner *et al.* [2013] propose an experiment to measure the work done in a nonequilibrium process (e.g. the process of the motional state of a trapped ion being altered by a change in the trapping potential)[1]. In short, the special qubit is used to probe the ensemble (i.e. the system of interest), which is initially in a prepared in a state of thermal equilibrium rather than the maximally mixed state.

4.4.5 Quantum Foundations

Quantum mechanics has a number of rather perplexing features. One such feature, made famous by the Schrödinger cat paradox [Schrödinger, 1935], is that it is not macrorealistic. In Souza *et al.* [2011], a DQC1 protocol is devised to test macrorealism.

Souza *et al.* [2011] implemented their protocol in a liquid-state NMR system. Because the protocol does not require the qubits in the ensemble to be individually addressed, one can straightforwardly envisage an equivalent

[1] A similar proposal was also conceived by Mazzola *et al.* [2013].

experiment being performed in a Rydberg DQC1 system. The use of Rydberg atoms may overcome some of the limitations (e.g. low detection efficiency) of the NMR experiment expressed in Knee *et al.* [2012].

Another feature of quantum mechanics is that it is contextual - the outcome of a quantum measurement cannot be understood as revealing the pre-existing definite value of some underlying "hidden variable." Moussa *et al.* [2010] propose a DQC1 protocol to test the violation of an inequality related to contextuality. The details of the protocol appear not to present any challenges to Rydberg-based implementation.

4.5 Summary

In this chapter, I have given a detailed introduction to the DQC1 model. I focussed on the DQC1 protocol for normalised trace estimation as it captures the essence of the model.

I then motivated the investigation of the DQC1 model. I did this by reference to cutting-edge research on nonclassical correlations and quantum speed-ups. I introduced the paradigmatic measures of correlations, entanglement and quantum discord, and discussed their roles in the DQC1 model. I also discussed two parameters related to correlations (namely, geometric discord and entangling power) and how they can be determined experimentally. Furthermore, I mentioned that in the work presented in Chapter 5, these parameters are investigated in numerical simulations of the proposed cold atom implementation.

Finally, I presented the wide variety of protocols within the DQC1 because they are possible avenues for future work.

Chapter 5

Cold Atom Realisation of the DQC1 Model

In this chapter, I detail the core of my work, namely a thorough proposal for an experimentally feasible implementation of the DQC1 model in a cold atom set-up. I benchmark the performance of the proposed implementation by numerically simulating the normalised trace estimation protocol for different numbers of atoms in the ensemble when they are all acted upon identically. Importantly, I describe how a cold atom implementation of this DQC1 protocol can be employed to investigate unitaries that are *non*-trivial[1].

I begin this chapter by giving an overview of the proposed DQC1 implementation based on cold atoms. I give a detailed description of the stages of the cold atom implementation of the DQC1 model: loading and initialising the atoms; performing the controlled unitary; and finally, reading out the result. For simplicity, I focus on the case where a trivial unitary is implemented, referring the reader to later in the chapter, where I discuss how such a trivial unitary can be useful for benchmarking the implementation.

I then discuss the modelling of the proposed cold atom implementation.

[1]Unitaries that describe strong, many-body, correlated (e.g. frustrated) interactions are typically non-trivial. The properties of such unitaries of considerable interest to a wide range of researchers [Amico *et al.*, 2008] [Bloch *et al.*, 2008].

The results of the modelling include estimates of the real and imaginary parts of the normalised trace as well as some measures of nonclassical correlations.

The subsequent sections of the chapter are devoted to dealing with various subtleties and issues involved with the Rydberg implementation. The first of these issues is the fluctuations in the number of atoms loaded into the traps. The second issue is a question about what unitaries can conceivably be investigated with ensemble of Rydberg atoms when there is no individual addressing.

Finally, I give a short description of the implementations of DQC1 protocols that have been achieved with other physical set-ups. I then emphasise that the proposed implementation with cold atoms constitutes a significant improvement on prior work because it allows vastly larger unitary matrices[1] to be investigated. Indeed, they are so large that brute force methods of finding their normalised trace (i.e. adding up their diagonal elements and dividing by the number of elements) would be classically intractable.

5.1 Overview of the Cold Atom Implementation

The physical set-up for the proposed cold atom implementation is as follows. There are two micrometre-sized optical dipole traps separated by a few micrometres. This separation is large enough that each trap can be individually optically addressed [Bergamini *et al.*, 2004] and small enough that there can be Rydberg blockade between the traps. One trap contains the system representing the special qubit and the other trap contains the system representing the ensemble. This is shown in Figure 5.1.

[1]The vast size of the unitary matrices stems from the large number of atoms in the ensemble and the use of strong, controllable, long-range Rydberg interactions to manipulate them unitarily. Recall that the size of a unitary matrix scales exponentially with the number of subsystems (e.g. qubits) taking part in the unitary process.

The special qubit can be represented by either a single atom or by an ensemble of atoms[1]. For clarity, I will refer to the special qubit as being encoded in a single atom but it is straightforward to use collective encoding instead. The ensemble of n qubits is represented by an ensemble of n atoms.

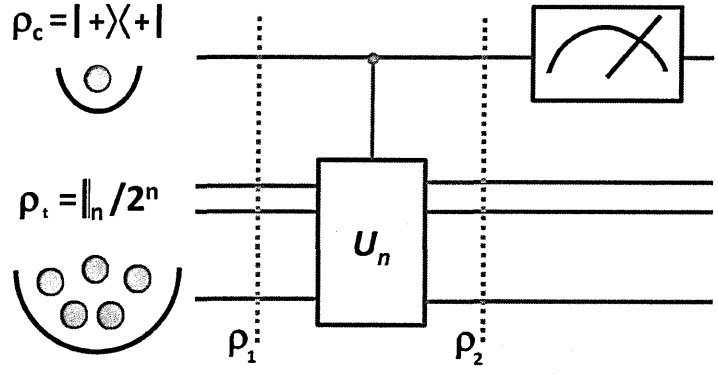

Figure 5.1: The roles of the trapped atoms as qubits. The special qubit is encoded in a single atom and the maximally mixed qubits are encoded in the ensemble of atoms.

For ^{87}Rb atoms, the qubits can be encoded in the two ground state hyperfine levels. For the single atom, these states are denoted by $|0\rangle_c$ and $|1\rangle_c$ and for the ensemble atoms, they are denoted by $|0\rangle_t$ and $|1\rangle_t$ (see Figure 5.2). The subscripts are dropped for conciseness where clarity allows.

For the initialisation stage of the protocol, the single atom is prepared in a pure state $\rho_c = |+\rangle\langle+|$, where $|+\rangle = (|0\rangle + |1\rangle)/\sqrt{2}$, whilst the n ensemble atoms are prepared in the maximally mixed state $\rho_t = \mathbb{I}_n/2^n$. For the processing stage, shown in Figure 5.2, the controlled unitary is implemented using the laser excitation scheme of Müller *et al.* [2009] based on Rydberg-Rydberg interaction and EIT (see section 3.3.2). The state of the special atom can be read out at the end of the protocol using florescence imaging (see Chapter 6).

The proposed physical implementation requires some modifications to the general, abstract analysis presented in Chapter 4. This is because the implementation requires states outside of the computational basis states (i.e. it

[1]An ensemble of atoms can be made to represent a qubit and undergo logic operations using the techniques based on strong interactions that were proposed by myself and colleagues Beterov *et al.* [2013] [Beterov *et al.*, 2014].

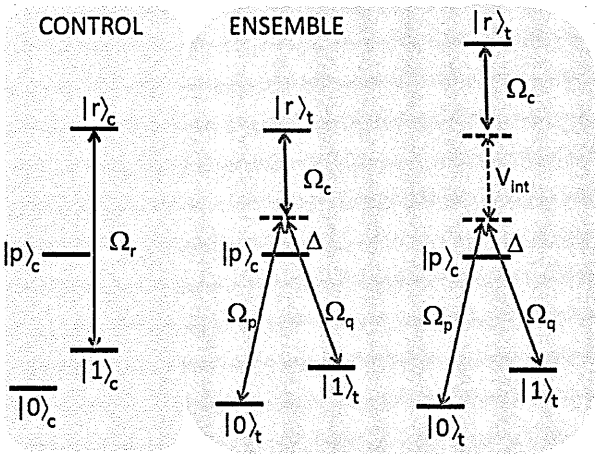

Figure 5.2: The scheme of Müller *et al.* [2009] that implements controlled off-resonant Raman rotation. The special qubit is encoded in the states $|0\rangle_c$ and $|1\rangle_c$ of a single atom. State $|1\rangle_c$ is coupled to a Rydberg state via Ω_r (left). Each of the n qubits in the ensemble is encoded in the states $|0\rangle_t$ and $|1\rangle_t$ which are coupled by a two-photon scheme. A beam coupling the intermediate state to the Rydberg state is added so that the EIT condition is fulfilled and the interaction with Ω_p and Ω_q is inhibited (centre). However the coupling of the special atom to Rydberg state can activate an additional shift that removes the condition for EIT, so that off-resonant Raman transfer is activated (right).

requires not only the two hyperfine ground states that encode $|0\rangle$ and $|1\rangle$ but also the intermediate and Rydberg states, $|p\rangle$ and $|r\rangle$, respectively, that are used to perform the logic operations). Hence, I now run through the protocol for one four-level control atom and one four-level target atom. I use the basis $(|0\rangle_c, |1\rangle_c, |p\rangle_c, |r\rangle_c) \otimes (|0\rangle_t, |1\rangle_t, |p\rangle_t, |r\rangle_t)$, where the subscripts c and t indicate the control atom and target atom respectively (see Figure 5.2).

The initial state of the system can be written in block form as

$$\rho_1 = \frac{1}{4}\begin{pmatrix} 1 & 1 & 0 & 0 \\ 1 & 1 & 0 & 0 \\ 0 & 0 & 0 & 0 \\ 0 & 0 & 0 & 0 \end{pmatrix} \otimes \begin{pmatrix} \mathbb{I}_2 & 0_2 \\ 0_2 & 0_2 \end{pmatrix}. \tag{5.1}$$

Note that there is no population in the $|p\rangle$ or $|r\rangle$ states of either atom. The controlled unitary, denoted cU, can be written as

$$cU = \begin{pmatrix} \mathbb{I}_4 & 0_4 & 0_4 & 0_4 \\ 0_4 & U & 0_4 & 0_4 \\ 0_4 & 0_4 & \mathbb{I}_4 & 0_4 \\ 0_4 & 0_4 & 0_4 & \mathbb{I}_4 \end{pmatrix}, \tag{5.2}$$

where the unitary itself can be written as

$$U = \begin{pmatrix} U_{\mathrm{TL}} & U_{\mathrm{TR}} \\ U_{\mathrm{BL}} & U_{\mathrm{BR}} \end{pmatrix}, \tag{5.3}$$

with the subscripts indicating the top left, top right, bottom left and bottom right (2-by-2) quarters of the matrix, U.

The controlled unitary leaves the system in the state

$$\rho_2 = cU\ \rho_1\ cU^\dagger \tag{5.4}$$

$$= \frac{1}{4}\begin{pmatrix} \mathbb{I}_2 & 0_2 & (U^\dagger)_{\mathrm{TL}} & (U^\dagger)_{\mathrm{TR}} & 0_2 & 0_2 & 0_2 & 0_2 \\ 0_2 & 0_2 & 0_2 & 0_2 & 0_2 & 0_2 & 0_2 & 0_2 \\ U_{\mathrm{TL}} & 0_2 & U_{\mathrm{TL}}(U^\dagger)_{\mathrm{TL}} & U_{\mathrm{TL}}(U^\dagger)_{\mathrm{TR}} & 0_2 & 0_2 & 0_2 & 0_2 \\ U_{\mathrm{BL}} & 0_2 & U_{\mathrm{BL}}(U^\dagger)_{\mathrm{TL}} & U_{\mathrm{BL}}(U^\dagger)_{\mathrm{TR}} & 0_2 & 0_2 & 0_2 & 0_2 \\ 0_2 & 0_2 & 0_2 & 0_2 & 0_2 & 0_2 & 0_2 & 0_2 \\ 0_2 & 0_2 & 0_2 & 0_2 & 0_2 & 0_2 & 0_2 & 0_2 \\ 0_2 & 0_2 & 0_2 & 0_2 & 0_2 & 0_2 & 0_2 & 0_2 \\ 0_2 & 0_2 & 0_2 & 0_2 & 0_2 & 0_2 & 0_2 & 0_2 \end{pmatrix}, \tag{5.5}$$

where $(U^\dagger)_{\mathrm{TL}}$, $(U^\dagger)_{\mathrm{TR}}$, $(U^\dagger)_{\mathrm{BL}}$ and $(U^\dagger)_{\mathrm{BR}}$ are, respectively, the top left, top right, bottom left and bottom right quarters of the unitary, $U^\dagger$.

The reduced state of the special qubit is

$$\rho_{\mathrm{special}} = \frac{1}{4}\begin{pmatrix} 2 & \mathrm{Tr}[(U^\dagger)_{\mathrm{TL}}] & 0 & 0 \\ \mathrm{Tr}[U_{\mathrm{TL}}] & \mathrm{Tr}[U_{\mathrm{TL}}(U^\dagger)_{\mathrm{TL}}] + \mathrm{Tr}[U_{\mathrm{BL}}(U^\dagger)_{\mathrm{TR}}] & 0 & 0 \\ 0 & 0 & 0 & 0 \\ 0 & 0 & 0 & 0 \end{pmatrix}. \tag{5.6}$$

One can see by inspection that the protocol works in the same way as explained in section 4.1.1 with the exception that when measurements of the special qubit are made in the Pauli-X and Pauli-Y bases, it is only the top left quarter of the unitary which has its normalised trace estimated[1]. The physical implementation of the protocol is therefore essentially the same as the abstract specification. However, being aware that it is only the top left quarter of the unitary which has its normalised trace estimated is crucial to interpreting the

[1]It is interesting to note that $U_{\mathrm{TL}}U_{\mathrm{TL}}^\dagger$ does not, in general, equal the identity. According to Dita [1982], one can parameterise the top left quarter of a 4-by-4 unitary matrix by 14 real parameters, whilst a 2-by-2 unitary matrix is parameterised by 4 parameters. Thus, the presence of states outside the computational basis states could add some flexibility to the protocol.

output of the protocol.

5.2 Stages of the Cold Atom Implementation

I now consider the stages of the cold atom implementation in more detail.

5.2.1 Loading and Initialisation

Both the special atom and the ensemble atoms are randomly loaded in small dipole traps [Bergamini *et al.*, 2004]. The trap for the special atom can be loaded with an 80% probability [Grünzweig *et al.*, 2010]. It is possible to conditionally start the experiment once the special atom is loaded.

The ensemble is typically loaded with a Poisson-distributed number of atoms around an average value $\overline{n}$. At small n, we can get the number of atoms in the trap to be exactly n for every run of the experiment by post-selection. This is reasonable at small n but at high n, the total number of runs required to get enough post-selected data would be infeasibly high.

Nevertheless, we find that experiments with high n and no post-selection can be useful for benchmarking the protocol. The basic idea is that: the average atom-number, $\overline{n}$, can be tuned by varying parameters such as the trap depth and the density of the reservoir; and for each value of $\overline{n}$, it is possible to compare whether the output of the (non-post-selected) protocol agrees with our theoretical predictions that are discussed in greater depth in section 5.3.

Once the ensemble is successfully loaded, it can be prepared in the maximally-mixed state by implementing a scheme inspired by Barreiro *et al.* [2010] for controlled decoherence in a trapped ion experiment. This scheme, adapted to cold Rubidium-87 atoms, consists of the following three steps.

- One can optically pump the atoms into the $5S_{1/2}F = 2, m_F = 2$ state using circularly polarised light. This is shown in Figure 5.3(a). Typical

fidelities for optical pumping are around 0.9999 (see Masterson *et al.* [1993] and section III A of Saffman & Walker [2005a]).

- One could perform an off-resonant Raman transition to create an equally weighted superposition of the $5S_{1/2}F = 2, m_F = 2$ state and the $5S_{1/2}F = 1, m_F = 1$ state. This is shown in Figure 5.3(b). This can also be done with similarly high fidelity [Saffman & Walker, 2005a].

- The final step in the preparation of the maximally mixed state is to destroy the phase coherence of the equally weighted superposition. This can be done by optically pumping the $5S_{1/2}F = 2, m_F = 2$ state with circularly polarised light into the $5P_{3/2}F = 3, m_F = 3$ state. This state spontaneously decays only to the $5S_{1/2}F = 2, m_F = 2$ state, destroying the phase coherence and thus turning the coherent superposition into a statistical mixture. This is shown in Figure 5.3(c).

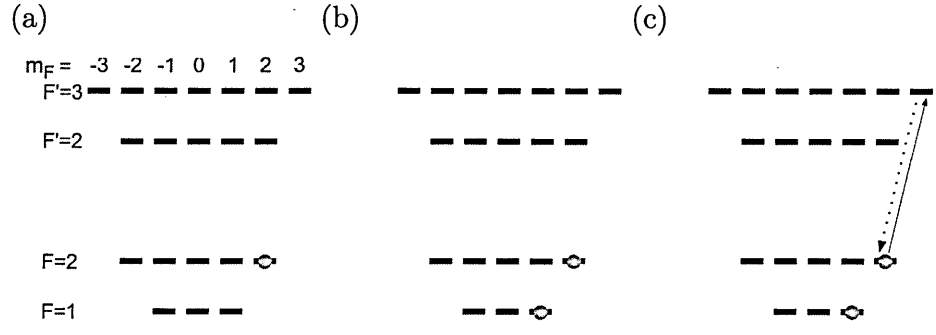

Figure 5.3: Scheme for preparing the maximally mixed state with Rubidium-87 atoms. See the main text for full details. (a) The atoms are optically pumped into one state. (b) An off-resonant Raman transition is used to create an equal superposition of two states. (c) Finally, optical pumping is used to destroy phase coherence and thus convert the equal superposition into the maximally mixed state.

Once the special atom successfully loaded, it can be prepared in the superposition state $|+\rangle = (|5S_{1/2}F = 1, m_F = 1\rangle + |5S_{1/2}F = 2, m_F = 2\rangle)/\sqrt{2}$ by following the scheme for preparing the maximally mixed state but leaving out the third step step where optical pumping is used to destroy the coherence. That is, one optically pumps the atom into the $5S_{1/2}F = 2, m_F = 2$ state using

circularly polarised light and then performs a high-fidelity off-resonant Raman rotation.

In the most general form of the DQC1 protocol for normalised trace estimation, the special atom is no longer completely pure (i.e. it has a polarization $\alpha < 1$). This can be achieved by modifying the second step of the preparation scheme so that the superposition state is *un*equally weighted.

One practical consideration is that an ideal maximally mixed state of n qubits, $\mathbb{I}/2^n$, will not be created but rather a state of the form

$$\rho = (1-\epsilon)\frac{\mathbb{I}}{2^n} + \epsilon\rho_a,$$

where ρ_a is any density matrix and ϵ is as small as practically possible. The imperfect preparation of the maximally mixed state is important because it affects whether nonclassical correlations other than entanglement can be investigated in the presence or in the absence of entanglement. The latter possibility would facilitate the interpretation of the results.

For $\epsilon < 2/4^n$ [Braunstein *et al.*, 1999], the mixed state is separable. Otherwise, there may be some entanglement. Hence, as n increases, the separability condition on ϵ gets more challenging to achieve. For a test of the role of discord in the DQC1 model with no entanglement in the ensemble and a preparation fidelity of $1-\epsilon = 1-10^{-3}$, the maximum value of n would be 5. Nevertheless, investigations of nonclassical correlations without entanglement in the high n regime can be made possible by reducing the purity α of the special qubit below 0.5. This is because for any value of n, when $\alpha \leq 0.5$, there is no entanglement [Datta *et al.*, 2005].

5.2.2 Processing: a Trivial Unitary

In the processing stage, a unitary is performed in a controlled manner. This unitary is clearly central to the protocol. I initially consider the case where

each of the n atoms in the ensemble experiences the same Hamiltonian and therefore evolves under the same unitary. To make this mathematically precise, note that the Kronecker sum obeys the property

$$e^{A\oplus B} \equiv e^A \otimes e^B. \tag{5.7}$$

From this, one can clearly see the following. If each of the n atoms in the ensemble experiences the Hamiltonian, $\mathcal{H}_1$, and evolves under the unitary, $U_1 = e^{-i\mathcal{H}_1 t}$, then the total Hamiltonian on the n ensemble atoms is $\mathcal{H}_n = \mathcal{H}_1^{\oplus n}$ and total unitary is $U_n = e^{-i\mathcal{H}_n t} = (e^{-i\mathcal{H}_1 t})^{\otimes n} = U_1^{\otimes n}$. That is, the total unitary is a tensor product of the single atom unitary. Hence, $\mathrm{Tr}[U_1^{\otimes n}] = (\mathrm{Tr}[U_1])^n$, which means that the calculation is not only classically tractable but also trivial. It is also trivial for the Rydberg implementation where only the top left quarter of the unitary has its normalised trace estimated because

$$\mathrm{Tr}_{\text{top left}}[U_n] = (\mathrm{Tr}_{\text{top left}}[U_1])(\mathrm{Tr}[U_1])^{n-1}. \tag{5.8}$$

Crucially for the importance of this work, I explain in section 5.5.2 how non-trivial unitaries can be investigated.

The physical implementation of the controlled unitary relies on the scheme of Müller *et al.* [2009]. There it was shown that Rydberg interactions, EIT and Raman transitions can be combined in such a way as to perform a CNOT gate between a single atom and an ensemble of atoms. The maximum number of atoms in the ensemble is simply the number that can be trapped within the blockade region. Since the blockade radius can be as large as several micrometres, several hundred atoms could undergo the controlled unitary.

The scheme of Müller *et al.* [2009] implements the CNOT gate by employing two Raman beams with Rabi frequencies of the same amplitude and no relative phase. The scheme can be adapted to employ a controlled rotation about the

x-axis of the Bloch sphere by simply choosing the pulse area (of the Raman beams) to give the desired rotation angle. Since Raman transitions can be used to perform arbitrary rotations in the Bloch sphere [Caillet & Simon, 2007], the controlled unitary in the processing stage of the DQC1 protocol can be yet further generalised to implement controlled arbitrary rotations. By varying the relative amplitudes and phases of the two Raman beams, the same controlled rotation can be applied to all the ensemble atoms (i.e. all the ensemble atoms can be rotated by the same angle about the same axis). Let the Raman beams have Rabi frequencies, Ω_1 and $\Omega_2 e^{i\alpha}$, where α is the relative phase. The axis of rotation in the Bloch sphere is (n_x, n_y, n_z) where:

$$n_x = \cos(\alpha)\sin(2\beta) \tag{5.9}$$

$$n_y = -\sin(\alpha)\sin(2\beta) \tag{5.10}$$

$$n_z = \cos(2\beta), \tag{5.11}$$

where $\beta = \arctan(\Omega_2/\Omega_1)$ and the rotation angle is given by the pulse area. Hence, by choosing α and β, it is possible for U_1 to be any single-qubit rotation.

To test that the desired controlled unitary is being applied appropriately and with high fidelity, one would construct a truth table for the operation by experimentally applying it to the atoms when they are in pure states.

I performed simulations of this scheme by numerically solving the time-dependent Schrödinger equation for a 4-level atomic system in the presence of finite Rydberg blockade and taking into account decay from the intermediate state (see section 5.4 for further details). I found that, for high fidelity operation, the following conditions have to be fulfilled:

(i) The Raman detuning Δ has to be much larger than the decay rate, Γ_p, of the intermediate state (which is approximately $2\pi \times 6$ MHz) so as to make sure that spontaneous decay is highly suppressed.

(ii) The lifetime of the Rydberg state, Γ_r^{-1}, chosen for the special atom has to be much larger than the operation time of the controlled Raman transition.

(iii) $\Omega_c \gg \Omega_p, \Omega_q$ to ensure that the Rydberg states are not populated in the ensemble, so that interactions between atoms do not affect the EIT-induced blocking of the Raman transfer.

(iv) The Raman detuning has to be much larger than the coupling Rabi frequency (i.e. $\Delta \gg \Omega_c$) so that, in the absence of EIT-induced blocking, the transfer proceeds with high fidelity.

These criteria are in full agreement with those specified in Müller *et al.* [2009], where the design of this logic gate was first reported.

Let us consider each of these conditions in more detail. Condition (i) sets the natural time scale of the problem because the decay rate of the intermediate state is the only parameter than cannot be experimentally tuned to any extent.

For condition (ii), the high-lying Rydberg states that can be routinely excited from the ground state via the intermediate state have lifetimes in the range of hundreds of microseconds. The operation time for the controlled Raman rotation is of the order of $2\Delta/(\Omega_p\Omega_q)$, so short rotation times require $2\Delta/\Omega_p\Omega_q \ll \Gamma_r^{-1}$.

Condition (iii) is the standard condition that needs to be fulfilled for there to be a strong EIT effect. The other side of this is condition (iv), which needs to be fulfilled so that there is very little residual EIT when the Rydberg-Rydberg interaction shift attempts to get rid of the EIT.

Together, these conditions require the various parameters to be as large as possible (compared to the natural time scale of the problem): $\Delta \gg \Omega_c \gg \Omega_p, \Omega_q \gg \Gamma_p$. There are, however, some factors that all Rydberg blockade experiments need to take into account. These include:

- the available power that can be produced from commercially available lasers and the magnitude of the transition dipole moments limit what Rydberg states can be excited within the appropriate time-scale.

- the proximity of the atom traps and the spatial extent of a Ryderg excited atom limit how close the atom traps can be placed without collisions between the valence electron of a Rydberg atom in one trap and the atoms of the other trap.

- as the principal quantum number increases, the energy level spacing between Rydberg states decreases and may become comparable to the energy difference between the $|0\rangle$ and $|1\rangle$ states encoded in the hyperfine ground state. At this point, accidental excitations of the Rydberg from the computational state that is not supposed to be coupled to Rydberg state become problematic Zhang *et al.* [2012]. In short, this means that the Rydberg state that provides the best blockade may not have the largest principal quantum number to which you could feasibly excite.

Attempting to fulfil these criteria for Rubidium-87, $|r\rangle_c = 64S$ and $|r\rangle_t = 63S$ and a separation between the traps of 1.7μm were chosen in order to achieve an interaction strength in excess of 15 GHz. The Raman beams both have Rabi frequency $\Omega_p = \Omega_q = 2\pi \times 70$ MHz and detuning $\Delta = 2\pi \times 1200$ MHz from the intermediate state. Ω_c is chosen to be $2\pi \times 700$ MHz. This coupling Rabi frequency can be obtained with commercially available intermediate power laser sources focused down to waists of tens of micrometers. With these parameters, the EIT-induced blocking of the Raman transfer works with a fidelity of more than 99.8% [Müller *et al.*, 2009].

5.2.3 Read-out

At the end of the protocol, the measurement of the state of the special qubit will allow us to retrieve the real and imaginary parts of the trace of the unitary

respectively. This is done by running the experiment numerous times so as to obtain the expectation values of the Pauli-X and Pauli-Y observables. The most appropriate way to experimentally perform measurements of these observables is to perform X (or Y) rotations on the special qubit and then perform a measurement in the computational basis (i.e. measure the populations of $|0\rangle_c$ and $|1\rangle_c$ states). The X (or Y) rotations can be performed with very high fidelity so that they negligibly affect the fidelity of the measurement result [Caillet & Simon, 2007]. To measure the expectation value with an accuracy ϵ requires the number of runs to be $\sim 1/\epsilon^2$, as shown Datta *et al.* [2005]. It is important to note that the number of runs necessary for a set accuracy does not depend on the number of qubits in the ensemble. The populations are measured via fluorescence imaging (see Chapter 6) and this suffers from limited efficiency, which translates to a non-negligible error rate, particularly when working with single atoms.

5.3 Loading Fluctuations

In any implementation of the DQC1 protocol for normalised trace estimation, multiple experimental runs will need to be performed in order to determine the expectation values of the measured observables. For the envisioned cold atom implementation, the number of atoms in the ensemble will vary from run to run. These variations in atom number are described by a Poissonian distribution.

For trivial unitaries, we can use equation 5.8 from section 5.2.2 to analyse how these fluctuations affect the output of the protocol. As an example, let us consider a unitary operator that performs a rotation of a single qubit about

the x-axis of the Bloch sphere. This unitary is given by the matrix:

$$R_x = \begin{pmatrix} \cos(\Omega t/2) & -i\ \sin(\Omega t/2) \\ -i\ \sin(\Omega t/2) & \cos(\Omega t/2) \end{pmatrix}, \tag{5.12}$$

where Ω is the Rabi frequency of the rotation and t is the time for which the unitary is applied.

The full normalised trace of this matrix is $\cos(\Omega t/2)$ and so is the top left normalised trace. Recalling equation 5.8, we find that for the Rydberg-based DQC1 protocol where all n the atoms of the ensemble are rotated around the x-axis of the Bloch sphere at the same rate, the top left normalised trace is $\cos^n(\Omega t/2)$.

For a plot of the top left normalised trace against time, the half width half maximum would occur when the rotation angle, $\Omega t/2$, is equal to $\arccos(0.5^{1/n})$. Figure 5.4 is a plot of the showing how the width of the top left normalised trace decreases with n.

As one can see in Figure 5.4, the width of the top left normalised trace that one would experimentally obtain when there are Poissonian fluctuations in the atom-loading is only a few percent different from the hypothetical situation in which every run could be performed with exactly 100 ensemble atoms. I thus arrive at the conclusion that the atom-number fluctuations do not present a significant weakness in the proposed experimental implementation of the DQC1 protocol for normalised trace estimation, even at high n. Furthermore, since the theoretical analysis outlined above can be readily compared with experimental data, the combination of trivial unitaries and Poissonian atom-number fluctuations can operate as a useful test bed for benchmarking the implementation.

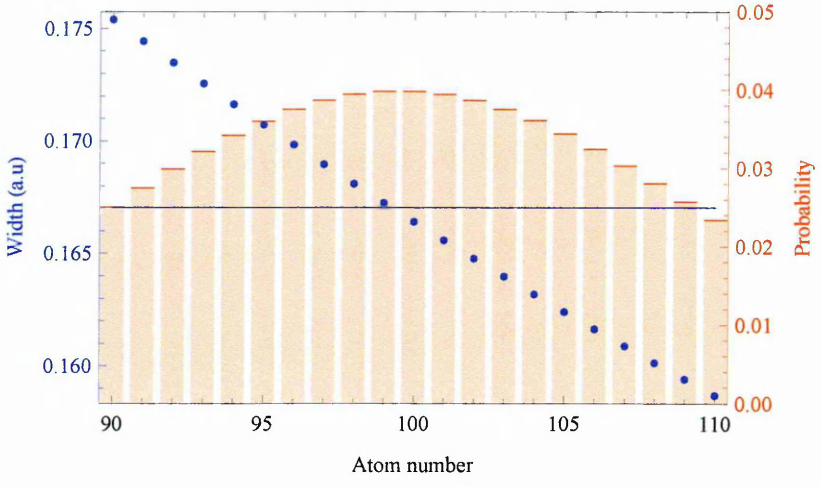

Figure 5.4: A plot showing the dependence of the width of the top left normalised trace on the number, n of ensemble atoms. Also shown in the plot is the probability that a given number of atoms will be loaded into the ensemble trap on any one experimental run when the mean number is 100. The horizontal line is the value of the width that one would obtain when the number of atoms in the ensemble varies with the shown distribution.

5.4 Modelling the Cold Atom Implementation

In this section, I describe the methods used to model the cold atom implementation and then proceed to discuss the results.

5.4.1 Methods

The modelling of the Rydberg implementation begins with the initialisation. This stage has a higher fidelity than the other stages. The fidelity is above 0.99 [Masterson *et al.*, 1993] [Saffman & Walker, 2005a] and so I approximated it as having unit fidelity. With only one atom in the ensemble, the initial state in

the basis $((|0\rangle_c, |1\rangle_c, |p\rangle_c, |r\rangle_c) \otimes (|0\rangle_t, |1\rangle_t, |p\rangle_t, |r\rangle_t)$ is:

$$\rho_1 = \frac{1}{4}\begin{pmatrix} 1 & 1 & 0 & 0 \\ 1 & 1 & 0 & 0 \\ 0 & 0 & 0 & 0 \\ 0 & 0 & 0 & 0 \end{pmatrix} \otimes \begin{pmatrix} \mathbb{I}_2 & 0_2 \\ 0_2 & 0_2 \end{pmatrix}. \tag{5.13}$$

For the processing stage, I considered the von Neumann equation,

$$i\hbar\frac{\partial\rho}{\partial t} = [\mathcal{H}, \rho]. \tag{5.14}$$

Continuing working in the same basis, the Hamiltonian is

$$\begin{aligned}\mathcal{H} =& \hbar\left(\begin{pmatrix} 0 & 0 & 0 & 0 \\ 0 & 0 & 0 & 0 \\ 0 & 0 & 0 & 0 \\ 0 & 0 & 0 & 0 \end{pmatrix} \oplus \begin{pmatrix} 0 & 0 & -i\Omega_p/2 & 0 \\ 0 & 0 & -i\Omega_q/2 & 0 \\ i\Omega_p/2 & i\Omega_q/2 & \Delta & -i\Omega_c/2 \\ 0 & 0 & i\Omega_c/2 & 0 \end{pmatrix}\right) \\ &+ B|r\rangle_c|r\rangle_t\,{}_t\langle r|_c\langle r|,\end{aligned} \tag{5.15}$$

where the Kronecker sum, $\oplus$, is defined as

$$A \oplus B = A \otimes \mathbb{I}_b + \mathbb{I}_a \otimes B, \tag{5.16}$$

A and B are square matrices of dimension a and b, respectively, $\mathbb{I}_n$ is the identity matrix of dimension n and $\otimes$ is the Kronecker product.

For a time-independent Hamiltonian, the analytical solution is

$$\rho(t) = e^{-i\mathcal{H}t/\hbar}\rho(0)e^{i\mathcal{H}t/\hbar}. \tag{5.17}$$

However, for the modelling of the processing stage to be realistic, it is important to include the decay of the intermediate state. To do this, I introduced the

Lindblad operator, $\mathcal{L}$, into equation 5.15 so that it becomes

$$i\hbar\frac{\partial\rho}{\partial t} = [\mathcal{H}, \rho] + i\mathcal{L}. \tag{5.18}$$

The Lindblad operator is given by

$$\mathcal{L} = -\sum_i 0.5(L_i^\dagger L_i \rho + \rho L_i^\dagger L_i) + L_i \rho L_i^\dagger, \tag{5.19}$$

where the L_i are specifically designed for the context. Here, for modelling the decay of the intermediate state, the L_i are defined as:

$$L_{pc0c} = 0.5\Gamma_{p0}|0\rangle_{c\ c}\langle p| \tag{5.20}$$

$$L_{pc1c} = 0.5\Gamma_{p1}|1\rangle_{c\ c}\langle p| \tag{5.21}$$

$$L_{pt0t} = 0.5\Gamma_{p0}|0\rangle_{t\ t}\langle p| \tag{5.22}$$

$$L_{pt1t} = 0.5\Gamma_{p1}|1\rangle_{t\ t}\langle p|. \tag{5.23}$$

where Γ_{p0} and Γ_{p1} is the decay rate from the intermediate state, $|p\rangle$, to the state $|0\rangle$ and $|1\rangle$ respectively. The *total* value of decay rate from the intermediate state is 36 MHz. However, to obtain the value of the decay from the intermediate state to the computational states, one has to multiply it by relevant branching ratios. So, given the atomic states that were chosen to be the qubit states and, for the sake of simplicity, assuming no leakage out of these computational states, $\Gamma_{p0} = (97/224)36$ MHz and $\Gamma_{p1} = (127/224)36$ MHz.

The final stage that needs to be modelled is the measurement stage. In this stage, the control qubit is measured in the X- or Y-basis. The measurements are repeated many times to obtain expectation values, $\langle X\rangle$ and $\langle Y\rangle$, which are the output of the protocol.

5.4.2 Results

For the Hamiltonian given in equation 5.15, I numerically calculated the evolution of the system after pulsed Raman rotations of varying durations (i.e. rotations corresponding to varying angles in the Bloch sphere) and retrieved the Pauli-X and Pauli-Y expectation values. I found that the real and imaginary parts of the top left normalised trace of the unitary acting on the ensemble of atoms take the form shown in Figures 5.5, 5.6 and 5.7 for different number of atoms in the ensemble. Also plotted in these Figures are the geometric discord, the adjusted geometric discord and the entangling power.

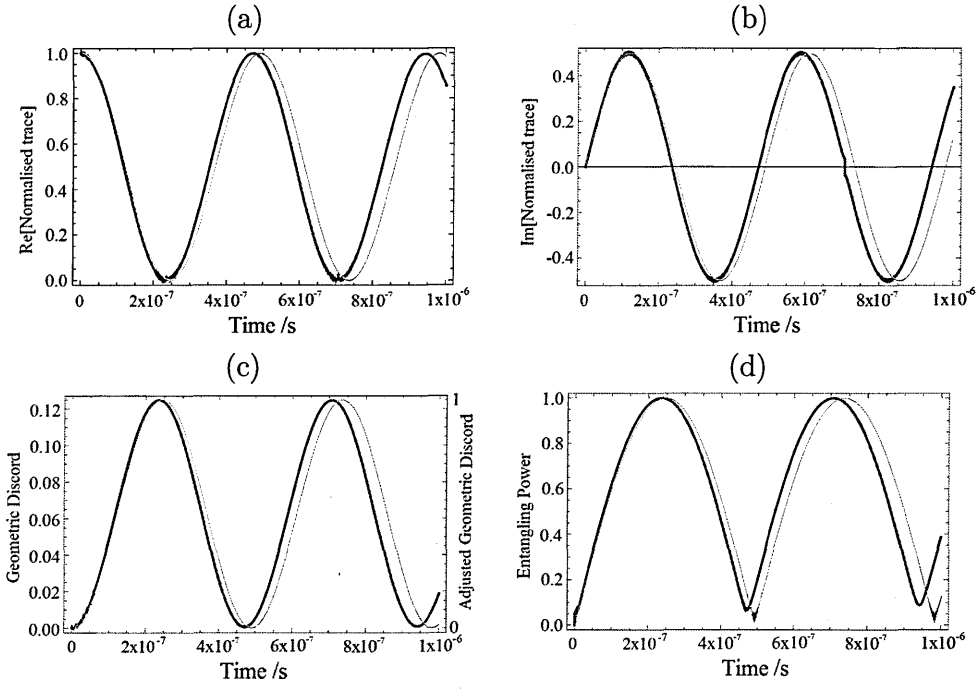

Figure 5.5: Results of the numerical estimate of (a) the real and (b) imaginary parts of the normalized trace, (c) the geometric discord and the adjusted geometric discord (i.e. rescaled geometric discord) and (d) the entangling power for one atom in the ensemble. The blue curve includes decay from the intermediate state and a finite blockade strength whilst the thin red curve shows the ideal case with no decay and perfect blockade. $\Omega_p = \Omega_q = 2\pi \times 70$ MHz, $\Delta = 2\pi \times 1200$ MHz from the intermediate state. The decay rate $2\pi \times 6$ MHz from the intermediate state is also taken into account. Ω_c is chosen to be $2\pi \times 700$ MHz. $|r\rangle_c = 64S$ and $|t\rangle_t = 63S$ for Rubidium 87 that, for a separation between the traps of 1.7μm, provide an interaction strength of 15 GHz.

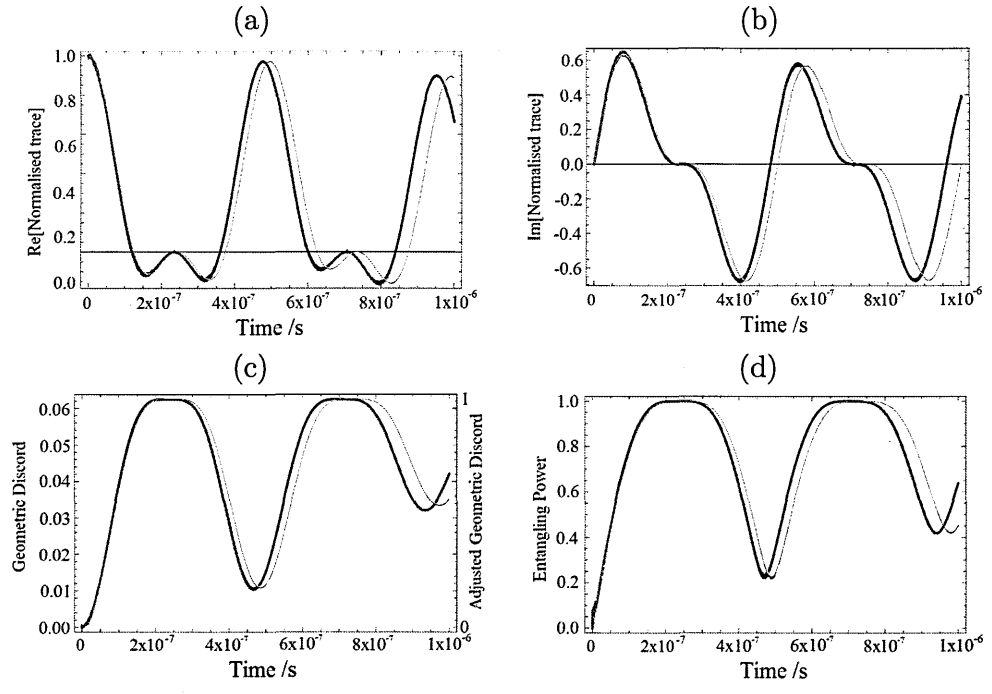

Figure 5.6: Results of the numerical estimate of (a) the real and (b) imaginary parts of the normalized trace, (c) the geometric discord and the adjusted geometric discord (i.e. rescaled geometric discord) and (d) the entangling power for two atoms in the ensemble. The blue curve includes decay from the intermediate state and a finite blockade strength whilst the thin red curve shows the ideal case. The parameters are the same as for Figure 5.5.

The plots show curves for the realistic case, where spontaneous decay and finite blockade strength are included, and for the ideal case, where there is no spontaneous decay and perfect blockade. There is good agreement between the two curves. It appears that the top left normalised trace evolves slightly more slowly in the realistic case than the ideal one. Determining the reason why this is so would require a careful theoretical analysis of the two cases. This is left for future work.

The plotted measures of nonclassical correlations are of interest for the reasons discussed in Chapter 4. In particular, geometric discord has been found to be useful in the analysis of a number of protocols [Dakic *et al.*, 2012b] [Giampaolo *et al.*, 2013] [Yao *et al.*, 2012] [Adhikari & Banerjee, 2012] whilst the concept of the entangling power of a unitary has been extended in several directions (e.g. it has inspired the related concepts of disentangling power

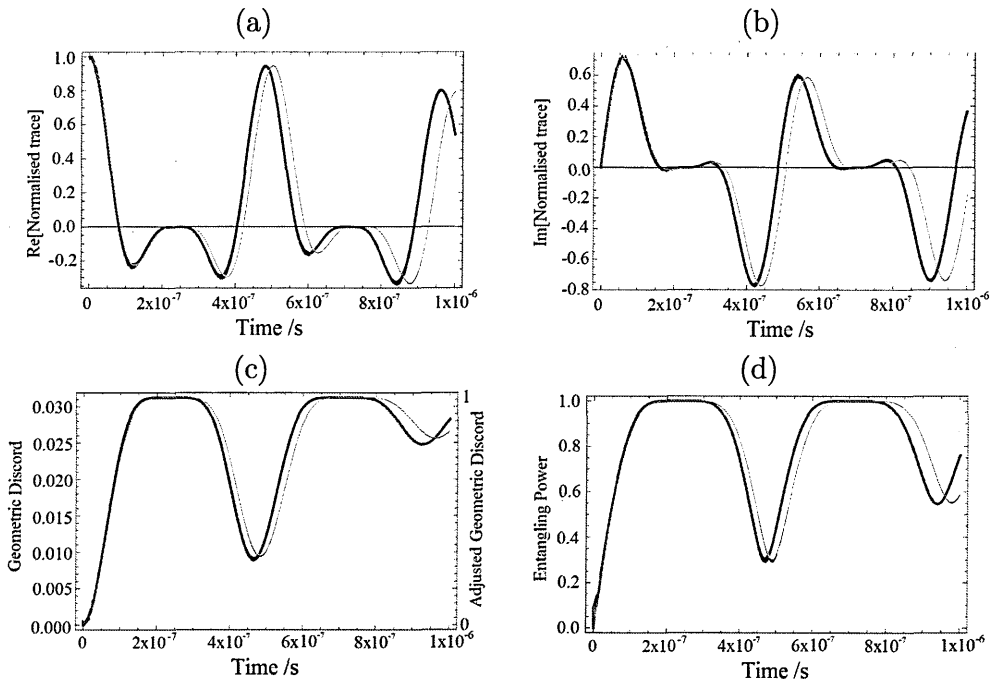

Figure 5.7: Results of the numerical estimate of (a) the real and (b) imaginary parts of the normalized trace, (c) the geometric discord and the adjusted geometric discord (i.e. rescaled geometric discord) and (d) the entangling power for three atoms in the ensemble. The blue curve includes decay from the intermediate state and a finite blockade strength whilst the thin red curve shows the ideal case. The parameters are the same as for Figure 5.5.

[Linden *et al.*, 2009] and discording power [Galve *et al.*, 2013]).

Note that I plotted both the adjusted geometric discord, defined in Eq. 4.20, as well as the originally defined geometric discord of Eq. 4.19 and Eq. 8.1. Importantly, the adjusted geometric discord is roughly 2^{n+1} times larger than the originally defined geometric discord. It therefore does not become negligible at high n, which leaves open the possibility that it is playing an important role in the protocol.

The conclusions that can be drawn from the plots of the measures of non-classical correlations are limited because the unitaries that have been modelled are trivial. However, since these measures are experimentally accessible, they can be investigated for non-trivial unitary processes (see the following section for details on how non-trivial unitaries can be implemented in a cold atom set-up). Given that theoretical studies have already highlighted the importance

of nonclassical correlations in a number of areas[1], experimental investigations are well-motivated.

Furthermore, as experimental control of cold atom systems improves, it may become feasible to investigate measures that are more challenging to experimentally determine, such as the measure proposed by Girolami & Adesso [2012], which requires up to four copies of the system and the measurement of nine observables. The task of finding measures of nonclassical correlations that have more physically insightful interpretations [Girolami *et al.*, 2013] and that are easier to experimentally investigate is an active area of research. Hence, there is considerable scope for future work in this direction.

5.5 Nontrivial Unitaries

A question may occur to the reader about how much of the Hilbert space can be explored. For experimental systems with poorly understood physics, it is possible to experimentally test the minimum Hilbert space dimension needed to successfully model a physical system [Brunner *et al.*, 2008] [Ahrens *et al.*, 2012] [Hendrych *et al.*, 2012]. However, for our purposes, the physics is sufficiently well-known to obtain a theoretical estimate.

As mentioned in Plesch & Bužek [2010], product states of N identical copies of a one-qubit state are a specific type of symmetric state. They span an $(N+1)$-dimensional subspace of the full, exponentially large Hilbert space that is available to general quantum states. If the many, identical atoms in an optical dipole trap remain in a product state during the experiment, very little of the Hilbert space will be explored.

In the limit of perfect blockade, the only accessible excited state is the

[1]For example, theoretical studies have shown nonclassical correlations to be important in quantum communication [Madhok & Datta, 2013], quantum metrology [Modi *et al.*, 2011], the quantum measurement problem [Piani & Adesso, 2012], quantum game theory [Zu *et al.*, 2012] and even in light-harvesting complexes at physiological temperatures [Bradler *et al.*, 2010].

symmetric Dicke state with one Rydberg excitation (also known a the W-state)[1]. As explained in Viteau *et al.* [2012], laser excitation preserves the symmetry of Dicke states. Since symmetric Dicke states of N two-level systems (e.g. systems with a ground and a Rydberg level) span only $N+1$ dimensions, one is again left with the atoms in the experiment exploring hardly any of the Hilbert space.

Fortunately, there is a way around this that will be described in the next chapter.

5.5.1 Investigating More Unitaries

For the DQC1 protocol to be able to implement an interesting unitary, one can make use of the results in Zhou *et al.* [2011]. The authors of this paper find that they can make *almost any* quantum operation depend on the state of a control qubit. This can be done simply by applying a certain gate that the authors call a "controlled-Xa gate" before the quantum operation and the same gate afterwards, as shown in Figure 5.8. This sequence is especially useful[2] for a DQC1 circuit because, as explained below, the quantum operation can be very general and because it is easier to find interesting unitaries than interesting *controlled* unitaries. For the cold atom implementation, use of the sequence reduces the task of finding interesting controlled unitaries (e.g. controlled many-body unitaries) that could be implemented (and thus investigated) to the task of finding a way to implement a cold atom version of the controlled-Xa gate.

To explain in more detail, the Xa gate operates on a four-dimensional Hilbert space spanned by the qubit states, $|0\rangle$ and $|1\rangle$, and two extra states, $|2\rangle$ and $|3\rangle$. The only condition that these extra states have to fulfil is that they

[1]Dicke states were first investigated by Dicke [1954]. The N-qubit Dicke state with k excitations is defined as: $|D_N^k\rangle = \left(\sum_j P_j\{|r\rangle^{\otimes k} \otimes |g\rangle^{\otimes(N-k)}\}\right) / \sqrt{\binom{N}{k}}$, where $P_j\{\cdot\}$ denotes the sum over all possible permutations.

[2]See Lanyon *et al.* [2009] for a discussion of how a similar scheme can drastically reduce the number of gates required in generic quantum circuits.

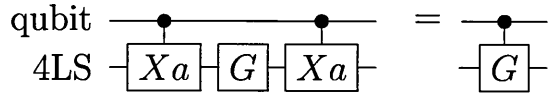

Figure 5.8: Circuit diagram involving a qubit, with basis states $|0\rangle$ and $|1\rangle$, and a four-level system (4LS) with two extra states $|2\rangle$ and $|3\rangle$. The diagram shows how two controlled-Xa gates can be used to implement a general operation, G, in a controlled way. The equality only holds when (i) the operation, G, only acts on the qubit states (not the extra states) and (ii) the 4LS initially has no population outside of the qubit states. For further details on these two conditions, see the main text.

are not acted upon by the quantum operations that act on the qubit states and that they are initially unpopulated. The Xa gate acts on the aforementioned states in the following way:

$$\begin{aligned} Xa|0\rangle &= |2\rangle \quad Xa|1\rangle = |3\rangle \\ Xa|2\rangle &= |0\rangle \quad Xa|3\rangle = |1\rangle \end{aligned} \tag{5.24}$$

It is written in the $|0\rangle, |1\rangle, |2\rangle, |3\rangle$ basis as:

$$Xa = \begin{pmatrix} 0 & 0 & 1 & 0 \\ 0 & 0 & 0 & 1 \\ 1 & 0 & 0 & 0 \\ 0 & 1 & 0 & 0 \end{pmatrix}. \tag{5.25}$$

One can show that the circuit diagram shown in Figure 5.8 to holds by performing some matrix multiplication. Let a general operation that only acts on the qubit states and not on extra states be written in the $|0\rangle, |1\rangle, |2\rangle, |3\rangle$ basis as:

$$G_q = \begin{pmatrix} G_{11} & G_{12} & 0 & 0 \\ G_{21} & G_{22} & 0 & 0 \\ 0 & 0 & 1 & 0 \\ 0 & 0 & 0 & 1 \end{pmatrix}. \tag{5.26}$$

One can verify that the matrix product XaG_qXa equals the following

matrix, G_e, that only acts on the extra states and not on the qubits.

$$G_e = \begin{pmatrix} 1 & 0 & 0 & 0 \\ 0 & 1 & 0 & 0 \\ 0 & 0 & G_{11} & G_{12} \\ 0 & 0 & G_{21} & G_{22} \end{pmatrix} \tag{5.27}$$

The left hand side of the identity in Figure 5.8, in the basis $(|0\rangle_c, |1\rangle_c) \otimes \mathbb{H}_t$ (where subscript c denotes the control qubit and $\mathbb{H}_t$ is the four dimensional Hilbert space of the target quantum system), is:

$$\begin{pmatrix} \mathbb{I} & 0 \\ 0 & Xa \end{pmatrix} \begin{pmatrix} G_q & 0 \\ 0 & G_q \end{pmatrix} \begin{pmatrix} \mathbb{I} & 0 \\ 0 & Xa \end{pmatrix} = \begin{pmatrix} G_q & 0 \\ 0 & G_e \end{pmatrix}. \tag{5.28}$$

This matrix is equivalent to a controlled version of G_q when the state upon which it acts initially has no population outside of the qubit states $|0\rangle$ and $|1\rangle$. This can be shown by explicit consideration of its action on such a state:

$$\begin{pmatrix} G_{11} & G_{12} & 0 & 0 & 0 & 0 & 0 & 0 \\ G_{21} & G_{22} & 0 & 0 & 0 & 0 & 0 & 0 \\ 0 & 0 & 1 & 0 & 0 & 0 & 0 & 0 \\ 0 & 0 & 0 & 1 & 0 & 0 & 0 & 0 \\ 0 & 0 & 0 & 0 & 1 & 0 & 0 & 0 \\ 0 & 0 & 0 & 0 & 0 & 1 & 0 & 0 \\ 0 & 0 & 0 & 0 & 0 & 0 & G_{11} & G_{12} \\ 0 & 0 & 0 & 0 & 0 & 0 & G_{21} & G_{22} \end{pmatrix} \begin{pmatrix} \alpha A \\ \alpha B \\ 0 \\ 0 \\ \beta A \\ \beta B \\ 0 \\ 0 \end{pmatrix} = \begin{pmatrix} \alpha(G_{11}A + G_{12}B) \\ \alpha(G_{21}A + G_{22}B) \\ 0 \\ 0 \\ \beta A \\ \beta B \\ 0 \\ 0 \end{pmatrix} \tag{5.29}$$

followed by explicit consideration of the action of a controlled version of G_q on

the same state:

$$\begin{pmatrix} G_{11} & G_{12} & 0 & 0 & 0 & 0 & 0 & 0 \\ G_{21} & G_{22} & 0 & 0 & 0 & 0 & 0 & 0 \\ 0 & 0 & 1 & 0 & 0 & 0 & 0 & 0 \\ 0 & 0 & 0 & 1 & 0 & 0 & 0 & 0 \\ 0 & 0 & 0 & 0 & 1 & 0 & 0 & 0 \\ 0 & 0 & 0 & 0 & 0 & 1 & 0 & 0 \\ 0 & 0 & 0 & 0 & 0 & 0 & 1 & 0 \\ 0 & 0 & 0 & 0 & 0 & 0 & 0 & 1 \end{pmatrix} \begin{pmatrix} \alpha A \\ \alpha B \\ 0 \\ 0 \\ \beta A \\ \beta B \\ 0 \\ 0 \end{pmatrix} = \begin{pmatrix} \alpha(G_{11}A + G_{12}B) \\ \alpha(G_{21}A + G_{22}B) \\ 0 \\ 0 \\ \beta A \\ \beta B \\ 0 \\ 0 \end{pmatrix}, \quad (5.30)$$

where: the basis is $(|0\rangle_c, |1\rangle_c) \otimes (|0\rangle_t, |1\rangle_t, |2\rangle_t, |3\rangle_t)$; the controlled-$G_q$ gates operates such that G_q is implemented conditional on the control qubit being in the state $|0\rangle$; and the initial state of the system was written as $|\alpha, \beta\rangle_c \otimes |A, B, 0, 0\rangle_t$ with α, β, A and B being general complex numbers fulfilling the usual conditions (such as normalisation) for representing a quantum state.

The controlled-Xa gate can be implemented in a cold atom set-up by using a slight modification of the EIT-based scheme of Müller *et al.* [2009] and the choice of states shown in Figure 5.9. The laser applied to the control atom remains the same as before, as does the coupling laser applied to the target ensemble. Now, however, the Raman transitions between the different states of the target ensemble must be carefully tailored to make sure that procedures on the extra states, $|2\rangle$ and $|3\rangle$, do not rotate the qubit states. Since the qubit states shown in Figure 5.9 are only coupled by Raman beams with circularly polarised light, this requirement is ensured by using linearly polarised light for the Raman beams of the controlled-Xa gate. The general quantum operation, G, acting on only the qubit states and not on the extra states, could be implemented with circularly polarised light. In order to make G non-trivial, the circularly polarised light beams would have to be employed in conjunction with other procedures (see, for example, Figure 5.11).

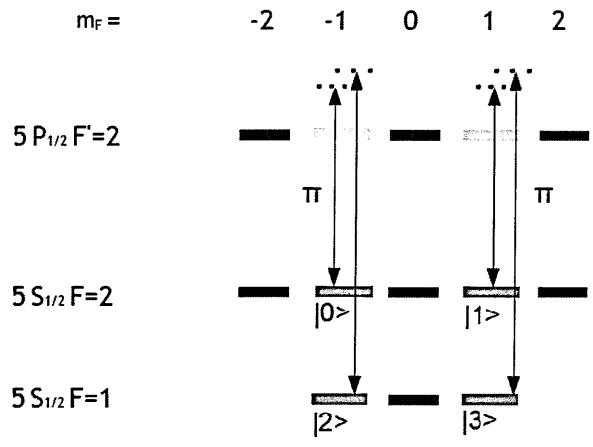

Figure 5.9: Cold atom implementation of the controlled-Xa gate. To transfer between $|0\rangle = |5S_{1/2}, F = 2, m_F = -1\rangle$ and $|2\rangle = |5S_{1/2}F = 1, m_F = -1\rangle$ (shown in dark green), one can perform an off-resonant Raman transition using linearly polarised light via $5P_{1/2}F' = 2, m'_F = -1$ (shown in light green). To transfer between $|1\rangle = |5S_{1/2}, F = 2, m_F = 1\rangle$ and $|3\rangle = |5S_{1/2}, F = 1, m_F = 1\rangle$ (shown in dark blue), one can perform an off-resonant Raman transition using linearly polarised light via $5P_{1/2}F' = 2, m'_F = 1$ (shown in light blue). When the transfer pulses are π-pulses, an Xa gate is implemented. A controlled-Xa gate can be performed by adding a coupling laser so that EIT occurs conditionally depending on the state of a control atom.

Encoding information in Zeeman states of the hyperfine ground state manifold is common practice (see, for example, Saffman & Walker [2005a], Brion *et al.* [2007] and Brion *et al.* [2008]). With such an encoding, it is important that the d.c. magnetic field used to split the Zeeman states is stable. Our choice of Zeeman states for the Rubidium-87 hyperfine ground state manifold was governed by the consideration that pairs of states $|F, m_F\rangle$ and $|F+1, -m_F\rangle$ experience the same linear Zeeman shifts.

The linear Zeeman shift can even be made equal to zero for: $|F = 1, m_F = \pm 1\rangle$ and $|2, m_F = \mp 1\rangle$ if the d.c. magnetic field is 3.23 G; and $|F = 1, m_F = \pm 1\rangle$ and $|2, m_F = \pm 1\rangle$ if the d.c. magnetic field is 1219 G [Saffman & Walker, 2005a]. Since one would like to get the greatest insensitivity to fluctuations for all of these pairs of states, we propose a field of intermediate strength of $\approx$ 600G, giving a splitting between adjacent m_F states of hundreds of MHz.

During the preparation of this thesis, three groups independently made

progress in this area. [Thompson *et al.*, 2013a] [Araújo *et al.*, 2013] [Nakayama *et al.*, 2013]. The outstanding result is that one can implement controlled unitaries where the unitary does not have to leave any part of the Hilbert space untouched. This result can be applied in the Rydberg system that I envision.

5.5.2 DQC1 to Probe Many-body Physics and Non-Trivial Unitaries

Van der Waals forces are the dominant interactions between neutral particles on nanometre-to-micrometre length scales Béguin *et al.* [2013], which makes their effects ubiquitous in physics, chemistry and biology Weidemüller [2013]. The relevant physics can become fairly involved. For example, Viteau *et al.* [2012] explain that when finite van der Waals interactions are taken into account, states with the same symmetry and those with different symmetries can be coupled. This expands the accessible regions of the Hilbert space so as to include interesting many-body states. Modelling such states has been done: with mean-field techniques [Tong *et al.*, 2004]; by dynamically reducing the size of the Hilbert space [Robicheaux & Hernández, 2005] [Hernández & Robicheaux, 2006]; by direct simulations with a truncated Hilbert space [Löw *et al.*, 2009] [Weimer *et al.*, 2008] [Wüster *et al.*, 2010]; by using rate equations [Ates *et al.*, 2006]; with a kinetic Monte Carlo analysis and a Hartree-Fock approximation [Chotia *et al.*, 2008]; and by using Dicke states as the basis states [Viteau *et al.*, 2012].

Interesting many-body problems can be tackled using Rydberg atoms. Finding the ground state of the 2- or 3-dimensional Ising model with a local transverse field with interactions beyond nearest neighbours is a hard computational problem [Barahona, 1982], which can be modelled with Rydberg atoms [Carr & Saffman, 2013]. In Stanojevic *et al.* [2012], the unitaries involved in collisions of Rydberg polaritons is theoretically investigated.

Whilst the above possibilities are left for future investigation, a more straightforward starting point is as follows. Consider a total Hamiltonian, $\mathcal{H}$, that is the sum of a light-matter Hamiltonian, $\mathcal{H}_{l-m}$, and a Hamiltonian written in the basis $\{ |g\rangle,|r\rangle \}^{\otimes n}$, where g denotes a ground state, r denotes a Rydberg state and n is the number of atoms. Let the Rydberg interaction strengths be much greater than any of the matrix elements (e.g. Rabi frequencies) of the light-matter Hamiltonian. For the case of $n = 4$ mutually equidistant atoms, the Hamiltonian is

$$\mathcal{H} = \mathcal{H}_{l-m} + \mathrm{diag}(0,0,0,x_2,0,x_2,x_2,x_3,0,x_2,x_2,x_3,x_2,x_3,x_3,x_4) \tag{5.31}$$

$$\sim \mathrm{diag}(0,0,0,x_2,0,x_2,x_2,x_3,0,x_2,x_2,x_3,x_2,x_3,x_3,x_4), \tag{5.32}$$

where x_i is the i-body Rydberg-Rydberg interaction shift, all terms other than x_i are completely neglected (i.e. a zeroth order approximation is made) and $x_i = (i-1)x_2$ in the case of additive interaction potentials (such as those encountered when a single $S_{1/2}$ Rydberg state is excited) and something else for non-additive interactions (such as those that occur for Förster interactions or when different $S_{1/2}$ Rydberg states are excited) [Younge *et al.*, 2009] [Cano & Fortágh, 2012].

It is straightforward to find the unitary corresponding to a diagonal Hamiltonian:

$$U \sim \mathrm{diag}(1,1,1,e^{\frac{ix_2t}{\hbar}},1,e^{\frac{ix_2t}{\hbar}},e^{\frac{ix_2t}{\hbar}},e^{\frac{ix_3t}{\hbar}},1,e^{\frac{ix_2t}{\hbar}},e^{\frac{ix_2t}{\hbar}},e^{\frac{ix_3t}{\hbar}},e^{\frac{ix_2t}{\hbar}},e^{\frac{ix_3t}{\hbar}},e^{\frac{ix_3t}{\hbar}},e^{\frac{ix_4t}{\hbar}}), \tag{5.33}$$

where t is time. The normalised trace of U is $(5+6e^{\frac{ix_2t}{\hbar}}+4e^{\frac{ix_3t}{\hbar}}+e^{\frac{ix_4t}{\hbar}})/16$. However, one must bear in mind the issues discussed in section 5.2 that only the top left half of the unitary, U_{TL} has its trace evaluated. The normalised trace of U_{TL} is $(4+3e^{\frac{ix_2t}{\hbar}}+e^{\frac{ix_3t}{\hbar}})/8$. For additive Rydberg-Rydberg interaction

potentials, $x_3 = 2x_2$ and the normalised trace of U_{TL} is $(4 + 3e^{\frac{ix_2t}{\hbar}} + e^{\frac{2ix_2t}{\hbar}})/8$.

If one can implement DQC1 to estimate the normalised trace at different times, as shown in Fig. 5.10, one can estimate the values of the x_i and thus one could investigate of the additivity, or lack thereof, of the Rydberg-Rydberg interaction potentials. This analysis could be extended to large values of n.

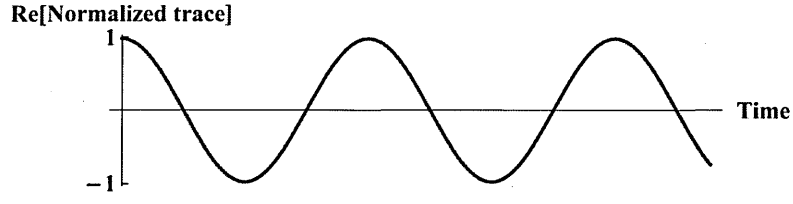

Figure 5.10: The estimates of the normalised trace can be plotted as a function of time. The shape of the curve would indicate the values of x_i. One could thus investigate of the additivity, or lack thereof, of the Rydberg-Rydberg interaction potentials .

The set-up is extremely versatile for investigating many-body physics. We have identified some particularly suitable configurations shown in Figure 5.11.

In Figure 5.11(a), the special atom is surrounded by a ring of traps, each loaded with an ensemble of atoms. Various collective phenomena can occur in traps arranged in a ring (e.g. phenomena involving symmetric entangled states [Olmos *et al.*, 2009a] or collective fermionic states [Olmos *et al.*, 2009b]). Square or triangular geometrical arrangements also lead to interesting physics [Laycock *et al.*, 2011]. By placing the special atom in the centre of the configuration, many traps can be placed within its blockade range. With traps that are individually addressable, the interactions between specific traps can be engineered as desired. Thus, the physics of the system can be explored in considerable depth.

In Figure 5.11(b), the atoms in the ensemble are coupled to Rydberg states. Many possible phenomena could be investigated in such a scenario. For example, it has been shown [Pohl *et al.*, 2010] that when a disordered ensemble is *not* fully blockaded, chirped laser excitation can lead to Rydberg atoms forming crystalline structures. As suggested in Pohl *et al.* [2010], one could

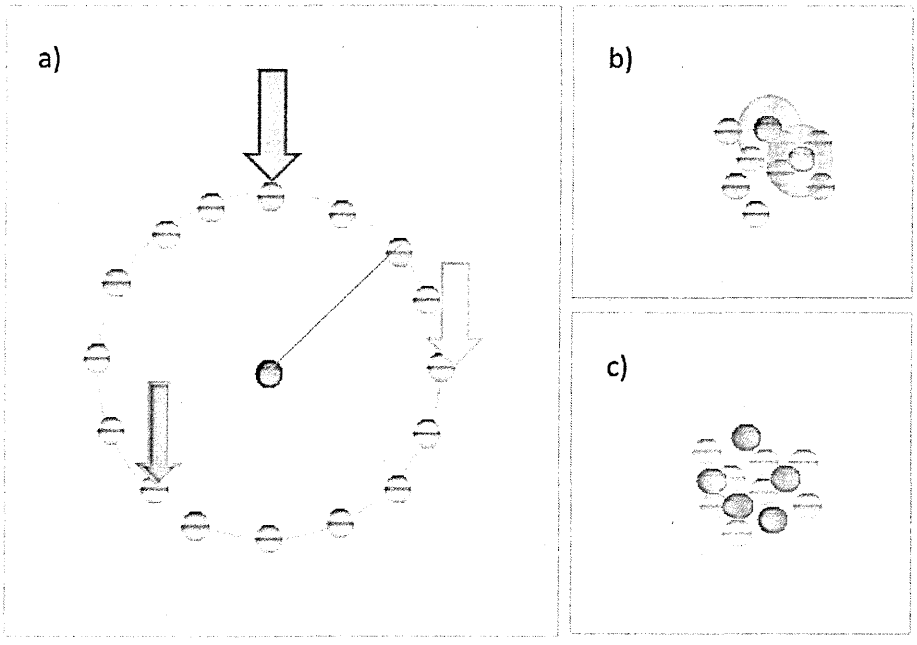

Figure 5.11: Non-trivial physical processes can be studied in various ways. One can (a) arrange the ensemble atoms (represented by the blue circles) in a ring of traps that can be individually addressed by focussed lasers (represented by the arrows). One can (b) couple the ensemble to Rydberg states (indicated by the large, pink-shaded circles). One can (c) load the ensemble with different atomic species or isotopes (represented by the different coloured circles).

then simulate the magnetism of long-range interacting spins and explore their quench dynamics through quantum phase transitions.

Another possibility, shown in Figure 5.11(c), is that different atomic isotopes or species could be loaded in the ensemble, so that they respond to different laser pulses[1]. The unequal masses and the different responses to external fields mean that experiments could probe a large parameter space [Petrov *et al.*, 2007]. The ultracold physics of mixed atomic species is expected to be extremely rich (e.g. the physics of two fermions combining to form a composite boson [Petrov *et al.*, 2005]).

Overall, the ability to individually address traps, excite to different Rydberg states and load different atomic species could open up a route to a wide variety of unitaries being implemented as part of mixed-state protocols.

[1]The individual addressing of different atomic isotopes or species is somewhat reminiscent of the quantum cellular automata techniques that were originally conceived by Lloyd [1993].

However, we have by no means considered all the possibilities for exploring large, many-body Hilbert spaces. There are options to make use of more of the energy levels of the atoms [Brion *et al.*, 2007] [Brion *et al.*, 2008][1]. There may even be opportunities to use nonholonomic control techniques [Brion *et al.*, 2011], which have been analysed for the specific case of ultracold Rydberg atoms in Brion *et al.* [2005], Brion *et al.* [2006] and Akulin *et al.* [2001]. The question of which of these numerous routes for further investigation are the most worthwhile to explore is left open.

5.6 DQC1 Implementations With Other Platforms

The DQC1 model has been implemented in other physical set-ups, such as NMR set-ups and linear optics set-ups. These previous experimental realisations have included implementations of the protocol for normalised trace estimation [Passante *et al.*, 2009] [Marx *et al.*, 2010] and investigations of nonclassical correlations [Passante *et al.*, 2011].

After briefly describing these implementations, I highlight the main differences between them and my proposed cold atom realisation. The key difference is that whilst the former were performed with a small number of qubits, the latter can be performed with many more.

5.6.1 Other Platforms

In section 4.1.1, it was mentioned that for an appropriate choice of the unitary, estimation of the normalised trace can be made equivalent to approximation of the Jones polynomial at the fifth root of unity [Shor & Jordan, 2008]. In Passante *et al.* [2009], an NMR experiment is performed to approximate the

[1] A particularly useful atomic species that could be used in this case is Holmium [Saffman & Mølmer, 2008b], which has 128 hyperfine ground states.

Jones polynomial for different unitaries that represented different knots.

A fundamental problem in knot theory is determining whether two knots are topologically different. Knot invariants, such as the Jones polynomial, have the same value for any representation of a given knot. The authors therefore tested whether they could perform the DQC1 protocol sufficiently reliably to correctly identify different knots. The authors had a success rate[1] of 91%.

Another NMR experiment for approximately evaluating the Jones polynomial was performedby Marx *et al.* [2010]. They applied a sequence of unitary transforms representing the trefoil knot, the figure-eight knot and the Borromean rings. The experimental results showed excellent agreement with the theory.

Nonclassical correlations been investigated in an NMR experiment [Passante *et al.*, 2011] and a linear optics experiment [Lanyon *et al.*, 2008]. The NMR experiment employed four qubits. The authors determine the value of a state-independent non-zero discord witness [Dakić *et al.*, 2010] at both the start and the end of the DQC1 protocol. They consistently find that there is discord at the end but not at the start. This is in accordance with the view that the DQC1 protocol generates nonclassical correlations during its implementation.

In the DQC1 protocol experimentally implemented in a linear optics architecture, there was only one maximally mixed qubit [Lanyon *et al.*, 2008] and the controlled unitary was a controlled rotation around the z-axis of the Bloch sphere. Correlations were analysed by performing tomography of the two-qubit output state and entanglement was quantified using the entanglement measure known as tangle. No entanglement was observed. Large amounts of discord were observed apart from in three cases. These cases were when the implemented unitary was a Clifford operation and so, according to the Gottesman-Knill theorem [Gottesman, 1998] [Gottesman, 1999] [Mari & Eisert,

[1]The success rate was defined to be the average of two percentages: the percentage of distinct knots correctly identified as being distinct and the percentage of identical knots corrects claimed to be indistinguishable to within experimental error.

2012], a classical simulation could efficiently be performed.

5.6.2 Differences With Other Platforms

Since the experiments performed to date in NMR systems and photonic systems have estimated the normalised trace of only small matrices (e.g. a two-by-two matrix [Lanyon *et al.*, 2008]), there may be platforms better suited to implementing the DQC1 model.

The key insight of this thesis is that the strong, long-range, controllable nature of Rydberg interactions can allow the special qubit in a DQC1 protocol to interact with a very large ensemble. Hence, a cold atom platform exploiting Rydberg interactions can estimate the normalised trace of extremely large unitaries.

As an illustrative example, consider one hundred atoms trapped in an optical dipole trap. A unitary operation on these atoms would be described by a 2^{100}-by-2^{100} matrix. Finding the normalised trace of this matrix is equivalent to adding up about 10^{30} numbers, which is a classically intractable task since modern supercomputers can perform 10^{12} operations per second and only about 10^{18} seconds have elapsed since the start of the universe.

As another example, consider 333 atoms trapped in an optical dipole trap. The unitary matrix describing an operation on these atoms would be a 2^{333}-by-2^{333} matrix. Finding the normalised trace of this matrix is equivalent to adding up about a googol numbers (i.e. 10^{100} numbers). To see how large a googol is, one can note that the mass of the observable universe is of the order of 10^{52} kg [Funkhouser, 2006] and that the mass of an electron is 9.109 x 10^{-31} kg [Mohr *et al.*, 2012] (i.e. of the order of 10^{-30}). The ratio of the mass of the universe to that of an electron is a number that is far less than a googol.

The idea to experimentally study the DQC1 model and nonclassical correlations in the intractably large Hilbert spaces of cold atom ensembles is thus a

novel and important departure from the small-scale studies performed to date.

5.7 Summary

In this chapter, I demonstrated that the cold atom platform is extremely suitable for large-scale implementations of the DQC1 model. For the case of a trivial unitary, I performed numerical simulations of the normalised trace estimation protocol. From these simulations, I plotted how experimentally accessible measures of nonclassical correlations vary throughout the protocol. Finally, I gave a detailed description of how the implementation can be adapted investigate non-trivial unitaries.

Ensuring there are no flaws is obviously important for any proposed experimental investigation. The work presented in this chapter, demonstrating the feasibility of the various aspects of the proposal, is important because it allows us to be confident that work put into its experimental realisation will be worthwhile. Indeed, the next chapter consists of an in-depth discussion of the practical details of the experimental apparatus.

Chapter 6

Experimental Implementation

In this chapter, I discuss the experimental set-up. I describe the techniques used to cool and trap neutral atoms [Metcalf & van der Straten, 2002]. I then describe a high-performance optical system that I designed to dipole-trap and image the atoms. The design employs a small number of aspheric lenses. Before inexpensive, moulded aspheric lenses were used for the purposes of imaging atoms, researchers had to work with a considerably larger number of spherical lenses [Alt, 2002].

Since systems were already being put in place to trap and cool the atoms, the design of the imaging system constituted the next important stage in the laboratory. It was, however, true that the atoms had not yet been trapped in an optical dipole trap. Hence, some considerations of the dipole trapping had to be made. Nevertheless, the greatest challenge was the imaging: if a design could successfully perform imaging (i.e. collect fluorescent light from a small region), then the task of creating a dipole trap (i.e. sending trapping light into a small region) should fall into place. The reasons for this are the following.

Aspheric lenses can be effective at minimising not only spherical aberrations but also chromatic aberrations. This means that a single dipole lens can be employed in service of both imaging and trapping. [Takamizawa *et al.*, 2006] provide some numbers for just how well this can be done. They define

chromatic aberration as the distance between the focal positions of the 830 nm trapping light and the 780 nm fluorescent light. They achieve chromatic aberrations that are consistently less than the Rayleigh lengths and as low as 2.9 μm. Furthermore, using optical design software, the optimal position for the atoms to be imaged can be accurately specified. It is then possible to straightforwardly, yet finely, adjust the convergence or divergence of the trapping light as it enters the dipole lens so that its focus is located at the optimal position for the imaging to be performed.

The importance of the imaging system is best seen in light of its applications. For some applications of cold atoms, it might be sufficient to use an imaging system to estimate the total number of trapped atoms. However, for many applications, including quantum computation, it is crucial to be able to measure the state of the atoms. This can be done as follows.

There are two hyperfine ground states of Rubidium-87. To see which of these an atom is in, one can shine light resonant between one of these states and the $5P$ state. If fluorescence is observed, the atom was in that state. If no fluorescence is observed, the atom was not in that state[1]. This procedure to measure the state of the atoms does not lead to any constraints on the design of imaging system.

The structure of the chapter is as follows. The chapter begins with a description of the experimental techniques employed to trap and cool atoms [Metcalf & van der Straten, 2002]. The lasers used to perform Rydberg excitation are briefly described. The layout of the optical design is then given. The majority of the chapter consists of an analysis of the expected performance of design. Finally, I discuss some tests of the performance of the experimental realisation of the design in the laboratory.

[1]Since the presence or absence of fluorescent light is crucial to this procedure and since this light is of the same frequency as the incident light, one must take care to ensure that the none of the incident light reaches the camera. This is done simply by shining the incident light along a path perpendicular to the imaging axis.

6.1 Laser Cooling

Energy and momentum are both conserved when an atom absorbs and emits a photon. The absorption can either be resonant or off-resonant. A resonant absorption is one where the energy difference between the excited state (with energy E_e) and the ground state (with energy E_g) is equal to the energy, $h\nu$, of the photon. An off-resonant absorption is one where this is not the case.

When the atom in its excited state returns to the ground state, it emits a photon with energy $E_e - E_g$. In order to conserve energy when an atom absorbs an off-resonant photon and then returns the ground state, the energy associated with another degree of freedom, namely the centre-of-mass motion of the atom, must also be considered.

The goal of laser cooling is to decrease the kinetic energy of an atom. This is achieved by an atom repeatedly absorbing red-detuned photons (i.e. photons with $h\nu < E_e - E_g$). When the atom in the excited state goes on to return to the ground state by emitting a photon (with energy $E_e - E_g$), the atom loses kinetic energy in order to conserve the total energy.

This leads us nicely onto a consider of momentum conservation [1]. Consider a photon propagating in the positive x-direction. When an atom absorbs this photon, the x-component of the momentum of the atom increases. The atom is then in its excited state. It spontaneously emits a photon in a random direction and the component of the momentum along this direction changes. This emission of photons is isotropic: there is no spatially preferred direction for the emission. Hence, spontaneous emission, on average, causes no net increase in the momentum of the atom. So, after many cycles of absorption and emission, the x-component of the momentum of the atom increases. If this x-component was initially negative (i.e. the atom was initially travelling in the

[1] The momentum of an atom is equal to the product of its mass, m, and velocity, $\vec{v}$, whilst the momentum of a photon is the product of its wave vector, $\vec{k}$, and Planck's constant, $\hbar$.

negative x-direction), an appropriately timed pulse of photons can be used to slow the atom.

6.1.1 Doppler Cooling

The theory of Doppler cooling is based on the concept of an atom with only two relevant energy levels subject to red-detuned photons from counter-propagating laser beams. The atom cycles between the two levels by absorbing the incident photons and spontaneously emitting them. These "cooling cycles" reduce the average momentum of the atom.

The Doppler effect is the change in the frequency of a wave for a body moving relative to the source of the wave. Due to this effect, the tuning of a laser beam to an atomic absorption resonance depends on the velocity of the atoms relative to the source of the photons: atoms moving towards the laser "see" the photons as being higher in frequency and atoms moving away the laser "see" the photons as being lower in frequency. The counter-propagating laser set-up employed in Doppler cooling exploits this effect to oppose the motion of the atoms. Figure 6.1 illustrates this.

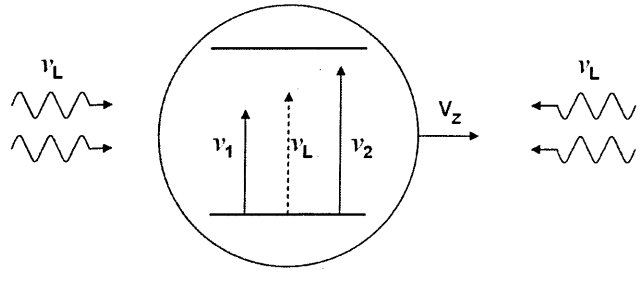

Figure 6.1: The principle of Doppler cooling. The laser light has a frequency ν_L that is tuned below the atomic resonance. As a result of the Doppler effect, the atom, regardless of the direction of its motion, is closer to resonance with the counter-propagating beam (with Doppler-shifted frequency ν_2) than with the co-propagating beam (with Doppler-shifted frequency ν_1). The atom therefore experiences a net force opposing its motion and is thus cooled.

The atom that we use in the laboratory at The Open University is Rubidium

[1]. Some of the atomic levels of Rubidium 87 are shown in Figure 8.2 in the appendix.

Even though Rubidium is clearly not a two-level system, we can employ selection rules to create an effective two level system and thus, implement Doppler cooling. For further details, see section 8.5.1 of the appendix.

6.2 Trapping

Objects can be confined in a potential well if their kinetic energy is less than the depth of the potential well. Consequently, once an atom has been laser-cooled (i.e. had its kinetic energy reduced), possibilities open up for trapping it.

6.2.1 Magneto Optical Trapping

Magneto-optical trapping relies on both magnetic fields and laser radiation. An atom with a magnetic moment $\vec{\mu}$ can be confined by an inhomogeneous magnetic field $\vec{B}$ because of the interaction between the moment and the field[2]. The combination of magnetic interactions and laser cooling processes employed in a MOT can trap millions of atoms at temperatures of tens of microKelvin. For further details on the operation of a MOT, see section 8.5.2 of the appendix.

The MOT in the laboratory consists of four beams rather than the standard six because the vacuum chamber has restricted optical access. This four-beam MOT has been characterised [Kowalczyk, 2013]. It traps between 1 $\times 10^5$ and 3 $\times 10^5$ atoms, depending on the angles between the beams. The number density was determined to be $\sim 2.5 \times 10^8$ atoms/cm^3. The temperature of the atoms was roughly 1 mK but this could be reduced to tens of microkelvin by turning

[1]The use of Rubidium is for several reasons. Rubidium only has single valence electron and consequently, lots of its basic properties can be estimated using analytical formulae existing for Hydrogen atoms. Inexpensive lasers are available for the transitions relevant to laser cooling.

[2]The energy shift experienced by the atom is $E = -\vec{\mu} \cdot \vec{B}$.

the magnetic fields off for 10 ms before measuring the temperature[1]. This temperature is sufficiently low to allow loading of an optical dipole trap.

6.2.2 Optical Dipole Trapping

Once atoms have been trapped in MOTs, it is possible to load them into other traps that are perhaps more appropriate for certain experiments. In this subsection on dipole traps, I motivate the use of optical dipole traps in cold atom quantum computation. I then give the basic physics of their operation. Finally, I highlight how flexibly these traps can be positioned with respect to one another and recall how this lends itself to detailed DQC1-based investigations of non-trivial physics.

6.2.2.1 Motivation

Experimental studies of Rydberg atoms have already been performed in MOTs and local blockade effects have been observed [Tong *et al.*, 2004] [Singer *et al.*, 2004]. However, in these experiments, the sample size (equal to the smaller of the trapped volume of atoms or the volume of the atoms exposed to the excitation laser beams) is larger than the blockade radius. This means that many collective Rydberg states can be excited at any one time.

The resulting Rydberg-Rydberg interactions are an additional source of dephasing. Even though it is possible to reduce this source of dephasing by exciting to Rydberg states that have repulsive Rydberg-Rydberg interactions, these types of MOT experiments were not intended to fully implement the quantum information processing schemes of Jaksch *et al.* [2000] or Lukin *et al.* [2001]. Rather, they were designed to investigate the key physics behind these schemes.

Unlike MOTs, optical dipole traps can be so small that they can trap single

[1]Turning the magnetic fields off is a standard technique. The atoms are no longer confined but their temperature is reduced. The atoms are said to be in optical molasses.

atoms, and thus are appropriate for carrying out the logic gate proposal of Jaksch *et al.* [2000]. Also unlike MOTs, the density of the atoms in dipole traps is sufficiently high that they may be able to achieve the regime where the blockade radius is larger than the multiple-atom sample size. This would make them appropriate for carrying out the proposal of Lukin *et al.* [2001].

6.2.2.2 Physics of an optical dipole trap

When an atom interacts with far detuned light, the electric field, **E**, induces an atomic dipole moment, **p**, that oscillates at the driving frequency of the light, ω. The resulting interaction potential, U_{dip}, of the induced dipole moment in the driving electric field can be used to trap the atom. More precisely, it is the spatial gradient of this potential, due to the spatial gradient of the intensity of the far detuned light, that creates the trapping force. Heating of the atoms in the trap, at a rate Γ_{sc}, is caused by the scattering of photons during the random, fluctuating cycles of absorption and spontaneous emission. Expressions for U_{dip} and Γ_{sc} for atoms trapped in an optical dipole trap are as follows [Grimm *et al.*, 2000]:

$$U_{dip}(\mathbf{r}) = \frac{3\pi c^2}{2\omega_0^3}\frac{\Gamma}{\Delta}I(\mathbf{r}) \tag{6.1}$$

$$\Gamma_{sc}(\mathbf{r}) = \frac{3\pi c^2}{2\hbar\omega_0^3}\left(\frac{\Gamma}{\Delta}\right)^2 I(\mathbf{r}), \tag{6.2}$$

where ω_0 is the resonant angular frequency of the transition, Γ is the spontaneous decay rate of the excited level, Δ is the detuning of the trapping light from resonance, I is the intensity of the trapping light, $\mathbf{r}$ is a spatial position coordinate, c is the speed of light and $\hbar$ is Planck's constant.

With red-detuned light (i.e. $\Delta < 0$), the potential minima, where the atoms get trapped, are positioned at the regions of highest intensity. Hence, the focus of a red-detuned laser acts as an optical dipole trap.

Whilst the interaction potential scales as I/Δ, the scattering rate scales as

I/Δ^2. Hence, to create an optical dipole trap with a large interaction potential and a small scattering rate, ones tries to achieve high intensities and large detunings.

6.2.2.3 Multiple dipole traps

It is possible to generate multiple dipole traps. Bergamini *et al.* [2004] generated multiple micron-sized optical dipole traps using holographic techniques and a programmable liquid crystal spatial light modulator. As shown in Figure 6.2, the traps can be placed in different geometrical arrangements. Furthermore, the distances between the traps can be controlled with micrometre precision (see Figure 6.3).

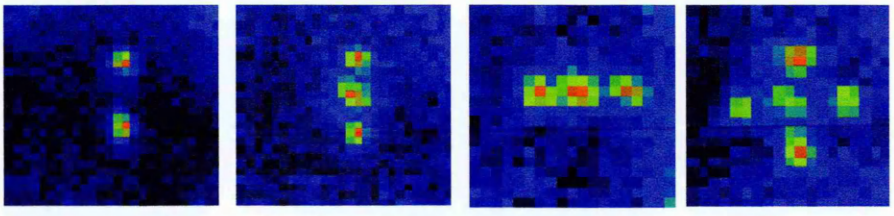

Figure 6.2: Figure from Bergamini *et al.* [2004] showing some different geometrical arrangements in which the traps can be placed.

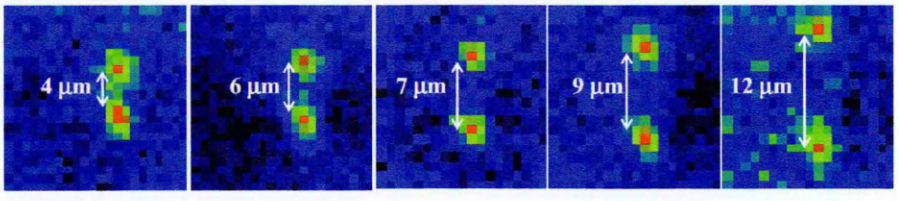

Figure 6.3: Figure from Bergamini *et al.* [2004] showing that the distance between the traps can be finely controlled.

As explained in section 5.5.2, using multiple dipole traps in a cold atom implementation of the DQC1 model would allow a wide variety of non-trivial unitary processes to be investigated. The ability to place different numbers of individually addressable traps in different relative positions, as illustrated in Figure 5.11(a), would be particularly suitable for studying collective phenomena [Olmos *et al.*, 2009a] [Olmos *et al.*, 2009b] [Laycock *et al.*, 2011].

6.3 Imaging Atoms

Once atoms have been cooled, trapped and an interesting phenomenon has occurred, it becomes important to image the atoms.

The collection of low levels of 780 nm fluorescent light from small numbers of atoms trapped in optical dipole traps requires a high numerical aperture ($N.A.$) objective lens. In the current context, the objective lens is also known as the dipole lens. For isotropically fluorescing atoms, we can calculate the fraction of fluorescent light collected by a given lens in the following way. Numerical aperture is defined as: $N.A. = n \cdot \sin(\theta)$, where n is the refractive index of the medium in which the lens operates and θ is the half-angle of the maximum cone of light that can enter the lens. The solid angle Ω of the lens subtended at the position of the trapped is given by: $\Omega = 2\pi(1 - \cos(\theta))$. The fraction of fluorescent light collected is thus $\frac{\Omega}{4\pi}$. So for the Paris ($N.A. = 0.5$), Wisconsin ($N.A. = 0.4$) and Bonn ($N.A. = 0.29$) groups, we find that $\frac{\Omega}{4\pi} = 6.7\%, 4.2\%, 2.1\%$ respectively.

In the next section, I give a detailed description of the imaging system that I designed to image the atoms in the laboratory at The Open University.

6.4 Design Layout

The imaging system was designed using an optical design software package called OpTaliX (see http://www.optenso.com/). The software performs three-dimension ray tracing. The values are kept at 64 bit precision throughout the programme. Once the coarse positions of the optical elements have been set, one can choose a parameter of interest that characterises the system and optimise it by allowing the software to finely adjust the positions of selected optical elements.

The design of the imaging system had to meet numerous requirements.

A simple example of one of the general requirements is that there must be sufficient space between the optical elements for them to be mounted on the optical table in the laboratory. The various requirements will become clear in the following sections. In order to arrive at the final design, I had to go through a lengthy process of trial and improvement. That is, I used the software package to explore different designs and see how well they met all the requirements.

The final design at which I arrived is shown in Figure 6.4. The success with which this design meets the requirements is discussed in section 6.8.

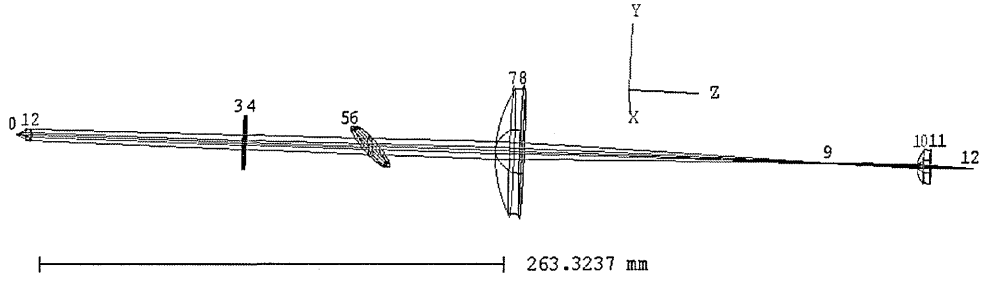

Figure 6.4: Diagram of the optical elements of the imaging system. See text for details.

Figure 6.4 shows the atoms are trapped at position 0. The fluorescence is collected and collimated by a high numerical aperture ($N.A. = 0.5$) aspheric lens (a 352240 lens from Geltech) (surfaces 1 and 2). The collimated light travels through the glass windows of the vacuum chamber (surfaces 3 and 4), through a dichroic beam-splitter (surfaces 5 and 6). The light is focussed by a large aspheric lens (a 75-150LPX lens from Asphericon) (surface 7 and 8). A 40 μm radius pinhole is placed at position 9. This pinhole will allow the fluorescent light to continue to propagate down the optical axis but will block stray light from getting any further. A high numerical aperture aspheric lenses (a 20-18HPX lens from Asphericon) then focusses the fluorescent light onto an intensified charge-coupled device (ICCD) at position 12. Ideally, the fluorescent light should be focussed onto a single pixel of the ICCD in order to maximise the signal-to-noise ratio (i.e. maximise the number of photons emitted by the

atoms compared to the number of photons from background sources of light).

6.5 On-axis Imaging Performance and Spot Diameter

This design gives an on-axis Strehl ratio of 0.99930 and a magnification of 9.31. The Strehl ratio is a parameter that compares the performance of the imaging optics to the diffraction-limited ideal case [Sortais *et al.*, 2007]. It serves to characterise the effect of the aberrations in the optics on the wave front of the light. The Strehl ratio, S, is given by

$$S = \frac{I_{\text{aberr}}}{I_{\text{ideal}}} \simeq 1 - \frac{4\pi^2\Delta^2}{\lambda^2}, \tag{6.3}$$

where I_{aberr} is the peak light intensity in the image plane in the presence of aberrations, I_{aberr} is the peak light intensity in the image plane in the ideal, diffraction-limited case (i.e. in the theoretical limit of no aberrations), Δ is the root-mean-square departure of the actual wave front with respect to the ideal one, and λ is the wavelength of the light that is being imaged.

It is important to have a Strehl ratio close to one because a distorted wave front would result in the energy of the collected fluorescent light being spread out, which would reduce the signal-to-noise ratio at the ICCD. Desirable values of the Strehl ratio are, arbitrarily, $S \gtrsim 0.8$ (i.e. $\Delta \lesssim \lambda/14$).

The on-axis point spread function (PSF) is shown in Figure 6.5. The spot diameter is 20 μm. This design would therefore be suitable for an ICCD with a pixel size of 20 μm.

The spot size can be characterised in other ways. The fraction of energy deposited in the image plane within a certain diameter is shown in Figure 6.6. This graph shows that about 80% of the energy is deposited within a diameter of 20 μm and the remaining energy is spread over a hundreds of micrometres.

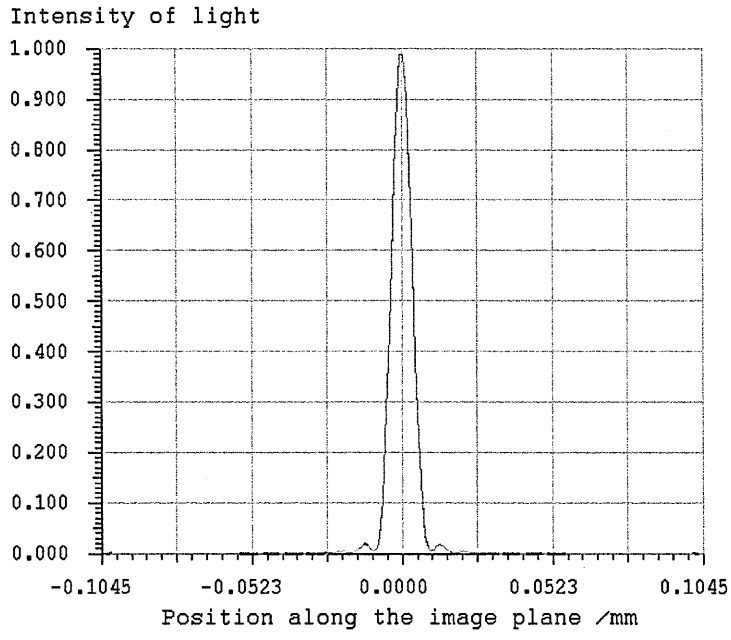

Figure 6.5: On-axis PSF.

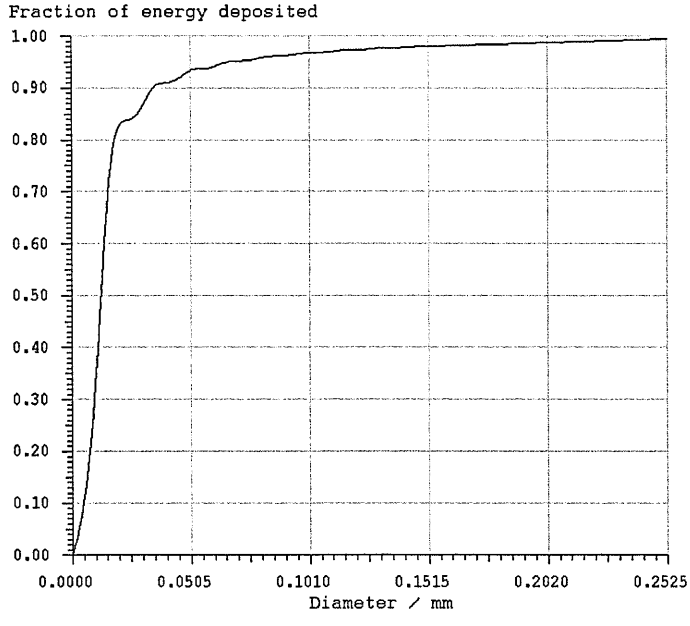

Figure 6.6: Fraction of energy deposited in the image plane within a certain diameter.

So far, we have just been considering the PSF. OpTaliX allows the imaging of extended objects to be simulated. Figure 6.7 shows image plane (in a false colour scale) when a 1 μm diameter object emits light with a Gaussian intensity profile. The scale on the diagram is in millimetres. The diagram shows that

most of the light forms a spot that has a diameter of about 20 μm. I chose the object to be as similar as possible to a point-like atom moving around in a micrometre-scale trap[1].

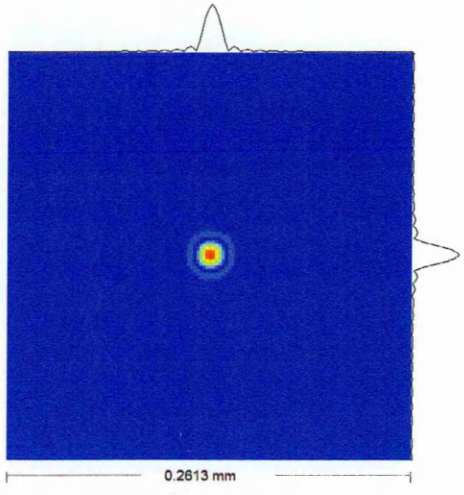

Figure 6.7: Image plane (in a false colour scale) when a 1 μm diameter object emits light with a Gaussian intensity profile.

The performance of an imaging system can also be characterised by the modulation transfer function (MTF). The MTF characterizes how the imaging optics attenuates the amplitudes of the emitted spatial frequencies. Spatial frequency is measured in line pairs per millimetre where a line pair is a black line next to a white line.

Figure 6.8 shows the on-axis MTF of the final design. The relative attenuation of emitted spatial frequencies is very close to the ideal, diffraction-limited case. MTF is quite useful for determining the optimal radius of the pinhole: the smaller the radius of the pinhole, the more stray light is prevented from reaching the ICCD; yet the pinhole radius should not be so small that it blocks out any of the spatial frequencies collected by the dipole lens. So by decreasing pinhole radius and comparing their MTF graphs, I determined that a pinhole with a radius of 40 μm or larger would be most suitable for filtering stray light.

[1]The spatial part of the wavefunction of an atom undergoing simple harmonic motion in a dipole trap is Gaussian.

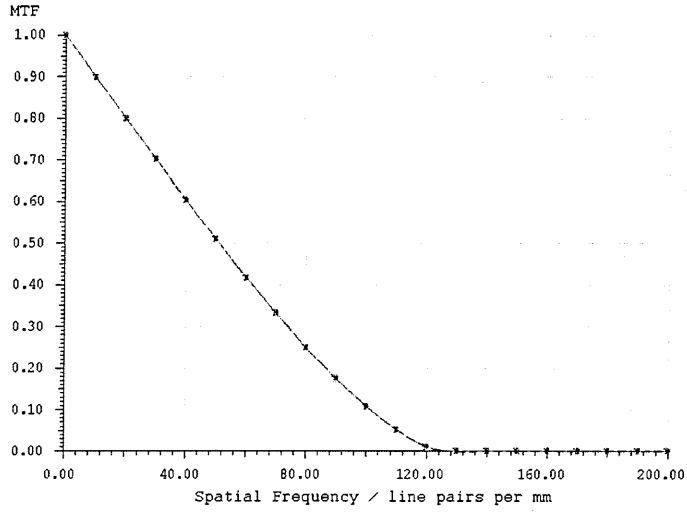

Figure 6.8: On-axis modulation transfer function (MTF) of the final design.

6.6 Off-axis Imaging Performance

In order to investigate the off-axis performance of the imaging system, I changed surface 9 so that it was no longer a pinhole, but rather a completely transparent surface (since for off-axis imaging it is not possible to achieve as aggressive filtering of stray light whilst still allowing all the collected spatial frequencies to reach the ICCD). This gave the result that $S > 0.8$ when the atom is moved < 60 μm away from the optical axis. This is a promising result since it shows that it may be possible to image a small, two-dimensional array of trapped atoms, even the atoms in the array that are trapped tens of micrometres away from the optical axis.

6.7 Tolerance

Whilst the performance of the imaging system is, as indicated in the previous sections, sufficient for our needs, we have so far only discussed the case of perfectly aligned optical elements. In reality, we cannot position the optical elements to arbitrary precision and accuracy. Hence, it is necessary to see how the performance of the imaging system will change in response to misalignments

of the optical elements. Such calculations have been performed in OpTaliX and are presented in Tables 6.1 and 6.2. See the following subsections for details.

Compensators:			THI S11		
Parameters:			STREHL	MAG	BFL
Nominal values:			0.99930	9.30698	24.32216
Surface	Tol.	(mm)			
0	*DLT*	0.1000 (+)	-0.09700	0.00000	5.18600
		(-)	-0.05372	0.00000	-27.67445
2	*DLT*	10.0000 (+)	-0.00004	-0.31456	0.18608
		(-)	0.00002	0.33736	-0.19906
3	*DLT*	1.0000 (+)	0.00000	-0.02149	0.01270
		(-)	0.00000	0.02159	-0.01276
4	*DLT*	10.0000 (+)	-0.00004	-0.31456	0.18608
		(-)	0.00002	0.33736	-0.19906
6	*DLT*	10.0000 (+)	-0.00004	-0.31456	0.18608
		(-)	0.00002	0.33736	-0.19906
8	*DLT*	1.0000 (+)	-0.00002	-0.29804	0.33080
		(-)	0.00001	0.31843	-0.35302
9	*DLT*	1.0000 (+)	-0.00002	-0.29804	0.33080
		(-)	0.00001	0.31843	-0.35302
	RSS		0.11089	1.00979	
7	*DLY*	1.0000 (+)	-0.06096	0.00000	0.11781
		(-)	-0.06505	0.00000	0.11465
10	*DLY*	1.0000 (+)	-0.01005	0.00000	0.03857
		(-)	-0.00883	0.00000	0.04345
	RSS		0.09015	0.00000	
	Total RSS		0.14291	1.00979	

Table 6.1: This table shows the how the value of the Strehl ratio, magnification (MAG) and back focal length (BFL) depend on the displacements of the lenses from their optimal positions, both along the optical axis (*DLT* tolerance) and transverse to the axis (*DLY* tolerance). See the main text for details.

The parameter *DLT* refers to the change in the distance between the indicated surface and the following one. The parameter *DLY* refers to the change in the displacement of the indicated surface away from the optical axis. RSS $= (\sum_i \Delta F_i^2)^{0.5}$ where ΔF_i denotes the change in a parameter (e.g. Strehl ratio or magnification) due a change in the distance between surfaces i and $i+1$.

When the calculations are performed with "THI S11" acting as a "compen-

		Compensators:		None	
		Parameters:		STREHL	MAG
		Nominal values:		0.99930	9.30698
Surface	Tol.	(mm)			
0	*DLT*	0.1000 (+)		-0.99160	0.00000
		(-)		-0.99191	0.00000
2	*DLT*	10.0000 (+)		-0.06918	-0.15998
		(-)		-0.06630	0.16568
3	*DLT*	1.0000 (+)		-0.00032	-0.01076
		(-)		-0.00029	0.01078
4	*DLT*	10.0000 (+)		-0.06918	-0.15998
		(-)		-0.06630	0.16568
6	*DLT*	10.0000 (+)		-0.06918	-0.15998
		(-)		-0.06630	0.16568
8	*DLT*	1.0000 (+)		-0.20225	-0.15144
		(-)		-0.19982	0.15654
9	*DLT*	1.0000 (+)		-0.20225	-0.15144
		(-)		-0.19982	0.15654
	RSS			1.46846	0.50423
7	*DLY*	1.0000 (+)		-0.01316	0.00000
		(-)		-0.01388	0.00000
10	*DLY*	1.0000 (+)		-0.00236	0.00000
		(-)		-0.00206	0.00000
	RSS			0.01938	0.00000
	Total RSS			1.46858	0.50423

Table 6.2: This table shows the how the value of the Strehl ratio, magnification (MAG) and back focal length (BFL) depend on the displacements of the lenses from their optimal positions, both along the optical axis (*DLT* tolerance) and transverse to the axis (*DLY* tolerance). See the main text for details.

sator," this means that the distance between surfaces 11 and 12 (i.e. between the final lens and the ICCD) is always readjusted before calculating the change in the performance of the system. However, when considering the tolerance of the positioning of each optical element, it may be also useful to look at the tolerance with no compensator (i.e. without always readjusting the distance between the final lens and the ICCD before calculating the change in the performance of the system). It is important to note that in the lab, the position of the ICCD will frequently be readjusted during alignment and so the tolerance data calculated without a compensator should not be taken as a direct indicator

of the precision with which we will need to align the optical elements. Rather, this set of tolerance data is included in the report because it serves to highlight which optical elements need to be aligned most precisely and because it gives a sense of the challenges that will be encountered during the alignment process.

With regards to misplacements along the axis (i.e. the *DLT* tolerances), it seems that getting the focus of the trapping light in exactly the right place relative to the dipole lens will be quite important. The results also show that how well the position and thickness of the vacuum chamber window have been modelled is not a concern since the decrease in performance of the imaging due to the window is negligible. This can be attributed to the fluorescent light being approximately collimated as it passes through the window. The tolerance on the positions of the lenses seems fairly good considering that it may be possible to mount these lenses on translation stages that can be moved with micrometre precision.

With regards to misalignments perpendicular to the optical axis (i.e. the *DLY* tolerances), it seems that the optical system is fairly tolerant. It may be possible to mount adjacent optical elements on the same piece of mounting apparatus and thus keep misalignments perpendicular to the axis to a minimum. Even this turns out not to be possible, the calculated values indicate that such misalignments will not decrease the image performing beyond acceptable limits.

Whilst calculating the tolerance parameters, both along and perpendicular to the optical axis, I changed surface 9 so that it was no longer a pinhole, but rather a completely transparent surface. I did this because the slight misalignments prevented the light from passing through the pinhole, thus preventing the tolerances from being calculated. Calculating the tolerance in this way reflects the way in which the optical components will be aligned in the lab (i.e. the pinhole will probably only be put in position once the rest of the optics have been aligned).

Tolerance analysis (not shown) with surface 9 as a 40 μm radius pinhole

shows that the pinhole must have a misalignment perpendicular to the optical axis of less than a few tens of microns (which is what one would expect given that the radius is a few tens of microns) and a misalignment along the optical axis of less than a few millimetres.

6.7.1 Tolerance on the Distance Between the Final Lens and the ICCD

		Compensators:	None
		Parameter:	STREHL
		Nominal value:	0.99930
Surface	Tol.	(mm)	
11	*DLT*	0.5000 (+)	-0.88708
		(-)	-0.91591
	RSS		1.27507
	DLT	0.1000 (+)	-0.07208
		(-)	-0.07400
	RSS		0.10330
	DLT	0.0500 (+)	-0.01862
		(-)	-0.01873
	RSS		0.02641

Table 6.3: This table shows the tolerance on the distance between the final lens and the ICCD.

The tolerance data on the distance between the final lens and the ICCD is shown in Table 6.3. The distance definitely needs to be controlled to a precision better than half a millimetre. However, a precision of tens of micrometres is required to give the desired optical performance.

6.8 Final Design Considerations

This design meets our requirements fairly well. A beam splitter has been included in the design in order to make sure that the optics for the trapping light and the imaging light are compatible. The beam splitter is 7 cm away from both the window and the large aspheric lens. This should give just enough

room for the mounting. The interference filter could be placed between the large aspheric lens and the pinhole. There is 5 cm between the pinhole and the final lens. We will put a flipper mirror in this space so that we can send all of the light to the APD when we perform fast time-scale experiments and all of the light to the ICCD when we would like to image the atoms. The distance between the final lens and the ICCD is 2.4 cm. This should be sufficient to allow us to mount the lens and the ICCD.

The distance between the final lens and the ICCD would need to be controlled to a precision of better than 50 μm in order to achieve a Strehl ratio of about $0.98(= 0.999 - 0.019)$. Achieving such precision may be possible if we mount the ICCD on a micrometre stage. In practice, all the degrees of freedom of this set-up will need to be aligned at once, so it would not be realistic to expect the quality of the image to be as high as 0.99 or 0.98 (e.g. experimentally, Sortais *et al.* [2007] achieve an on-axis Strehl ratio of 0.93).

For the filtering of stray light, we can try pinholes of various radii and see how aggressively we need to filter. The model suggests that the pinhole radius should be greater than 40 μm so that we do not filter out the spatial frequencies that we want to collect. This design gives a spot diameter of about 20 μm. Hence, the suitability of this design will have to be compared with the suitability and the expense of ICCDs with 20 μm pixels.

6.9 Experimental Implementation of the Design

After I finished the design, the optical system was successfully assembled in the laboratory, as shown in Figure 6.9.

The imaging system was then tested by inserting a 200 line/mm grating in the imaging plane of the system. The obtained image is shown in Figure

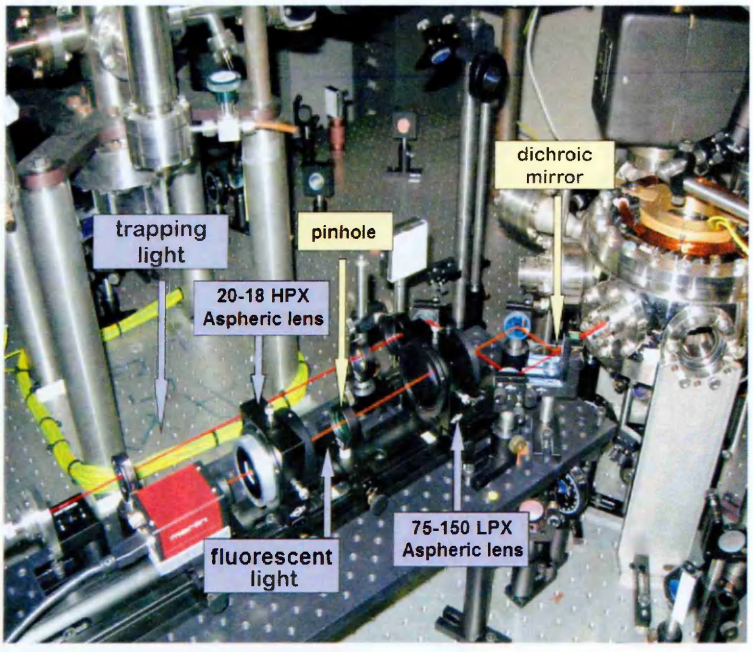

Figure 6.9: Experimental implementation of the optical system. The 352240 lens from Geltech is inside the vacuum chamber. The camera shown in the figure is an ordinary camera (which will be replaced with an ICCD in due time).

6.10(a). The measured magnification was 9.31, which is just as it was designed to be. In Figure 6.10(b), the counts are plotted and compared to a simple curve.

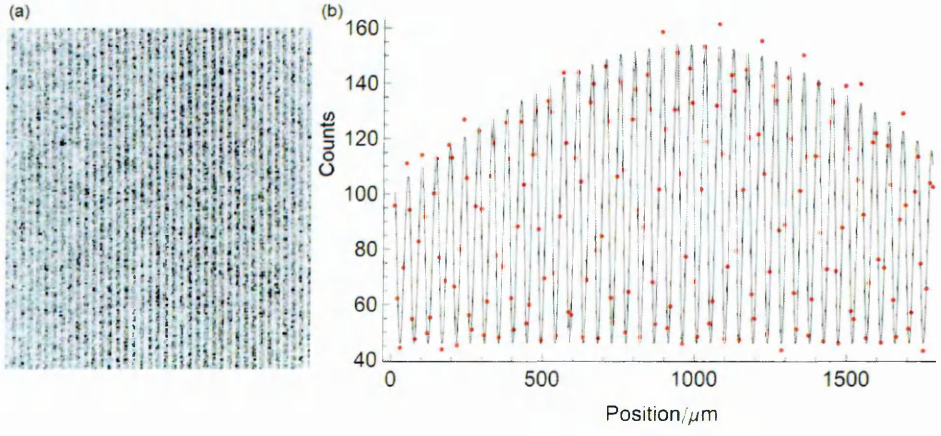

Figure 6.10: Test of the imaging system with 780 nm light. (a) An image of a grating with 200 lines per millimetre. The measured magnification is 9.31. (b) Analysis of the image. The red dots are the data points and the curve is a damped sinusoidal function.

Finally, I sent 50 mW of trapping light into the chamber. The trapping light has a wavelength of 830 nm, which constitutes a red-detuning of 50 nm from the 780 nm, $5P_{3/2}$ to $5S_{1/2}$ transition. With the MOT and the dipole trap overlapping, I loaded the optical dipole trap. The experimental sequence involved creating the dipole trap, loading the MOT for 3 ms, turning the magnetic fields off for 5 ms, turning everything apart from the dipole trap off for 2.5 ms and then imaging the dipole-trapped atoms for 25 μs [Kowalczyk, 2013]. Approximately 65 atoms were trapped (see Figure 6.11).

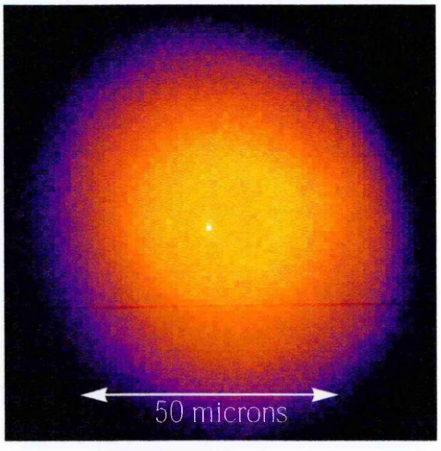

Figure 6.11: Image of the dipole trap. Note how the light from the trap is incident on only one pixel.

6.10 Summary

In this chapter, I discussed the laboratory equipment that will be used to implement DQC1 protocols using cold atoms. I outlined the techniques for cooling and trapping neutral atoms and I mentioned the lasers that can perform two-photon excitation of the atoms to Rydberg states.

I then presented my design of a high-performance optical system for imaging cold, trapped atoms. The system was designed with realistic conditions in mind (e.g. the tolerance on the positioning of the optical elements). I implemented the design and tested it by imaging a grating. Finally, I dipole-trapped and

imaged tens of atoms.

Chapter 7

Conclusions

The central conclusion of this thesis is that the DQC1 model can be implemented in a cold atom set-up that is both technologically feasible and highly versatile. To arrive at this conclusion, I showed that:

- atoms can be prepared in optical dipole traps in the states required for DQC1 (see Chapter 5);
- controlled, Rydberg-based logic gates can be performed with ensembles of atoms (see Chapter 3)[1];
- a high performance optical system can be built to collect fluorescent light from the atoms and thus determine the outcome of a DQC1 protocol (see Chapter 6).

Furthermore, from the detailed considerations presented in Chapter 5, one can conclude that the cold atom implementation of the DQC1 model can be extremely large-scale (e.g. the normalised trace of a 2^{100}-by-2^{100} unitary matrix could be estimated [Mansell & Bergamini, 2014]). The numerical simulations showed that large, trivial unitaries can be used to benchmark the experimental implementation even in the presence of run-to-run fluctuations in the number of atoms loaded into the ensemble dipole trap.

[1]This chapter includes the work of myself and colleagues [Beterov *et al.*, 2013] [Beterov *et al.*, 2014] in which we devise a logic gate that would allow the special qubit of the DQC1 protocol to be encoded not in a single atom but in an ensemble. The advantages of working with ensembles rather than single atoms is discussed in section 3.2.2.

The work presented in Chapter 5 included a scheme for implementing cold atom unitaries in a controlled way, thus allowing such unitaries to be investigated in the proposed cold atom implementation of the DQC1 model. Given the flexibility of the cold atom set-up, one can conclude that non-trivial unitaries, such as those related to many-body processes, could be investigated. This is an important finding because non-trivial quantum dynamics is currently an area of intensive research [Amico *et al.*, 2008] [Bloch *et al.*, 2008].

The work on the optical system, presented in Chapter 6, was an important step towards the laboratory implementation of the DQC1 model. The remaining steps include: exciting the trapped atoms to a Rydberg state such that the resulting blockaded region is larger than the sample size; using a spatial light modulator to create multiple traps; observing inter-trap Rydberg blockade; observing EIT; and setting up the necessary lasers to perform Raman transitions. With these steps completed, everything would be in place to attempt experimental runs of the protocol for normalised trace estimation.

Overall, the ability to investigate non-trivial processes in extremely large Hilbert spaces is an exciting prospect, especially when one recalls (see Chapter 2) that cold atom systems are very versatile and their quantum mechanical degrees of freedom can be well-controlled [Miroshnychenko *et al.*, 2006] [Beugnon *et al.*, 2007]. Other avenues for exploration include investigations of nonclassical correlations and the implementation of the rich variety of protocols within the DQC1 model (see Chapter 4).

The goal of quantum technology superseding the achievements of classical technology is being approached by the community of quantum physics researchers on many fronts [Preskill, 2011]. The work described in this thesis, taken in conjunction with some recent theoretical results on the hardness of classically simulating the DQC1 model [Morimae *et al.*, 2014] [Morimae & Koshiba, 2014], constitutes progress towards this goal.

Chapter 8

Appendix

8.1 Historical Context of the Research

Quantum computation and the laser cooling of neutral atoms are fields that, as shown in Figure 8.1, began at roughly the same time and developed in parallel. The 1980s and 1990s were decades of tremendous experimental progress for laser cooling. During this time, some important theoretical discoveries were made in the field of quantum computation. By the turn of the millennium, many researchers had begun the task of experimentally building a quantum computer. There were far too many developments to summarise in a diagram like Figure 8.1, so instead of attempting this, I focussed on the strands of research most relevant to this thesis: Rydberg physics and DQC1.

8.2 Rubidium-87 Energy Levels

The energy levels of Rubidium-87 are shown in Figure 8.2.

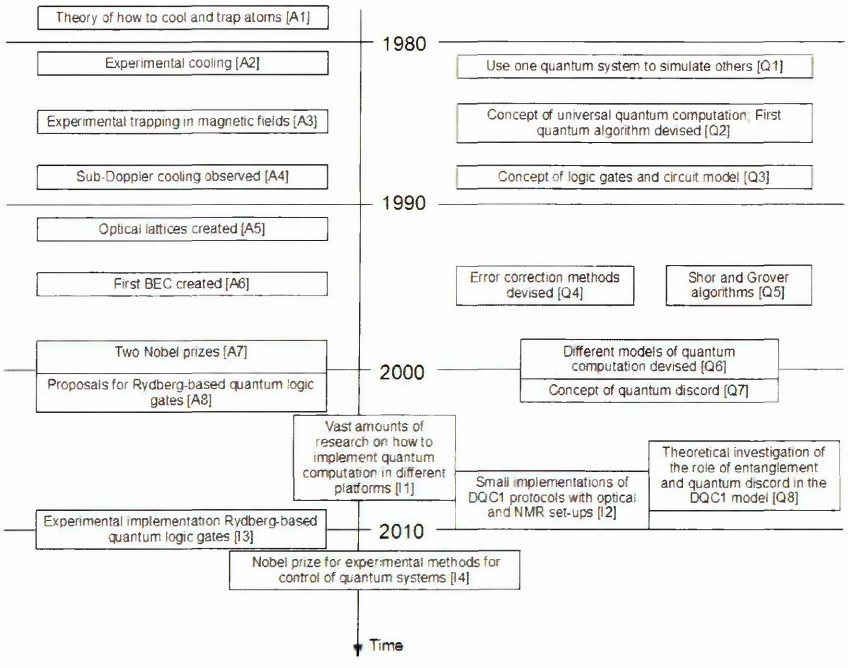

Figure 8.1: A potted history of the relevant fields. The references for the research related to cold atoms, quantum computation and implementations of quantum computers are given in footnotes [1], [2] and [3] respectively.

8.3 Further Rydberg Phenomena

Some Rydberg phenomena that are not central to the main thesis are now mentioned for the sake of giving the reader a more complete flavour of the richness of Rydberg physics.

8.3.1 Macrodimers

In 2000, Greene *et al.* [2000] proposed the creation of "trilobite" Rydberg molecules, so named due to the similarity between the shapes of the probability

[1] A1=[Ashkin, 1978]. A2=[Phillips & Metcalf, 1982]. A3=[Migdall *et al.*, 1985] [Raab *et al.*, 1987]. A4=[Lett *et al.*, 1988]. A5=[Jessen *et al.*, 1992] [Verkerk *et al.*, 1992] A6=[Anderson *et al.*, 1995] [Davis *et al.*, 1995]. A7=[Chu *et al.*, 1997] [Cornell *et al.*, 2001]. A8=Jaksch *et al.* [2000] Lukin *et al.* [2001].

[2] Q1=[Feynman, 1982]. Q2=[Deutsch, 1985]. Q3=[Deutsch, 1989]. Q4=[Shor, 1995] [Steane, 1996b] [Steane, 1996a] [Calderbank & Shor, 1996]. Q5=[Shor, 1994] [Grover, 1996]. Q6=[Kitaev, 2003] [Kitaev, 1997] [Knill & Laflamme, 1998] [Farhi *et al.*, 2001] [Raussendorf & Briegel, 2001]. Q7=[Henderson & Vedral, 2001] [Ollivier & Zurek, 2001]. Q8=[Datta *et al.*, 2005] [Datta *et al.*, 2008].

[3] I1=[Beth *et al.*, 2008] [Hughes *et al.*, 2004] [Ladd *et al.*, 2010]. I2=[Lanyon *et al.*, 2008] Passante *et al.* [2009][Marx *et al.*, 2010]. I3=[Isenhower *et al.*, 2010] [Wilk *et al.*, 2010]. I4=[Haroche & Wineland, 2012].

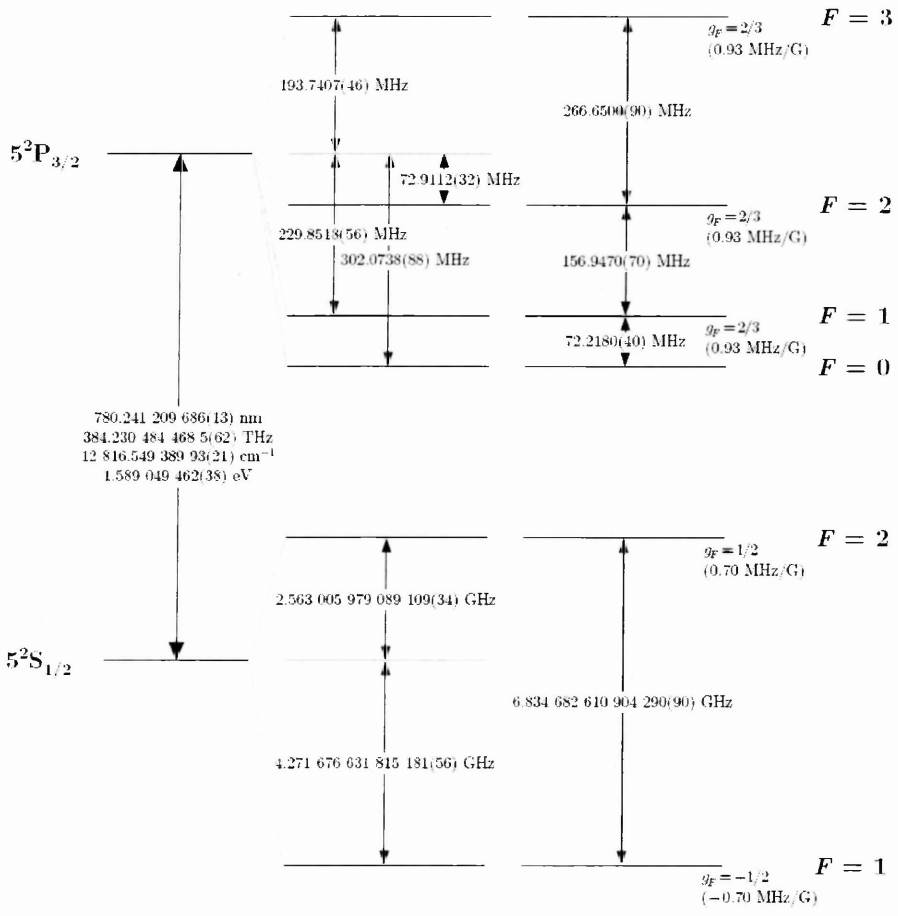

Figure 8.2: An energy level diagram for Rubidium-87 (taken from the website http://steck.us/alkalidata/).

density of the electron and the appearance of a extinct marine animals, trilobites.

In 2002, Boisseau *et al.* [2002] predicted the existence of macrodimers: ultralong range Rydberg dimers with equilibrium separations of many thousands of Bohr radii. They analysed np-np macrodimers. In 2009, Bendkowsky *et al.* [2009] observed ns-ns macrodimers.

8.3.2 Rydberg excited ensembles and quantum optical effects

Ensembles interact more strongly with a radiation field than single quantum objects and may thus be less experimentally challenging (e.g. there is less need to place them inside reflective cavities).

There are cooperative photon emission effects such as superradiance [Dicke, 1954]. Wang *et al.* [2007] obtained excellent agreement between their experimental and theoretical investigations of superradiant effects in high density ultracold atom samples. Since the wavelengths, λ, of the transitions between Rydberg states are long, the cooperative parameter, $C = N\lambda^3/4\pi^2$, in sample with a high density of atoms, N, is large. Superradiance competes with excitation transfer effects [Day *et al.*, 2008]. However superradiant effects are not expected to occur in fully blockaded samples (i.e blockade radius > sample size).

Superradiance could be employed to help create a quantum network [Vuletic, 2006].

The proposals for deterministic repeaters require conversion of atomic qubits into photonic qubits. This would also be very useful for linking quantum computers together over a quantum internet.

8.3.3 Ultracold Plasmas

Ultracold plasmas have ion temperatures ranging from tens of milliKelvin to a few Kelvin and electron temperatures ranging from a few Kelvin to one thousand Kelvin [Killian *et al.*, 2007]. They are quite unique systems since other plasmas typically have temperatures of thousands of Kelvin or more.

Cold, dense Rydberg gases can evolve into ultracold plasmas [Vitrant *et al.*, 1982]. Strong, attractive Rydberg-Rydberg forces (e.g. due to resonant dipole-dipole interactions [Li *et al.*, 2005]) can lead to ionising collisions. The resulting ions create an electric field which traps the recently freed electrons in the vicinity of the atoms and ions. These electrons can then collide with the remaining Rydberg atoms, leading to the formation of an ultracold plasma [Robinson *et al.*, 2000].

Recombination of electrons and ions in an ultracold plasma leads to the

formation of Rydberg gases [Killian *et al.*, 2001]. Three body recombination (TBR), in which an ion and two electrons collide, dominates in ultracold plasmas whilst at the temperatures of typical plasmas (i.e. about 1000 K), TBR is only important when the plasma is very dense. This is due to the rate of TBR scaling with electron temperature to the power of -9/2.

8.4 Geometric Discord

Geometric discord quantifies the distance to the closest state with no quantum correlations, where the distance measure is the Hilbert-Schmidt distance and the closest state is found by minimisation. That is:

$$D_{\mathrm{G}} = \min_{\chi \epsilon \Omega_0^A} ||\rho - \chi||^2. \tag{8.1}$$

Here, A and B denote the two subsystems, Ω_0^A is the set of all zero-discord states $\{\chi\}$ where χ can be written as $\sum_j p_j |j\rangle\langle j| \otimes \rho_j^B$ for some complete orthonormal basis $\{|j\rangle\}$. The superscript B denotes that ρ_j^B is the reduced state of B. The Hilbert-Schmidt distance is evaluated according to

$$||\rho - \chi||^2 = \mathrm{Tr}\left[(\rho - \chi)^2\right] \tag{8.2}$$

Geometric discord has found operational interpretations (in terms of remote state preparation for pure two-qubit states [Dakic *et al.*, 2012b] and in quantifying the global impact of local unitary evolutions [Giampaolo *et al.*, 2013]). It has also been found to be useful in analysis of quantum random access codes [Yao *et al.*, 2012] and quantum teleportation [Adhikari & Banerjee, 2012]. However, it is important to note that geometric discord may not be a good measure of non-classical correlations in generic settings [Piani, 2012].

The main problem is that D_{G}^A can increase at no cost to the mutual information when local operations are performed on subsystem B. So, for example,

adding an ancillary state to subsystem B would change D_{G} by a factor equal to the purity of the ancillary state. This problem does not apply to the adjusted version of geometric discord (equation 4.20) [Tufarelli *et al.*, 2013].

8.5 Laser Cooling

In this section, I give further details on the Doppler cooling of Rubidium-87 and the operation of magneto-optical traps.

8.5.1 Doppler Cooling of Rubidium-87

The Doppler cooling of Rubidium-87 requires the use of selection rules to create an effective two-level system. This achieved by using a laser red-detuned from the $5^2S_{1/2}$ F $= 2$ level to the $5^2P_{3/2}$ F $= 3$ transition (see Figure 8.3). Due to the ΔF $= 0, \pm 1$ selection rule on the spontaneous emission of the $5^2P_{3/2}$ F $= 3$ level, we effectively have a two level system.

However, there are no selection rules preventing the $5^2P_{3/2}$ F $= 2$ level from being populated and then decaying to the $5^2S_{1/2}$ F$= 1$ level (see Figure 8.3). Atoms that populate this level are so far detuned from the incident laser light that they remain in this level and consequently stop undergoing cooling cycles. This problem can be solved by using "repumper" light to excite from $5^2S_{1/2}$ F$= 1$ to the $5^2P_{3/2}$ F $= 2$ level, so that there is then a non-zero probability for decay into the $5^2S_{1/2}$ F$= 2$ level and thus for the cooling cycles in the effective two-level system to restart.

8.5.2 Magneto-optical Traps

In the following, I explain the operation of a MOT.

The magnetic field required for a MOT is created two identical coils carrying opposite currents. The coils are separated by 1.25 times their radius, which

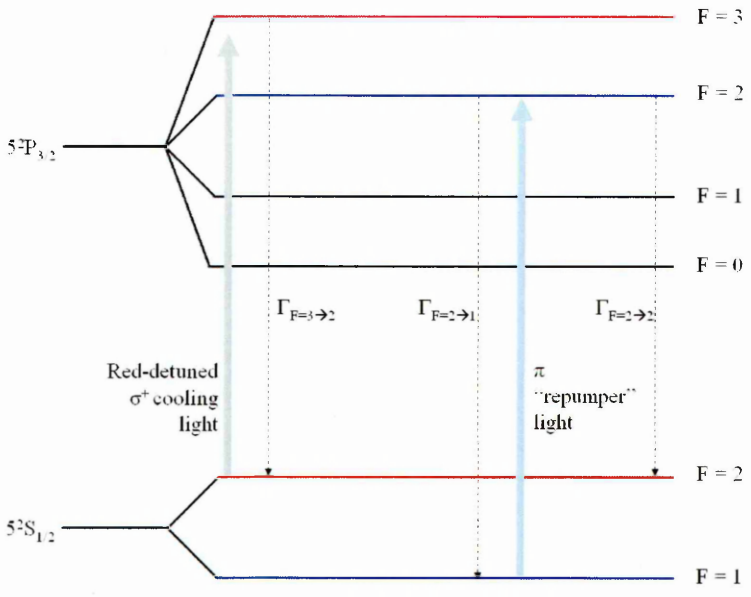

Figure 8.3: Schematic diagram showing Doppler cooling of Rubidium 87. A closed two level system is effectively formed by the $5^2S_{1/2}$ F = 2 level and the $5^2P_{3/2}$ F = 3 shown in red. The red-detuned σ^+ polarised light (grey arrow) and spontaneous F = 3 → 2 emission are called "cycling" or "cooling" transitions. Even though the $5^2P_{3/2}$ F = 2 and $5^2S_{1/2}$ F= 1 levels, shown in blue, do get populated, the linearly polarised "repumper" light and the spontaneous F = 2 → 2 emission serve to return the atoms to the states that are subject to Doppler cooling.

results in a magnetic field, B, that is zero at the centre of the trap and linearly inhomogeneous along the axis of the coils. If this axis is the z-axis of a Cartesian coordinate system, the modulus of the magnetic field is $|B| = B'\sqrt{x^2 + y^2 + 4z^2}$, where B' is the gradient of the magnetic field.

Let us consider a one-dimensional example (with z as the position coordinate) where two counter propagating laser beams of opposite circular polarization (σ^+ and σ^-) are incident on a gas of atoms. Each laser is detuned below the zero magnetic field atomic resonance by δ, as shown in Figure 8.4[1]. Due to the Zeeman effect, in positions with positive values of z, the $\Delta m_F = +1$ transition (coupled by the σ^+ light) is shifted further from resonance and the $\Delta m_F = -1$

[1]The atoms shown in the Figure are Rubidium-87 atoms with the lasers operating on the $5^2S_{1/2}$ F= 2, $m_F = 2$ to $5^2P_{3/2}$ F = 3 $m_F = 3$ and $m_F = 1$ transitions. The $\Delta m_F = 0$ transition is forbidden due to a selection rule. Other atoms, e.g. other alkali atoms, have similar transitions, obey similar selection rules and can also be confined in a MOT.

transition (coupled by the σ^- light) is shifted closer to resonance. Thus, atoms in positions with positive values of z preferentially absorb σ^- polarised light. Similarly, atoms in positions with negative values of z preferentially absorb σ^+ polarised light.

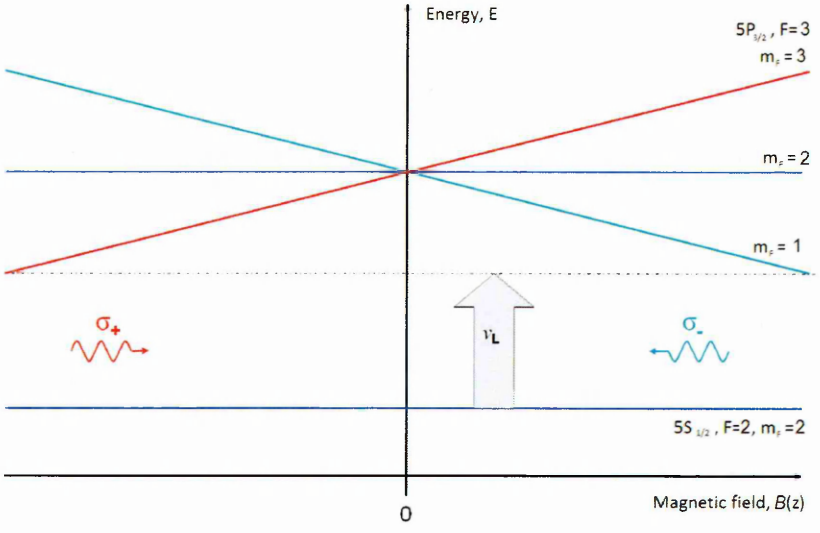

Figure 8.4: A schematic diagram of a MOT, showing two, oppositely circularly polarised, counter-propagating lasers. Both these lasers have the same frequency, ν_L, which is below the resonant frequency of the atomic transitions. The energy, E, of the atomic levels is shown as a function of the applied magnetic field, B, which, in turn, is a function of the spatial position (see the main text for further details).

One can recall from section 6.1 that when an atom is subject to red-detuned photons from a laser beam, the many cycles of absorption and spontaneous emission lead to a change in the component of the momentum of the atom in the direction of the photon propagation. Hence, with the lasers propagating as shown in Figure 8.4 (i.e. with σ^- polarised light propagating in the negative z direction and σ^+ polarised light propagating in the positive z direction), all the atoms experience a net force pushing them towards $z = 0$: the atoms in the positions with positive values of z experience a net force pushing them in the negative z direction whilst the atoms in positions with negative values of z experience a net force pushing them in the positive z direction. Hence, the centre of the trap is at $z = 0$.

It is important to note that the absorption of photons is more highly preferential for atoms further away the centre of the trap than for atoms closer to the centre. This means that magnitude of the net force that the atoms experience is larger for atoms further from trap centre[1]. The net force is therefore a restoring force that confines, or traps, the atoms near $z = 0$.

[1]That is, the net force is proportional to $-z$.

References

AARONSON, S. & ARKHIPOV, A. (2011). The computational complexity of linear optics. In *Proceedings of the 43rd annual ACM symposium on Theory of computing*, STOC '11, 333–342, ACM, New York, NY, USA. 12, 72

ABEYESINGHE, A., DEVETAK, I., HAYDEN, P. & WINTER, A. (2009). The mother of all protocols: restructuring quantum informations family tree. *Proceedings of the Royal Society A: Mathematical, Physical and Engineering Science*, **465**, 2537–2563. 74

ADESSO, G. & DATTA, A. (2010). Quantum versus classical correlations in gaussian states. *Phys. Rev. Lett.*, **105**, 030501.

ADHIKARI, S. & BANERJEE, S. (2012). Operational meaning of discord in terms of teleportation fidelity. *Phys. Rev. A*, **86**, 062313. 103, 147

AHRENS, J., BADZIACEDILG, P., CABELLO, A. & BOURENNANE, M. (2012). Experimental device-independent tests of classical and quantum dimensions. *Nature Physics*, **8**, 592–595. 105

AKULIN, V.M., GERSHKOVICH, V. & HAREL, G. (2001). Nonholonomic quantum devices. *Phys. Rev. A*, **64**, 012308. 115

ALICKI, R., PIANI, M. & RYN, N.V. (2008). Quantumness witnesses. *Journal of Physics A: Mathematical and Theoretical*, **41**, 495303. 81

ALT, W. (2002). An objective lens for efficient fluorescence detection of single atoms. *Optik*, **113**, 142–144. 119

AMICO, L., FAZIO, R., OSTERLOH, A. & VEDRAL, V. (2008). Entanglement

in many-body systems. *Rev. Mod. Phys.*, **80**, 517–576. 85, 142

ANDERLINI, M., LEE, P.J., BROWN, B.L., SEBBY-STRABLEY, J., PHILLIPS, W.D. & PORTO, J.V. (2007). Controlled exchange interaction between pairs of neutral atoms in an optical lattice. *Nature*, **448**, 452–456. 20

ANDERS, J., OI, D.K.L., KASHEFI, E., BROWNE, D.E. & ANDERSSON, E. (2010). Ancilla-driven universal quantum computation. *Phys. Rev. A*, **82**, 020301. 12

ANDERSON, M., ENSHER, J., MATTHEWS, M., WIEMAN, C. & CORNELL, E. (1995). Observation of bose-einstein condensation in a dilute atomic vapor. *Science*, **269**, 198–201. 144

ANDERSON, W.R., VEALE, J.R. & GALLAGHER, T.F. (1998). Resonant dipole-dipole energy transfer in a nearly frozen rydberg gas. *Phys. Rev. Lett.*, **80**, 249–252. 31, 40

ANDRÉ, A., SØRENSEN, A.S. & LUKIN, M.D. (2004). Stability of atomic clocks based on entangled atoms. *Phys. Rev. Lett.*, **92**, 230801. 81

ANISIMOV, P.M., DOWLING, J.P. & SANDERS, B.C. (2011). Objectively discerning autler-townes splitting from electromagnetically induced transparency. *Phys. Rev. Lett.*, **107**, 163604.

AOYAMA, T., HAYAKAWA, M., KINOSHITA, T. & NIO, M. (2012). Tenth-order qed contribution to the electron g - 2 and an improved value of the fine structure constant. *Phys. Rev. Lett.*, **109**, 111807. 5

ARAÚJO, M., FEIX, A., COSTA, F. & BRUKNER, Č. (2013). Quantum circuits cannot control unknown operations, arXiv:1309.7976 [quant-ph]. 111

ASHKIN, A. (1978). Trapping of atoms by resonance radiation pressure. *Phys. Rev. Lett.*, **40**, 729–732. 18, 144

ATES, C., POHL, T., PATTARD, T. & ROST, J.M. (2006). Strong interaction effects on the atom counting statistics of ultracold rydberg gases. *Journal of*

Physics B: Atomic, Molecular and Optical Physics, **39**, L233. 111

AUBIN, S., MYRSKOG, S., EXTAVOUR, M., LEBLANC, L., MCKAY, D., STUMMER, A. & THYWISSEN, J. (2006). Rapid sympathetic cooling to fermi degeneracy on a chip. *Nature Physics*, **2**, 384–387. 17

BAKR, W.S., GILLEN, J.I., PENG, A., FOLLING, S. & GREINER, M. (2009). A quantum gas microscope for detecting single atoms in a hubbard-regime optical lattice. *Nature*, **462**, 74–77. 21

BALENTS, L. (2010). Spin liquids in frustrated magnets. *Nature*, **464**, 199–208. 32

BARAHONA, F. (1982). On the computational complexity of ising spin glass models. *Journal of Physics A: Mathematical and General*, **15**, 3241. 111

BARENDS, R., KELLY, J., MEGRANT, A., VEITIA, A., SANK, D., JEFFREY, E., WHITE, T., MUTUS, J., FOWLER, A., CAMPBELL, B. *et al.* (2014). Superconducting quantum circuits at the surface code threshold for fault tolerance. *Nature*, **508**, 500–503. 15

BARREIRO, J.T., SCHINDLER, P., GÜHNE, O., MONZ, T., CHWALLA, M., ROOS, C.F., HENNRICH, M. & BLATT, R. (2010). Experimental multiparticle entanglement dynamics induced by decoherence. *Nature Physics*, **6**, 943–946. 2, 90

BEALS, T.R., VALA, J. & WHALEY, K.B. (2008). Scalability of quantum computation with addressable optical lattices. *Phys. Rev. A*, **77**, 052309. 18

BÉGUIN, L., VERNIER, A., CHICIREANU, R., LAHAYE, T. & BROWAEYS, A. (2013). Direct measurement of the van der waals interaction between two rydberg atoms. *Phys. Rev. Lett.*, **110**, 263201. 111

BENDKOWSKY, V., BUTSCHER, B., NIPPER, J., SHAFFER, J.P., LW, R. & PFAU1, T. (2009). Observation of ultralong-range rydberg molecules. *Nature*, **458**, 1005–1008. 145

BERGAMINI, S., DARQUIÉ, B., JONES, M., JACUBOWIEZ, L., BROWAEYS, A. & GRANGIER, P. (2004). Holographic generation of microtrap arrays for single atoms by use of a programmable phase modulator. *J. Opt. Soc. Am. B*, **21**, 1889–1894. xxi, 18, 86, 90, 126

BERGMANN, K., THEUER, H. & SHORE, B.W. (1998). Coherent population transfer among quantum states of atoms and molecules. *Rev. Mod. Phys.*, **70**, 1003–1025. 48, 51

BERNON, S., HATTERMANN, H., BOTHNER, D., KNUFINKE, M., WEISS, P., JESSEN, F., CANO, D., KEMMLER, M., KLEINER, R., KOELLE, D. *et al.* (2013). Manipulation and coherence of ultra-cold atoms on a superconducting atom chip. *Nature communications*, **4**, 2380. 17

BETEROV, I.I., TRETYAKOV, D.B., ENTIN, V.M., YAKSHINA, E.A., RYABTSEV, I.I., MACCORMICK, C. & BERGAMINI, S. (2011). Deterministic single-atom excitation via adiabatic passage and rydberg blockade. *Phys. Rev. A*, **84**, 023413. 51, 52, 53, 64

BETEROV, I.I., SAFFMAN, M., YAKSHINA, E.A., ZHUKOV, V.P., TRETYAKOV, D.B., ENTIN, V.M., RYABTSEV, I.I., MANSELL, C.W., MACCORMICK, C., BERGAMINI, S. & FEDORUK, M.P. (2013). Quantum gates in mesoscopic atomic ensembles based on adiabatic passage and rydberg blockade. *Phys. Rev. A*, **88**, 010303. 3, 28, 47, 51, 63, 64, 87, 141

BETEROV, I.I., SAFFMAN, M., ZHUKOV, V.P., TRETYAKOV, D.B., ENTIN, V.M., YAKSHINA, E.A., RYABTSEV, I.I., MANSELL, C.W., MACCORMICK, C., BERGAMINI, S. & FEDORUK, M.P. (2014). Coherent control of mesoscopic atomic ensembles for quantum information. *Laser Physics*, **24**, 074013. 3, 28, 47, 51, 63, 64, 87, 141

BETH, T., BLATT, R., BRIEGEL, H., BRUSS, D., CALARCO, T., CIRAC, J., DEUTSCH, D., EISERT, J., EKERT, A., FABRE, C., GISIN, N., GRANGIER, P., ABD S. HAROCHE, M.G., IMAMOGLU, A., KARLSON, A., KEMPE, J.,

KOUWENHOVEN, L., KRLL, S., LEUCHS, G., LEWENSTEIN, M., LOSS, D., LTKENHAUS, N., MASSAR, S., MOOIJ, J.E., PLENIO, M.B., POLZIK, E., POPESCU, S., REMPE, G., SERGIENKO, A., SUTER, D., THEW, R., TWAMLEY, J., WENDIN, G., WERNER, R., WINTER, A., WRACHTRUP, J., ZANARDI, P., ZEILINGER, A. & ZOLLER, P. (2008). Quantum information processing and comunication - strategic report on current status, visions and goals for research in europe. 144

BEUGNON, J., TUCHENDLER, C., MARION, H., GATAN, A., MIROSHNYCHENKO, Y., SORTAIS, Y.R.P., LANCE, A.M., JONES, M.P.A., MESSIN, G., BROWAEYS, A. & GRANGIER, P. (2007). Two-dimensional transport and transfer of a single atomic qubit in optical tweezers. *Nature Physics*, **3**, 696–699. 15, 142

BLOCH, I. (2005). Ultracold quantum gases in optical lattices. *Nature Physics*, **1**, 23–30. xi, 17

BLOCH, I. (2008). Quantum coherence and entanglement with ultracold atoms in optical lattices. *Nature*, **453**, 1016–1022. 17, 20

BLOCH, I., DALIBARD, J. & ZWERGER, W. (2008). Many-body physics with ultracold gases. *Rev. Mod. Phys.*, **80**, 885–964. 85, 142

BOCHMANN, J., MÜCKE, M., GUHL, C., RITTER, S., REMPE, G. & MOEHRING, D.L. (2010). Lossless state detection of single neutral atoms. *Phys. Rev. Lett.*, **104**, 203601. 22

BOHR, N. (1913). I. on the constitution of atoms and molecules. *Philosophical Magazine Series 6*, **26**, 1–25. 28

BOHR, N. (1935). Can quantum-mechanical description of physical reality be considered complete? *Phys. Rev.*, **48**, 696–702. 73

BOISSEAU, C., SIMBOTIN, I. & CÔTÉ, R. (2002). Macrodimers: Ultralong range rydberg molecules. *Phys. Rev. Lett.*, **88**, 133004. 145

BOLLER, K.J., IMAMOLU, A. & HARRIS, S.E. (1991). Observation of elec-

tromagnetically induced transparency. *Phys. Rev. Lett.*, **66**, 2593–2596. 41

BRADLER, K., WILDE, M.M., VINJANAMPATHY, S. & USKOV, D.B. (2010). Identifying the quantum correlations in light-harvesting complexes. *Phys. Rev. A*, **82**, 062310. 105

BRAGA, H.C., RULLI, C.C., DE OLIVEIRA, T.R. & SARANDY, M.S. (2012). Monogamy of quantum discord by multipartite correlations. *Phys. Rev. A*, **86**, 062106.

BRAUNSTEIN, S.L., CAVES, C.M., JOZSA, R., LINDEN, N., POPESCU, S. & SCHACK, R. (1999). Separability of very noisy mixed states and implications for nmr quantum computing. *Phys. Rev. Lett.*, **83**, 1054–1057. 92

BREKKE, E., DAY, J.O. & WALKER, T.G. (2008). Four-wave mixing in ultracold atoms using intermediate rydberg states. *Phys. Rev. A*, **78**, 063830. 23

BREMNER, M.J., MORA, C. & WINTER, A. (2009). Are random pure states useful for quantum computation? *Phys. Rev. Lett.*, **102**, 190502. 73

BREMNER, M.J., JOZSA, R. & SHEPHERD, D.J. (2011). Classical simulation of commuting quantum computations implies collapse of the polynomial hierarchy. *Proceedings of the Royal Society A: Mathematical, Physical and Engineering Science*, **467**, 459–472. 72

BRENNEN, G.K. (2003). An observable measure of entanglement for pure states of multi-qubit systems. *Quantum Information and Computation*, **3**, 619–626. 81

BRIEGEL, H., BROWNE, D., DÜR, W., RAUSSENDORF, R. & VAN DEN NEST, M. (2009). Measurement-based quantum computation. *Nature Physics*, **5**, 19–26. 20

BRIGGS, G.A.D., BUTTERFIELD, J.N. & ZEILINGER, A. (2013). The oxford questions on the foundations of quantum physics. *Proceedings of the Royal Society A: Mathematical, Physical and Engineering Science*, **469**, 20130299.

5

BRION, E., AKULIN, V.M., COMPARAT, D., DUMER, I., HAREL, G., KÉBAILI, N., KURIZKI, G., MAZETS, I. & PILLET, P. (2005). Coherence protection by the quantum zeno effect and nonholonomic control in a rydberg rubidium isotope. *Phys. Rev. A*, **71**, 052311. 115

BRION, E., COMPARAT, D. & HAREL, G. (2006). Implementation of a cnot gate in two cold rydberg atoms by the nonholonomic control technique. *The European Physical Journal D - Atomic, Molecular, Optical and Plasma Physics*, **38**, 381–387. 115

BRION, E., MØLMER, K. & SAFFMAN, M. (2007). Quantum computing with collective ensembles of multilevel systems. *Physical Review Letters*, **99**, 260501. 39, 110, 115

BRION, E., PEDERSEN, L.H., SAFFMAN, M. & MØLMER, K. (2008). Error correction in ensemble registers for quantum repeaters and quantum computers. *Phys. Rev. Lett.*, **100**, 110506. 110, 115

BRION, E., CARLIER, F., HAREL, G. & AKULIN, V.M. (2011). Nonholonomic quantum control. *Journal of Physics B: Atomic, Molecular and Optical Physics*, **44**, 154001. 115

BRUNNER, N., PIRONIO, S., ACIN, A., GISIN, N., MÉTHOT, A.A. & SCARANI, V. (2008). Testing the dimension of hilbert spaces. *Phys. Rev. Lett.*, **100**, 210503. 105

BULUTA, I. & NORI, F. (2009). Quantum simulators. *Science*, **326**, 108–111. 1

BULUTA, I., ASHHAB, S. & NORI, F. (2011). Natural and artificial atoms for quantum computation. *Reports on Progress in Physics*, **74**, 104401. 15

BURKE, K. & MITCHELL, K.A. (2009). Chaotic ionization of a rydberg atom subjected to alternating kicks: Role of phase-space turnstiles. *Phys. Rev. A*, **80**, 033416. 32

CAILLET, X. & SIMON, C. (2007). Precision of single-qubit gates based on raman transitions. *The European Physical Journal D*, **42**, 341–348. 94, 97

CALDERBANK, A.R. & SHOR, P.W. (1996). Good quantum error-correcting codes exist. *Phys. Rev. A*, **54**, 1098–1105. 144

CAMPBELL, G.K., MUN, J., BOYD, M., MEDLEY, P., LEANHARDT, A.E., MARCASSA, L.G., PRITCHARD, D.E. & KETTERLE, W. (2006). Imaging the mott insulator shells by using atomic clock shifts. *Science*, **313**, 649–652. 20, 40

CANO, D. & FORTÁGH, J. (2012). Nonadditive potentials between three rydberg atoms. *Physical Review A*, **86**, 043422. 112

CARR, A.W. & SAFFMAN, M. (2013). Preparation of entangled and antiferromagnetic states by dissipative rydberg pumping. *Phys. Rev. Lett.*, **111**, 033607. 111

CÉLERI, L.C., MAZIERO, J. & SERRA, R.M. (2011). Theoretical and experimental aspects of quantum discord and related measures. *International Journal of Quantum Information*, **09**, 1837–1873.

CHOTIA, A., VITEAU, M., VOGT, T., COMPARAT, D. & PILLET, P. (2008). Kinetic monte carlo modeling of dipole blockade in rydberg excitation experiment. *New Journal of Physics*, **10**, 045031. 111

CHU, S., COHEN-TANNOUDJI, C. & PHILLIPS, W.D. (1997). The nobel prize in physics 1997, awarded for development of methods to cool and trap atoms with laser light. 144

CIRAC, J.I. & ZOLLER, P. (1995). Quantum computations with cold trapped ions. *Phys. Rev. Lett.*, **74**, 4091–4094. 14

CLAUDON, J., BLEUSE, J., MALIK, N.S., BAZIN, M., JAFFRENNOU, P., GREGERSEN, N., SAUVAN, C., LALANNE, P. & GÉRARD, J.M. (2010). A highly efficient single-photon source based on a quantum dot in a photonic nanowire. *Nature Photonics*, **4**, 174–177. 14

COMPARAT, D. (2009). General conditions for quantum adiabatic evolution. *Phys. Rev. A*, **80**, 012106. 48

COMPARAT, D. & PILLET, P. (2010). Dipole blockade in a cold rydberg atomic sample [invited]. *J. Opt. Soc. Am. B*, **27**, A208–A232. 30

COOPER, J.J., HALLWOOD, D.W. & DUNNINGHAM, J.A. (2010). Entanglement-enhanced atomic gyroscope. *Phys. Rev. A*, **81**, 043624. 81

CORNELL, E.A., KETTERLE, W. & WIEMAN, C.E. (2001). The nobel prize in physics 2001, awarded for the achievement of Bose-Einstein condensation in dilute gases of alkali atoms, and for early fundamental sutdies of the properties of the condensates. 144

CORY, D.G., PRICE, M.D., MAAS, W., KNILL, E., LAFLAMME, R., ZUREK, W.H., HAVEL, T.F. & SOMAROO, S.S. (1998). Experimental quantum error correction. *Phys. Rev. Lett.*, **81**, 2152–2155. 15

DAKIC, B., LIPP, Y.O., MA, X., RINGBAUER, M., KROPATSCHEK, S., BARZ, S., PATEREK, T., VEDRAL, V., ZEILINGER, A., BRUKNER, C. & WALTHER, P. (2012a). Quantum discord as optimal resource for quantum communication, arXiv:1203.1629v1 [quant-ph]. 74

DAKIC, B., LIPP, Y.O., MA, X., RINGBAUER, M., KROPATSCHEK, S., BARZ, S., PATEREK, T., VEDRAL, V., ZEILINGER, A., BRUKNER, C. & WALTHER, P. (2012b). Quantum discord as resource for remote state preparation. *Nature Physics*, **8**, 666–670. 103, 147

DAKIĆ, B., VEDRAL, V. & BRUKNER, I.C.V. (2010). Necessary and sufficient condition for nonzero quantum discord. *Phys. Rev. Lett.*, **105**, 190502. 78, 116

DATTA, A. & SHAJI, A. (2011). Quantum discord and quantum computing: An appraisal. *International Journal of Quantum Information*, **09**, 1787–1805. 71

DATTA, A., FLAMMIA, S.T. & CAVES, C.M. (2005). Entanglement and the

power of one qubit. *Phys. Rev. A*, **72**, 042316. 67, 71, 74, 92, 97, 144

DATTA, A., SHAJI, A. & CAVES, C.M. (2008). Quantum discord and the power of one qubit. *Phys. Rev. Lett.*, **100**, 050502. 71, 73, 78, 144

DAVIS, K., MEWES, M., ANDREWS, M., VAN DRUTEN, N., DURFEE, D., KURN, D. & KETTERLE, W. (1995). Bose-einstein condensation in a gas of sodium atoms. *Physical Review Letters*, **75**, 3969–3973. 144

DAY, J.O., BREKKE, E. & WALKER, T.G. (2008). Dynamics of low-density ultracold rydberg gases. *Phys. Rev. A*, **77**, 052712. 146

DEREVIANKO, A. & KATORI, H. (2011). Physics of optical lattice clocks. *Review of Modern Physics*, **83**, 331–347. 17

DEUTSCH, C., RAMIREZ-MARTINEZ, F., LACROÛTE, C., REINHARD, F., SCHNEIDER, T., FUCHS, J.N., PIÉCHON, F., LALOË, F., REICHEL, J. & ROSENBUSCH, P. (2010). Spin self-rephasing and very long coherence times in a trapped atomic ensemble. *Phys. Rev. Lett.*, **105**, 020401. 15

DEUTSCH, D. (1985). Theory, the church-turing principle and the universal quantum computer. *Proceedings of the Royal Society of London*, **400**, 97–117. 5, 72, 144

DEUTSCH, D. (1989). Quantum computational networks. *Proceedings of the Royal Society of London. A. Mathematical and Physical Sciences*, **425**, 73–90. 144

DEUTSCH, D. & JOZSA, R. (1992). Rapid solution of problems by quantum computation. *Proceedings: Mathematical and Physical Sciences*, **439**, 553–558. 6

DICKE, R.H. (1954). Coherence in spontaneous radiation processes. *Physical Review*, **93**, 99–110. 106, 146

DITA, P. (1982). Parametrisation of unitary matrices. *Journal of Physics A: Mathematical and General*, **15**, 3465. 89

DiVincenzo, D.P. (2000). The physical implementation of quantum computation. *Fortschritte der Physik*, **48**, 771–783. 11

Dorner, R., Clark, S.R., Heaney, L., Fazio, R., Goold, J. & Vedral, V. (2013). Extracting quantum work statistics and fluctuation theorems by single-qubit interferometry. *Phys. Rev. Lett.*, **110**, 230601. 80, 82

Dudin, Y.O. & Kuzmich, A. (2012). Strongly interacting rydberg excitations of a cold atomic gas. *Science*, **336**, 887–889. 23, 41, 65

Dudin, Y.O., Li, L., Bariani, F. & Kuzmich, A. (2012). Observation of coherent many-body rabi oscillations. *Nature Physics*, **8**, 790–794. 23, 41, 65

Dumke, R., Volk, M., Müther, T., Buchkremer, F.B.J., Birkl, G. & Ertmer, W. (2002). Micro-optical realization of arrays of selectively addressable dipole traps: A scalable configuration for quantum computation with atomic qubits. *Phys. Rev. Lett.*, **89**, 097903. 18

Dür, W., Vidal, G. & Cirac, J.I. (2000). Three qubits can be entangled in two inequivalent ways. *Phys. Rev. A*, **62**, 062314. 39

Eastin, B. (2010). Simulating concordant computations, arXiv:1006.4402v1 [quant-ph].

Einstein, A., Podolsky, B. & Rosen, N. (1935). Can quantum-mechanical description of physical reality be considered complete? *Phys. Rev.*, **47**, 777–780. 73

Ekert, A.K., Alves, C.M., Oi, D.K.L., Horodecki, M., Horodecki, P. & Kwek, L.C. (2002). Direct estimations of linear and nonlinear functionals of a quantum state. *Phys. Rev. Lett.*, **88**, 217901. 81

Ernst, P.T., Gtze, S., Krauser, J.S., Pyka, K., Lhmann, D.S., Pfannkuche, D. & Sengstock, K. (2009). Probing superfluids in optical lattices by momentum-resolved bragg spectroscopy. *Nature Physics*, **6**, 56–61. 17

FARHI, E., GOLDSTONE, J., GUTMANN, S., LAPAN, J., LUNDGREN, A. & PREDA, D. (2001). A quantum adiabatic evolution algorithm applied to random instances of an np-complete problem. *Science*, **292**, 472–475. 12, 144

FERRARO, A., AOLITA, L., CAVALCANTI, D., CUCCHIETTI, F.M. & ACIN, A. (2010). Almost all quantum states have nonclassical correlations. *Phys. Rev. A*, **81**, 052318.

FEYNMAN, R.P. (1982). Simulating physics with computers. *International Journal of Theoretical Physics*, **21**, 467–488. 144

FILIP, R. (2002). Overlap and entanglement-witness measurements. *Phys. Rev. A*, **65**, 062320. 81

FLEISCHHAUER, M., IMAMOGLU, A. & MARANGOS, J.P. (2005). Electromagnetically induced transparency: Optics in coherent media. *Rev. Mod. Phys.*, **77**, 633–673. 42

FÖLLING, S., WIDERA, A., MÜLLER, T., GERBIER, F. & BLOCH, I. (2006). Formation of spatial shell structure in the superfluid to mott insulator transition. *Phys. Rev. Lett.*, **97**, 060403. 20, 40

FOLMAN, R., KRÜGER, P., SCHMIEDMAYER, J., DENSCHLAG, J. & HENKEL, C. (2002). Microscopic atom optics: from wires to an atom chip. *Advances in Atomic, Molecular, and Optical Physics*, **48**, 263–356. 16

FORTÁGH, J. & ZIMMERMANN, C. (2007). Magnetic microtraps for ultracold atoms. *Rev. Mod. Phys.*, **79**, 235–289. 16

FRESE, D., UEBERHOLZ, B., KUHR, S., ALT, W., SCHRADER, D., GOMER, V. & MESCHEDE, D. (2000). Single atoms in an optical dipole trap: Towards a deterministic source of cold atoms. *Phys. Rev. Lett.*, **85**, 3777–3780. 22

FUNKHOUSER, S. (2006). The large number coincidence, the cosmic coincidence and the critical acceleration. *Proceedings of the Royal Society A: Mathematical, Physical and Engineering Science*, **462**, 3657–3661. 117

GALINDO, A. & MARTÍN-DELGADO, M.A. (2002). Information and computation: Classical and quantum aspects. *Rev. Mod. Phys.*, **74**, 347–423. 1

GALLAGHER, T.F. (1988). Rydberg atoms. *Reports on Progress in Physics*, **51**, 143. 29

GALLAGHER, T.F. & PILLET, P. (2008). Dipole-dipole interactions of rydberg atoms. *Advances in Atomic, Molecular and Optical Physics*, **56**, 161–218. 41

GALVE, F., PLASTINA, F., PARIS, M.G.A. & ZAMBRINI, R. (2013). Discording power of quantum evolutions. *Phys. Rev. Lett.*, **110**, 010501. 104

GATAN, A., EVELLIN, C., WOLTERS, J., GRANGIER, P., WILK, T. & BROWAEYS, A. (2010). Analysis of the entanglement between two individual atoms using global raman rotations. *New Journal of Physics*, **12**, 065040. 36

GAUBATZ, U., RUDECKI, P., BECKER, M., SCHIEMANN, S., KÜLZ, M. & BERGMANN, K. (1988). Population switching between vibrational levels in molecular beams. *Chemical physics letters*, **149**, 463–468. 48

GAUBATZ, U., RUDECKI, P., SCHIEMANN, S. & BERGMANN, K. (1990). Population transfer between molecular vibrational levels by stimulated raman scattering with partially overlapping laser fields. a new concept and experimental results. *The Journal of Chemical Physics*, **92**, 5363–5376. 48

GEORGESCU, M., I. ASHHAB, S. & NORI, F. (2014). Quantum simulation. *Rev. Mod. Phys.*, **86**, 153–185. 1, 24

GERICKE, T., WÜRTZ, P., REITZ, D., LANGEN, T. & OTT, H. (2008). High-resolution scanning electron microscopy of an ultracold quantum gas. *Nature Physics*, **4**, 949–953. 21

GIAMPAOLO, S.M., STRELTSOV, A., ROGA, W., BRUSS, D. & ILLUMINATI, F. (2013). Quantifying nonclassicality: Global impact of local unitary evolutions. *Phys. Rev. A*, **87**, 012313. 103, 147

GIORDA, P. & PARIS, M.G.A. (2010). Gaussian quantum discord. *Phys. Rev. Lett.*, **105**, 020503.

GIOVANNETTI, V., LLOYD, S. & MACCONE, L. (2011). Advances in quantum metrology. *Nature Photonics*, **5**, 222–229. 1

GIROLAMI, D. & ADESSO, G. (2011). Quantum discord for general two-qubit states: Analytical progress. *Phys. Rev. A*, **83**, 052108. 74

GIROLAMI, D. & ADESSO, G. (2012). Observable measure of bipartite quantum correlations. *Phys. Rev. Lett.*, **108**, 150403. 105

GIROLAMI, D., TUFARELLI, T. & ADESSO, G. (2013). Characterizing non-classical correlations via local quantum uncertainty. *Phys. Rev. Lett.*, **110**, 240402. 105

GOTTESMAN, D. (1998). The heisenberg representation of quantum computers, arXiv:quant-ph/9807006. 73, 116

GOTTESMAN, D. (1999). The heisenberg representation of quantum computers. In *Proceedings of the XXII International Colloquium on Group Theoretical Methods in Physics*. 73, 116

GRANGIER, P., SANDERS, B. & VUCKOVIC, J. (2004). Focus on single photons on demand. *New Journal of Physics*, **6**. 14

GREENE, C.H., DICKINSON, A.S. & SADEGHPOUR, H.R. (2000). Creation of polar and nonpolar ultra-long-range rydberg molecules. *Phys. Rev. Lett.*, **85**, 2458–2461. 144

GRIMM, R., WEIDEMÜLLER, M. & OVCHINNIKOV, Y. (2000). Optical dipole traps for neutral atoms. *Adv. at. mol. opt. phys*, **42**, 130. 18, 125

GROSS, D., FLAMMIA, S.T. & EISERT, J. (2009). Most quantum states are too entangled to be useful as computational resources. *Phys. Rev. Lett.*, **102**, 190501. 73

GROVER, L. (1996). A fast quantum mechanical algorithm for database search.

In *Proceedings of the twenty-eighth annual ACM symposium on Theory of computing*, 219, ACM. 6, 144

GRÜNZWEIG, T., HILLIARD, A., MCGOVERN, M. & ANDERSEN, M.F. (2010). Near-deterministic preparation of a single atom in an optical microtrap. *Nature Physics*, **Advanced On-line Publication**, Advanced On–line Publication. 90

GU, M., CHRZANOWSKI, H.M., ASSAD, S.M., SYMUL, T., MODI, K., RALPH, T.C., VEDRAL, V. & LAM, P.K. (2012). Observing the operational significance of discord consumption. *Nature Physics*, **AOP**, AOP. 74

HADFIELD, R.H. (2009). Single-photon detectors for optical quantum information applications. *Nature photonics*, **3**, 696–705. 14

HAMMERER, K., SØRENSEN, A.S. & POLZIK, E.S. (2010). Quantum interface between light and atomic ensembles. *Rev. Mod. Phys.*, **82**, 1041–1093. 39

HÄNSEL, W., HOMMELHOFF, P., HÄNSCH, T. & REICHEL, J. (2001). Bose–einstein condensation on a microelectronic chip. *Nature*, **413**, 498–501. 17

HAROCHE, S. & WINELAND, D. (2012). The nobel prize in physics 2012, awarded for ground-breaking experimental methods that enable measuring and manipulation of individual quantum systems. 60, 144

HARRIS, S.E., FIELD, J.E. & IMAMOĞLU, A. (1990). Nonlinear optical processes using electromagnetically induced transparency. *Phys. Rev. Lett.*, **64**, 1107–1110. 41

HARROW, A.W., HASSIDIM, A. & LLOYD, S. (2009). Quantum algorithm for linear systems of equations. *Physical Review Letters*, **103**, 1–4. 6

HAU, L.V., HARRIS, S.E., DUTTON, Z. & BEHROOZI, C.H. (1999). Light speed reduction to 17 metres per second in an ultracold atomic gas. *Nature*, **397**, 594–598. 43

HAYES, D., JULIENNE, P.S. & DEUTSCH, I.H. (2007). Quantum logic via

the exchange blockade in ultracold collisions. *Phys. Rev. Lett.*, **98**, 070501. 19

HEIDEMANN, R., RAITZSCH, U., BENDKOWSKY, V., BUTSCHER, B., LÖW, R., SANTOS, L. & PFAU, T. (2007). Evidence for coherent collective rydberg excitation in the strong blockade regime. *Phys. Rev. Lett.*, **99**, 163601. 41

HENDERSON, K., RYU, C., MACCORMICK, C. & BOSHIER, M.G. (2009). Experimental demonstration of painting arbitrary and dynamic potentials for boseeinstein condensates. *New Journal of Physics*, **11**, 043030. 18

HENDERSON, L. & VEDRAL, V. (2001). Classical, quantum and total correlations. *Journal of Physics A: Mathematical and General*, **34**, 6899. 73, 77, 144

HENDRYCH, M., GALLEGO, R., MIUDA, M., BRUNNER, N., ACN, A. & TORRES, J.P. (2012). Experimental estimation of the dimension of classical and quantum systems. *Nature Physics*, **8**, 588–591. 105

HERNÁNDEZ, J.V. & ROBICHEAUX, F. (2006). Coherence conditions for groups of rydberg atoms. *Journal of Physics B: Atomic, Molecular and Optical Physics*, **39**, 4883. 111

HOME, J.P., HANNEKE, D., JOST, J.D., AMINI, J.M., LEIBFRIED, D. & WINELAND, D.J. (2009). Complete methods set for scalable ion trap quantum information processing. *Science*, **325**, 1227–1230. 14

HORODECKI, R., HORODECKI, P., HORODECKI, M. & HORODECKI, K. (2009). Quantum entanglement. *Rev. Mod. Phys.*, **81**, 865–942. 73

HOWARD, M., WALLMAN, J.J., VEITCH, V. & EMERSON, J. (2014). Contextuality supplies the magic for quantum computation, arXiv:1401.4174 [quant-ph]. 72

HUAI-ZHI, W., ZHEN-BIAO, Y. & SHI-BIAO, Z. (2012). Quantum state swap for two trapped rydberg atoms. *Chinese Physics B*, **21**, 040305. 81

HUBER, B., BALUKTSIAN, T., SCHLAGMÜLLER, M., KÖLLE, A., KÜBLER, H., LÖW, R. & PFAU, T. (2011). Ghz rabi flopping to rydberg states in hot atomic vapor cells. *Phys. Rev. Lett.*, **107**, 243001. 22

HUGHES, D.R., DOOLEN, G., AWSCHALOM, D., CAVES, C., CHAPMAN, M., CLARK, R., CORY, D., DIVINCENZO, D., EKERT, A., HAMMEL, P.C., KWIAT, P., LLOYD, S., MILBURN, G., ORLANDO, T., STEEL, D., VAZIRANI, U., WHALEY, K.B. & WINELAND, D. (2004). Quantum information science and technology roadmapping project: Quantum computation project. 144

ISENHOWER, L., WILLIAMS, W., DALLY, A. & SAFFMAN, M. (2009). Atom trapping in an interferometrically generated bottle beam trap. *Opt. Lett.*, **34**, 1159–1161. 19

ISENHOWER, L., URBAN, E., ZHANG, X.L., GILL, A.T., HENAGE, T., JOHNSON, T.A., WALKER, T.G. & SAFFMAN, M. (2010). Demonstration of a neutral atom controlled-not quantum gate. *Phys. Rev. Lett.*, **104**, 010503. 22, 35, 144

ISENHOWER, L., SAFFMAN, M. & MØLMER, K. (2011). Multibit c k not quantum gates via rydberg blockade. *Quantum Information Processing*, **10**, 755–770.

JAKSCH, D. & ZOLLER, P. (2005). The cold atom hubbard toolbox. *Annals of Physics*, **315**, 52–79. 17, 32

JAKSCH, D., BRIEGEL, H.J., CIRAC, J.I., GARDINER, C.W. & ZOLLER, P. (1999). Entanglement of atoms via cold controlled collisions. *Phys. Rev. Lett.*, **82**, 1975–1978. 19

JAKSCH, D., CIRAC, J.I., ZOLLER, P., ROLSTON, S.L., CÔTÉ, R. & LUKIN, M.D. (2000). Fast quantum gates for neutral atoms. *Phys. Rev. Lett.*, **85**, 2208–2211. 22, 27, 33, 62, 124, 125, 144

JESSEN, P.S., GERZ, C., LETT, P.D., PHILLIPS, W.D., ROLSTON, S.L.,

SPREEUW, R.J.C. & WESTBROOK, C.I. (1992). Observation of quantized motion of rb atoms in an optical field. *Phys. Rev. Lett.*, **69**, 49–52. 144

JOZSA, R. & LINDEN, N. (2003). On the role of entanglement in quantum-computational speed-up. *Proceedings of the Royal Society of London. Series A: Mathematical, Physical and Engineering Sciences*, **459**, 2011–2032. 73

JRDENS, R., STROHMAIER, N., G

"UNTER, K., MORITZ, H. & ESSLINGER, T. (2008). A mott insulator of fermionic atoms in an optical lattice. *Nature*, **455**, 204–207. 17

KASEVICH, M. & CHU, S. (1992). Laser cooling below a photon recoil with three-level atoms. *Phys. Rev. Lett.*, **69**, 1741–1744. 21

KAUFMAN, A.M., LESTER, B.J. & REGAL, C.A. (2012). Cooling a single atom in an optical tweezer to its quantum ground state. *Phys. Rev. X*, **2**, 041014. 18

KILLIAN, T., PATTARD, T., POHL, T. & ROST, J. (2007). Ultracold neutral plasmas. *Physics Reports*, **449**, 77–130. 146

KILLIAN, T.C., LIM, M.J., KULIN, S., DUMKE, R., BERGESON, S.D. & ROLSTON, S.L. (2001). Formation of rydberg atoms in an expanding ultracold neutral plasma. *Phys. Rev. Lett.*, **86**, 3759–3762. 147

KIMBLE, H.J. (2008). The quantum internet. *Nature*, **453**, 1023–1030. 1

KITAEV, A.Y. (1997). Fault-tolerant quantum computation by anyons, arXiv:quant-ph/9707021v1. 12, 144

KITAEV, A.Y. (2003). Fault-tolerant quantum computation by anyons. *Annals of Physics*, **303**, 2–30. 12, 144

KLEIN, A. (2007). *Special purpose quantum information processing with atoms in optical lattices*. Ph.D. thesis, Keble College, University of Oxford. 18, 20

KNEE, G.C., GAUGER, E.M., BRIGGS, G.A.D. & BENJAMIN, S.C. (2012). Comment on "a scattering quantum circuit for measuring bell's time inequal-

ity: a nuclear magnetic resonance demonstration using maximally mixed states". *New Journal of Physics*, **14**, 058001. 83

KNILL, E. & LAFLAMME, R. (1998). Power of one bit of quantum information. *Phys. Rev. Lett.*, **81**, 5672–5675. 2, 12, 67, 68, 144

KNILL, E., LAFLAMME, R., MARTINEZ, R. & NEGREVERGNE, C. (2001a). Benchmarking quantum computers: The five-qubit error correcting code. *Phys. Rev. Lett.*, **86**, 5811–5814. 15

KNILL, E., LAFLAMME, R. & MILBURN, G.J. (2001b). A scheme for efficient quantum computation with linear optics. *nature*, **409**, 46–52. 14

KOWALCZYK, A.U. (2013). *Ultracold Rydberg atoms*. Ph.D. thesis, The Open University. 123, 139

KRÁL, P., THANOPULOS, I. & SHAPIRO, M. (2007). Colloquium: Coherently controlled adiabatic passage. *Rev. Mod. Phys.*, **79**, 53–77. 48

LADD, T.D., JELEZKO, F., LAFLAMME, R., NAKAMURA, Y., MONROE, C. & OBRIEN, J.L. (2010). Quantum computers. *Nature*, **464**, 45–53. 1, 6, 12, 144

LANDAUER, R. (1996). The physical nature of information. *Physics letters A*, **217**, 188–193. 10

LANDOUER, R. (1991). Information is physical. *Physics Today*, 25. 10

LANGER, C., OZERI, R., JOST, J.D., CHIAVERINI, J., DEMARCO, B., BEN-KISH, A., BLAKESTAD, R.B., BRITTON, J., HUME, D.B., ITANO, W.M., LEIBFRIED, D., REICHLE, R., ROSENBAND, T., SCHAETZ, T., SCHMIDT, P.O. & WINELAND, D.J. (2005). Long-lived qubit memory using atomic ions. *Phys. Rev. Lett.*, **95**, 060502. 14

LANYON, B.P., BARBIERI, M., ALMEIDA, M.P. & WHITE, A.G. (2008). Experimental quantum computing without entanglement. *Phys. Rev. Lett.*, **101**, 200501. 2, 116, 117, 144

LANYON, B.P., BARBIERI, M., ALMEIDA, M.P., JENNEWEIN, T., RALPH, T.C., RESCH, K.J., PRYDE, G.J., O'BRIEN, J.L., GILCHRIST, A. & WHITE, A.G. (2009). Simplifying quantum logic using higher-dimensional hilbert spaces. *Nature Physics*, **5**, 134–140. 106

LAYCOCK, T., OLMOS, B. & LESANOVSKY, I. (2011). Creation of collective many-body states and single photons from two-dimensional rydberg lattice gases. *Journal of Physics B: Atomic, Molecular and Optical Physics*, **44**, 184017. 113, 126

LEGGETT, A.J. (2002). Testing the limits of quantum mechanics: motivation, state of play, prospects. *Journal of Physics: Condensed Matter*, **14**, R415.

LETT, P.D., WATTS, R.N., WESTBROOK, C.I., PHILLIPS, W.D., GOULD, P.L. & METCALF, H.J. (1988). Observation of atoms laser cooled below the doppler limit. *Phys. Rev. Lett.*, **61**, 169–172. 144

LEUNG, D., VANDERSYPEN, L., ZHOU, X., SHERWOOD, M., YANNONI, C., KUBINEC, M. & CHUANG, I. (1999). Experimental realization of a two-bit phase damping quantum code. *Phys. Rev. A*, **60**, 1924–1943. 15

LI, L., DUDIN, Y.O. & KUZMICH, A. (2013). Entanglement between light and an optical atomic excitation. *Nature*, **498**, 466–469. 23, 41, 65

LI, W., TANNER, P.J. & GALLAGHER, T.F. (2005). Dipole-dipole excitation and ionization in an ultracold gas of rydberg atoms. *Phys. Rev. Lett.*, **94**, 173001. 146

LIEBISCH, T.C., REINHARD, A., BERMAN, P.R. & RAITHEL, G. (2005). Atom counting statistics in ensembles of interacting rydberg atoms. *Phys. Rev. Lett.*, **95**, 253002. 41

LINDEN, N., SMOLIN, J.A. & WINTER, A. (2009). Entangling and disentangling power of unitary transformations are not equal. *Phys. Rev. Lett.*, **103**, 030501. 104

LITA, A.E., MILLER, A.J. & NAM, S.W. (2008). Counting near-infrared

single-photons with 95% efficiency. *Opt. Express*, **16**, 3032–3040. 14

LIU, L., BELLANCA, M.J. & METCALF, H. (2002). Evolution of coherent dark states. *Phys. Rev. A*, **65**, 043401. 46

LLOYD, S. (1993). A potentially realizable quantum computer. *Science*, **261**, 1569–1571. 12, 114

LLOYD, S. (2000). Ultimate physical limits to computation. *Nature*, **406**, 1047–1054. 10

LOSS, D. & DIVINCENZO, D.P. (1998). Quantum computation with quantum dots. *Phys. Rev. A*, **57**, 120–126. 19

LÖW, R., WEIMER, H., KROHN, U., HEIDEMANN, R., BENDKOWSKY, V., BUTSCHER, B., BÜCHLER, H.P. & PFAU, T. (2009). Universal scaling in a strongly interacting rydberg gas. *Phys. Rev. A*, **80**, 033422. 111

LOY, M.M.T. (1974). Observation of population inversion by optical adiabatic rapid passage. *Phys. Rev. Lett.*, **32**, 814–817. 48

LUKIN, M.D. (2003). Colloquium: Trapping and manipulating photon states in atomic ensembles. *Rev. Mod. Phys.*, **75**, 457–472. 39

LUKIN, M.D., FLEISCHHAUER, M., COTE, R., DUAN, L.M., JAKSCH, D., CIRAC, J.I. & ZOLLER, P. (2001). Dipole blockade and quantum information processing in mesoscopic atomic ensembles. *Phys. Rev. Lett.*, **87**, 037901. 27, 33, 36, 37, 39, 40, 41, 62, 124, 125, 144

LUO, S. & FU, S. (2010). Geometric measure of quantum discord. *Phys. Rev. A*, **82**, 034302. 78

MADHOK, V. & DATTA, A. (2013). Quantum discord as a resource in quantum communication. *International Journal of Modern Physics B*, **27**, 1345041. 74, 105

MADHOK, V., GUPTA, V., HAMEL, A.M. & GHOSE, S. (2013). Signatures of chaos in the dynamics of quantum discord, arXiv:1307.1405v2 [quant-ph].

81

MANSELL, C.W. & BERGAMINI, S. (2014). A cold-atoms based processor for deterministic quantum computation with one qubit in intractably large hilbert spaces. *New Journal of Physics*, **16**, 053045. 141

MANSFIELD, S.M. & KINO, G.S. (1990). Solid immersion microscope. *Applied Physics Letters*, **57**, 2615–2616. 21

MANTHEY, T., WEBER, T.M., NIEDERPRM, T., LANGER, P., GUARRERA, V., BARONTINI, G. & OTT, H. (2014). Scanning electron microscopy of rydberg-excited boseeinstein condensates. *New Journal of Physics*, **16**, 083034. 49

MARI, A. & EISERT, J. (2012). Positive wigner functions render classical simulation of quantum computation efficient. *Phys. Rev. Lett.*, **109**, 230503. 73, 116

MARTIN, M.J., BISHOF, M., SWALLOWS, M.D., ZHANG, X., BENKO, C., VON STECHER, J., GORSHKOV, A.V., REY, A.M. & YE, J. (2013). A quantum many-body spin system in an optical lattice clock. *Science*, **341**, 632–636. 81

MARX, R., FAHMY, A., KAUFFMAN, L., LOMONACO, S., SPÖRL, A., POMPLUN, N., SCHULTE-HERBRÜGGEN, T., MYERS, J.M. & GLASER, S.J. (2010). Nuclear-magnetic-resonance quantum calculations of the jones polynomial. *Phys. Rev. A*, **81**, 032319. 115, 116, 144

MASTERSON, B.P., TANNER, C., PATRICK, H. & WIEMAN, C.E. (1993). High-brightness, high-purity spin-polarized cesium beam. *Phys. Rev. A*, **47**, 2139–2145. 91, 99

MAZZOLA, L., DE CHIARA, G. & PATERNOSTRO, M. (2013). Measuring the characteristic function of the work distribution. *Phys. Rev. Lett.*, **110**, 230602. 80, 82

MERALI, Z. (2011). Quantum computing: The power of discord. *Nature*, **474**,

24–26.

METCALF, H.J. & VAN DER STRATEN, P. (2002). *Laser Cooling and Trapping.* Springer. 2, 119, 120

MIGDALL, A. & DOWLING, J. (2004). Introduction to the journal of modern optics special issue on single-photon: Detectors, applications, and measurement methods. Tech. rep., DTIC Document. 14

MIGDALL, A.L., PRODAN, J.V., PHILLIPS, W.D., BERGEMAN, T.H. & METCALF, H.J. (1985). First observation of magnetically trapped neutral atoms. *Phys. Rev. Lett.*, **54**, 2596–2599. 144

MIROSHNYCHENKO, Y., ALT, W., DOTSENKO, I., FORSTER, L., KHUDAVERDYAN, M., MESCHEDE, D., SCHRADER, D. & RAUSCHENBEUTEL, A. (2006). An atom-sorting machine. *Nature*, **442**, 151. 15, 23, 142

MODI, K., CABLE, H., WILLIAMSON, M. & VEDRAL, V. (2011). Quantum correlations in mixed-state metrology. *Phys. Rev. X*, **1**, 021022. 80, 82, 105

MODI, K., BRODUTCH, A., CABLE, H., PATEREK, T. & VEDRAL, V. (2012). The classical-quantum boundary for correlations: Discord and related measures. *Rev. Mod. Phys.*, **84**, 1655–1707. 73, 74, 77

MOHR, P.J., TAYLOR, B.N. & NEWELL, D.B. (2012). Codata recommended values of the fundamental physical constants: 2010. *Rev. Mod. Phys.*, **84**, 1527–1605. 117

MØLLER, D., MADSEN, L.B. & MØLMER, K. (2008). Quantum gates and multiparticle entanglement by rydberg excitation blockade and adiabatic passage. *Phys. Rev. Lett.*, **100**, 170504. 52

MØLMER, K. & SØRENSEN, A. (1999). Multiparticle entanglement of hot trapped ions. *Phys. Rev. Lett.*, **82**, 1835–1838. 14

MONROE, C. (2002). Quantum information processing with atoms and photons. *Nature*, **416**, 238–246. xii, 19

MORIMAE, T. & KOSHIBA, T. (2014). Classical simulatability of the one clean qubit model, arXiv:1405.6840 [quant-ph]. 142

MORIMAE, T., FUJII, K. & FITZSIMONS, J.F. (2014). Hardness of classically simulating the one-clean-qubit model. *Phys. Rev. Lett.*, **112**, 130502. 142

MOURACHKO, I., COMPARAT, D., DE TOMASI, F., FIORETTI, A., NOSBAUM, P., AKULIN, V.M. & PILLET, P. (1998). Many-body effects in a frozen rydberg gas. *Phys. Rev. Lett.*, **80**, 253–256. 31, 40

MOUSSA, O., RYAN, C.A., CORY, D.G. & LAFLAMME, R. (2010). Testing contextuality on quantum ensembles with one clean qubit. *Phys. Rev. Lett.*, **104**, 160501. 80, 83

MÜLLER, M., LESANOVSKY, I., WEIMER, H., BÜCHLER, H.P. & ZOLLER, P. (2009). Mesoscopic rydberg gate based on electromagnetically induced transparency. *Phys. Rev. Lett.*, **102**, 170502. xiv, xviii, 27, 41, 43, 44, 45, 46, 47, 52, 63, 87, 88, 93, 95, 96, 109

MÜLLER, M.M., MURPHY, M., MONTANGERO, S., CALARCO, T., GRANGIER, P. & BROWAEYS, A. (2014). Implementation of an experimentally feasible controlled-phase gate on two blockaded rydberg atoms. *Phys. Rev. A*, **89**, 032334. 24, 36

MÜLLER, T., ZHANG, B., FERMANI, R., CHAN, K.S., WANG, Z.W., ZHANG, C.B., LIM, M.J. & DUMKE, R. (2010). Trapping of ultra-cold atoms with the magnetic field of vortices in a thin-film superconducting micro-structure. *New Journal of Physics*, **12**, 043016. 17

MÜNTINGA, H., AHLERS, H., KRUTZIK, M., WENZLAWSKI, A., ARNOLD, S., BECKER, D., BONGS, K., DITTUS, H., DUNCKER, H., GAALOUL, N., GHERASIM, C., GIESE, E., GRZESCHIK, C., HÄNSCH, T.W., HELLMIG, O., HERR, W., HERRMANN, S., KAJARI, E., KLEINERT, S., LÄMMERZAHL, C., LEWOCZKO-ADAMCZYK, W., MALCOLM, J., MEYER, N., NOLTE, R., PETERS, A., POPP, M., REICHEL, J., ROURA, A.,

RUDOLPH, J., SCHIEMANGK, M., SCHNEIDER, M., SEIDEL, S.T., SENGSTOCK, K., TAMMA, V., VALENZUELA, T., VOGEL, A., WALSER, R., WENDRICH, T., WINDPASSINGER, P., ZELLER, W., VAN ZOEST, T., ERTMER, W., SCHLEICH, W.P. & RASEL, E.M. (2013). Interferometry with bose-einstein condensates in microgravity. *Phys. Rev. Lett.*, **110**, 093602. 82

NAKAYAMA, S., SOEDA, A. & MURAO, M. (2013). Universal implementation of projective measurement of energy, arXiv:1310.3047 [quant-ph]. 111

NEGRETTI, A., TREUTLEIN, P. & CALARCO, T. (2011). Quantum computing implementations with neutral particles. *Quantum Information Processing*, **10**, 721–753. 15

NELSON, K.D., LI, X. & WEISS, D.S. (2007). Imaging single atoms in a three-dimensional array. *Nature Physics*, **3**, 556–560. 20

NG, H.T. (2013). Quantum-limited measurement of magnetic-field gradient with entangled atoms. *Phys. Rev. A*, **87**, 043602. 82

NIELSEN, M.A. & CHUANG, I.L. (2010). *Quantum computation and quantum information*. Cambridge University Press. 1, 10

NOGRETTE, F., LABUHN, H., RAVETS, S., BARREDO, D., BÉGUIN, L., VERNIER, A., LAHAYE, T. & BROWAEYS, A. (2014). Single-atom trapping in holographic 2d arrays of microtraps with arbitrary geometries. *Phys. Rev. X*, 4, 021034. 18

O'BRIEN, J.L. (2007). Optical quantum computing. *Science*, **318**, 1567–1570. 14

OLLIVIER, H. & ZUREK, W.H. (2001). Quantum discord: A measure of the quantumness of correlations. *Phys. Rev. Lett.*, **88**, 017901. 73, 77, 144

OLMOS, B., GONZÁLEZ-FÉREZ, R. & LESANOVSKY, I. (2009a). Collective rydberg excitations of an atomic gas confined in a ring lattice. *Phys. Rev. A*, **79**, 043419. 113, 126

OLMOS, B., GONZÁLEZ-FÉREZ, R. & LESANOVSKY, I. (2009b). Fermionic collective excitations in a lattice gas of rydberg atoms. *Phys. Rev. Lett.*, **103**, 185302. 113, 126

OLMOS, B., GONZÁLEZ-FÉREZ, R. & LESANOVSKY, I. (2010). Creating collective many-body states with highly excited atoms. *Phys. Rev. A*, **81**, 023604. 32

OREG, J., HIOE, F.T. & EBERLY, J.H. (1984). Adiabatic following in multilevel systems. *Phys. Rev. A*, **29**, 690–697. 48

OREG, J., HAZAK, G. & EBERLY, J.H. (1985). Multilevel inversion schemes in and beyond the adiabatic limit. *Phys. Rev. A*, **32**, 2776–2783. 48

OSTERWALDER, A. & MERKT, F. (1999). Using high rydberg states as electric field sensors. *Phys. Rev. Lett.*, **82**, 1831–1834. 32

OTT, H., FORTAGH, J., SCHLOTTERBECK, G., GROSSMANN, A. & ZIMMERMANN, C. (2001). Bose-einstein condensation in a surface microtrap. *Phys. Rev. Lett.*, **87**, 230401. 17

PARKER, S. & PLENIO, M.B. (2002). Entanglement simulations of shor's algorithm. *Journal of Modern Optics*, **49**, 1325–1353. 68

PASSANTE, G., MOUSSA, O., RYAN, C.A. & LAFLAMME, R. (2009). Experimental approximation of the jones polynomial with one quantum bit. *Phys. Rev. Lett.*, **103**, 250501. 115, 144

PASSANTE, G., MOUSSA, O., TROTTIER, D.A. & LAFLAMME, R. (2011). Experimental detection of nonclassical correlations in mixed-state quantum computation. *Phys. Rev. A*, **84**, 044302. 115, 116

PASSANTE, G., MOUSSA, O. & LAFLAMME, R. (2012). Measuring geometric quantum discord using one bit of quantum information. *Phys. Rev. A*, **85**, 032325. 78, 79, 80

PATTON, K.R. & FISCHER, U.R. (2013). Ultrafast quantum random access

memory utilizing single rydberg atoms in a bose-einstein condensate. *Phys. Rev. Lett.*, **111**, 240504. 17

PERES, A. (1984). Stability of quantum motion in chaotic and regular systems. *Phys. Rev. A*, **30**, 1610–1615.

PÉREZ-DELGADO, C.A. & KOK, P. (2011). Quantum computers: Definition and implementations. *Phys. Rev. A*, **83**, 012303. 12

PETROV, D.S., SALOMON, C. & SHLYAPNIKOV, G.V. (2005). Diatomic molecules in ultracold fermi gases: novel composite bosons. *Journal of Physics B: Atomic, Molecular and Optical Physics*, **38**, S645. 114

PETROV, D.S., ASTRAKHARCHIK, G.E., PAPOULAR, D.J., SALOMON, C. & SHLYAPNIKOV, G.V. (2007). Crystalline phase of strongly interacting fermi mixtures. *Phys. Rev. Lett.*, **99**, 130407. 114

PHILLIPS, D.F., FLEISCHHAUER, A., MAIR, A., WALSWORTH, R.L. & LUKIN, M.D. (2001). Storage of light in atomic vapor. *Phys. Rev. Lett.*, **86**, 783–786. 43

PHILLIPS, W.D. & METCALF, H. (1982). Laser deceleration of an atomic beam. *Phys. Rev. Lett.*, **48**, 596–599. 144

PIANI, M. (2012). Problem with geometric discord. *Phys. Rev. A*, **86**, 034101. 147

PIANI, M. & ADESSO, G. (2012). Quantumness of correlations revealed in local measurements exceeds entanglement. *Phys. Rev. A*, **85**, 040301. 105

PIOTROWICZ, M.J., LICHTMAN, M., MALLER, K., LI, G., ZHANG, S., ISENHOWER, L. & SAFFMAN, M. (2013). Two-dimensional lattice of blue-detuned atom traps using a projected gaussian beam array. *Phys. Rev. A*, **88**, 013420. 19

PLESCH, M. & BUŽEK, V. (2010). Efficient compression of quantum information. *Phys. Rev. A*, **81**, 032317. 105

POHL, T., DEMLER, E. & LUKIN, M.D. (2010). Dynamical crystallization in the dipole blockade of ultracold atoms. *Phys. Rev. Lett.*, **104**, 043002. 113

POULIN, D., LAFLAMME, R., MILBURN, G.J. & PAZ, J.P. (2003). Testing integrability with a single bit of quantum information. *Phys. Rev. A*, **68**, 022302. 80, 81

POULIN, D., BLUME-KOHOUT, R., LAFLAMME, R. & OLLIVIER, H. (2004). Exponential speedup with a single bit of quantum information: Measuring the average fidelity decay. *Phys. Rev. Lett.*, **92**, 177906. 74, 80, 81

POULIN, D., QARRY, A., SOMMA, R. & VERSTRAETE, F. (2011). Quantum simulation of time-dependent hamiltonians and the convenient illusion of hilbert space. *Phys. Rev. Lett.*, **106**, 170501. 72

PRESKILL, J. (2011). Quantum computing and the entanglement frontier. In *The Theory of the Quantum World - Proceedings of the 25th Solvay Conference on Physics*, vol. 1, 210–249. 1, 142

PRITCHARD, J.D., ISAACS, J.A., BECK, M.A., MCDERMOTT, R. & SAFFMAN, M. (2014). Hybrid atom-photon quantum gate in a superconducting microwave resonator. *Phys. Rev. A*, **89**, 010301. 17

RAAB, E.L., PRENTISS, M., CABLE, A., CHU, S. & PRITCHARD, D.E. (1987). Trapping of neutral sodium atoms with radiation pressure. *Phys. Rev. Lett.*, **59**, 2631–2634. 144

RAMSEY, N.F. (1950). A molecular beam resonance method with separated oscillating fields. *Phys. Rev.*, **78**, 695–699. 60

RAUSSENDORF, R. & BRIEGEL, H.J. (2001). A one-way quantum computer. *Phys. Rev. Lett.*, **86**, 5188–5191. 12, 144

REICHEL, J. (2002). Microchip traps and bose einstein condensation. *Applied Physics B*, **74**, 469–487. 16

ROBICHEAUX, F. & HERNÁNDEZ, J.V. (2005). Many-body wave function in

a dipole blockade configuration. *Phys. Rev. A*, **72**, 063403. 111

ROBINSON, M.P., TOLRA, B.L., NOEL, M.W., GALLAGHER, T.F. & PILLET, P. (2000). Spontaneous evolution of rydberg atoms into an ultracold plasma. *Phys. Rev. Lett.*, **85**, 4466–4469. 146

ROOS, C., CHWALLA, M., KIM, K., RIEBE, M. & BLATT, R. (2006). designer atoms for quantum metrology. *Nature*, **443**, 316–319. 81

RULLI, C.C. & SARANDY, M.S. (2011). Global quantum discord in multipartite systems. *Phys. Rev. A*, **84**, 042109.

RYABTSEV, I.I., TRETYAKOV, D.B., BETEROV, I.I. & ENTIN, V.M. (2010a). Observation of the stark-tuned förster resonance between two rydberg atoms. *Phys. Rev. Lett.*, **104**, 073003. 53

RYABTSEV, I.I., TRETYAKOV, D.B., BETEROV, I.I., ENTIN, V.M. & YAKSHINA, E.A. (2010b). Stark-tuned förster resonance and dipole blockade for two to five cold rydberg atoms: Monte carlo simulations for various spatial configurations. *Phys. Rev. A*, **82**, 053409. 53

RYAN, C.A., LAFOREST, M. & LAFLAMME, R. (2009). Randomized benchmarking of single- and multi-qubit control in liquid-state nmr quantum information processing. *New Journal of Physics*, **11**, 013034. 14

SAEEDI, K., SIMMONS, S., SALVAIL, J.Z., DLUHY, P., RIEMANN, H., ABROSIMOV, N.V., BECKER, P., POHL, H.J., MORTON, J.J.L. & THEWALT, M.L.W. (2013). Room-temperature quantum bit storage exceeding 39 minutes using ionized donors in silicon-28. *Science*, **342**, 830–833. 15

SAFFMAN, M. & MØLMER, K. (2008a). Scaling the neutral-atom rydberg gate quantum computer by collective encoding in holmium atoms. *Phys. Rev. A*, **78**, 012336. 18, 39

SAFFMAN, M. & MØLMER, K. (2008b). Scaling the neutral-atom rydberg gate quantum computer by collective encoding in holmium atoms. *Phys. Rev. A*, **78**, 012336. 115

SAFFMAN, M. & WALKER, T.G. (2002). Creating single-atom and single-photon sources from entangled atomic ensembles. *Phys. Rev. A*, **66**, 065403. 23, 39

SAFFMAN, M. & WALKER, T.G. (2005a). Analysis of a quantum logic device based on dipole-dipole interactions of optically trapped rydberg atoms. *Phys. Rev. A*, **72**, 022347. 22, 91, 99, 110

SAFFMAN, M. & WALKER, T.G. (2005b). Entangling single- and n -atom qubits for fast quantum state detection and transmission. *Phys. Rev. A*, **72**, 042302. 23

SAFFMAN, M., WALKER, T.G. & MØLMER, K. (2010). Quantum information with rydberg atoms. *Rev. Mod. Phys.*, **82**, 2313–2363. xi, 2, 13, 20

SAFINYA, K.A., DELPECH, J.F., GOUNAND, F., SANDNER, W. & GALLAGHER, T.F. (1981). Resonant rydberg-atom-rydberg-atom collisions. *Phys. Rev. Lett.*, **47**, 405–408. 30

SANGOUARD, N., SIMON, C., DE RIEDMATTEN, H. & GISIN, N. (2011). Quantum repeaters based on atomic ensembles and linear optics. *Rev. Mod. Phys.*, **83**, 33–80. 24

SCHMIDT, H. & IMAMOGLU, A. (1996). Giant kerr nonlinearities obtained by electromagnetically induced transparency. *Optics letters*, **21**, 1936–1938. 43

SCHNEIDER, U., HACKERMULLER, L., WILL, S., BEST, T., BLOCH, I., COSTI, T.A., HELMES, R.W., RASCH, D. & ROSCH, A. (2008). Metallic and insulating phases of repulsively interacting fermions in a 3d optical lattice. *Science*, **322**, 1520–1525. 17

SCHRADER, D., DOTSENKO, I., KHUDAVERDYAN, M., MIROSHNYCHENKO, Y., RAUSCHENBEUTEL, A. & MESCHEDE, D. (2004). Neutral atom quantum register. *Phys. Rev. Lett.*, **93**, 150501. 15

SCHRÖDINGER, E. (1935). Present status of quantum mechanics. *Die Naturwissenschaften*, **23**. 73, 82

SCHUMM, T., HOFFERBERTH, S., ANDERSSON, L.M., WILDERMUTH, S., GROTH, S., BAR-JOSEPH, I., SCHMIEDMAYER, J. & KRÜGER, P. (2005). Matter-wave interferometry in a double well on an atom chip. *Nature Physics*, **1**, 57–62. 17

SCHWINDT, P.D.D., KNAPPE, S., SHAH, V., HOLLBERG, L., KITCHING, J., LIEW, L.A. & MORELAND, J. (2004). Chip-scale atomic magnetometer. *Applied Physics Letters*, **85**, 6409–6411. 32

SEDLACEK, J.A., SCHWETTMANN, A., KÜBLER, H., LÖW, R., PFAU, T. & SHAFFER, J.P. (2012). Microwave electrometry with rydberg atoms in a vapour cell using bright atomic resonances. *Nature Physics*, **8**, 819–824. 32

SEDLACEK, J.A., SCHWETTMANN, A., KÜBLER, H. & SHAFFER, J.P. (2013). Atom-based vector microwave electrometry using rubidium rydberg atoms in a vapor cell. *Phys. Rev. Lett.*, **111**, 063001. 32

SHANNON, C. (1948). A mathematical theory of communication. *Bell System Technical Journal*, **27**, 379–423, 623–656. 5

SHEPHERD, D. & BREMNER, M.J. (2009). Temporally unstructured quantum computation. *Proceedings of the Royal Society A: Mathematical, Physical and Engineering Science*, **465**, 1413–1439. 12

SHOCKLEY, W.B., BARDEEN, J. & BRATTAIN, W.H. (1956). The nobel prize in physics 1956, awarded for their researches on semiconductors and their discovery of the transistor effect. 5

SHOR, P. (1994). Algorithms for quantum computation: Discrete logarithms and factoring. In *ANNUAL SYMPOSIUM ON FOUNDATIONS OF COMPUTER SCIENCE*, vol. 35, 124–124, Citeseer. 6, 144

SHOR, P.W. (1995). Scheme for reducing decoherence in quantum computer memory. *Phys. Rev. A*, **52**, R2493–R2496. 144

SHOR, P.W. & JORDAN, S.P. (2008). Estimating jones polynomials is a complete problem for one clean qubit. *Quantum Info. Comput.*, **8**, 681–714.

68, 115

SIMMONS, S., JONES, J.A., KARLEN, S.D., ARDAVAN, A. & MORTON, J.J.L. (2010). Magnetic field sensors using 13-spin cat states. *Phys. Rev. A*, **82**, 022330. 82

SINGER, K., REETZ-LAMOUR, M., AMTHOR, T., MARCASSA, L.G. & WEIDEMÜLLER, M. (2004). Suppression of excitation and spectral broadening induced by interactions in a cold gas of rydberg atoms. *Phys. Rev. Lett.*, **93**, 163001. 41, 124

SØRENSEN, A. & MØLMER, K. (1999). Quantum computation with ions in thermal motion. *Phys. Rev. Lett.*, **82**, 1971–1974. 14

SORTAIS, Y., MARION, H., TUCHENDLER, C., LANCE, A., LAMARE, M., FOURNET, P., ARMELLIN, C., MERCIER, R., MESSIN, G., BROWAEYS, A. & GRANGIER, P. (2007). Diffraction-limited optics for single-atom manipulation. *Physical Review A*, **75**, 13406. 129, 137

SOUZA, A.M., OLIVEIRA, I.S. & SARTHOUR, R.S. (2011). A scattering quantum circuit for measuring bell's time inequality: a nuclear magnetic resonance demonstration using maximally mixed states. *New Journal of Physics*, **13**, 053023. 80, 82

STANOJEVIC, J., PARIGI, V., BIMBARD, E., OURJOUMTSEV, A., PILLET, P. & GRANGIER, P. (2012). Generating non-gaussian states using collisions between rydberg polaritons. *Phys. Rev. A*, **86**, 021403. 111

STEANE, A. (1996a). Multiple-particle interference and quantum error correction. *Proceedings of the Royal Society of London. Series A: Mathematical, Physical and Engineering Sciences*, **452**, 2551–2577. 144

STEANE, A.M. (1996b). Error correcting codes in quantum theory. *Phys. Rev. Lett.*, **77**, 793–797. 144

STEANE, A.M. (2003). A quantum computer only needs one universe. *Studies in History and Philosophy of Science Part B: Studies in History and Philosophy*

of Modern Physics, **34**, 469–478. 72

STOLZE, J. & SUTER, D. (2008). *Quantum computing: a short course from theory to experiment*. John Wiley & Sons. 1

SWALLOWS, M.D., BISHOF, M., LIN, Y., BLATT, S., MARTIN, M.J., REY, A.M. & YE, J. (2011). Suppression of collisional shifts in a strongly interacting lattice clock. *Science*, **331**, 1043–1046. 81

TAKAMIZAWA, A., STEINMETZ, T., DELHUILLE, R., HÄNSCH, T.W. & REICHEL, J. (2006). Miniature fluorescence detector for single atom observation on a microchip. *Opt. Express*, **14**, 10976–10983. 119

THOMPSON, J., GU, M., MODI, K. & VEDRAL, V. (2013a). Quantum computing with black-box subroutines, arXiv:1310.2927 [quant-ph]. 111

THOMPSON, J.D., TIECKE, T.G., ZIBROV, A.S., VULETIĆ, V. & LUKIN, M.D. (2013b). Coherence and raman sideband cooling of a single atom in an optical tweezer. *Phys. Rev. Lett.*, **110**, 133001. 18

TONG, D., FAROOQI, S.M., STANOJEVIC, J., KRISHNAN, S., ZHANG, Y.P., CÔTÉ, R., EYLER, E.E. & GOULD, P.L. (2004). Local blockade of rydberg excitation in an ultracold gas. *Phys. Rev. Lett.*, **93**, 063001. 41, 111, 124

TORII, Y., SUZUKI, Y., KOZUMA, M., SUGIURA, T., KUGA, T., DENG, L. & HAGLEY, E.W. (2000). Mach-zehnder bragg interferometer for a bose-einstein condensate. *Phys. Rev. A*, **61**, 041602. 81

TOWNES, C.H., BASOV, N.G. & PROKHOROV, A.M. (1964). The nobel prize in physics 1964, awarded for fundamental work in the field of quantum electronics, which has led to the construction of oscillators and amplifiers based on the maser-laser principle. 5

TREUTLEIN, P., HOMMELHOFF, P., STEINMETZ, T., HÄNSCH, T.W. & REICHEL, J. (2004). Coherence in microchip traps. *Phys. Rev. Lett.*, **92**, 203005. 15

TUFARELLI, T., MACLEAN, T., GIROLAMI, D., VASILE, R. & ADESSO, G. (2013). The geometric approach to quantum correlations: computability versus reliability. *Journal of Physics A: Mathematical and Theoretical*, **46**, 275308. 79, 148

TURING, A.M. (1936). On computable numbers, with an application to the entscheidungsproblem. *Proceedings of the London Mathematical Society*, **42**, 230–265. 5

VAN DEN NEST, M. (2013). Universal quantum computation with little entanglement. *Phys. Rev. Lett.*, **110**, 060504. 73

VANDERSYPEN, L.M., STEFFEN, M., BREYTA, G., YANNONI, C.S., SHERWOOD, M.H. & CHUANG, I.L. (2001). Experimental realization of shor's quantum factoring algorithm using nuclear magnetic resonance. *Nature*, **414**, 883–887. 14

VARNAVA, M., BROWNE, D.E. & RUDOLPH, T. (2006). Loss tolerance in one-way quantum computation via counterfactual error correction. *Phys. Rev. Lett.*, **97**, 120501. 14

VEDRAL, V. (2010). The elusive source of quantum speedup. *Foundations of Physics*, **40**, 1141–1154. 72

VERKERK, P., LOUNIS, B., SALOMON, C., COHEN-TANNOUDJI, C., COURTOIS, J.Y. & GRYNBERG, G. (1992). Dynamics and spatial order of cold cesium atoms in a periodic optical potential. *Phys. Rev. Lett.*, **68**, 3861–3864. 144

VITANOV, N. & STENHOLM, S. (1997). Properties of stimulated raman adiabatic passage with intermediate-level detuning. *Optics Communications*, **135**, 394 - 405. 51

VITANOV, N.V., HALFMANN, T., SHORE, B.W. & BERGMANN, K. (2001). Laser-induced population transfer by adiabatic passage techniques. *Annual review of physical chemistry*, **52**, 763–809. 48

VITEAU, M., HUILLERY, P., BASON, M.G., MALOSSI, N., CIAMPINI, D., MORSCH, O., ARIMONDO, E., COMPARAT, D. & PILLET, P. (2012). Cooperative excitation and many-body interactions in a cold rydberg gas. *Phys. Rev. Lett.*, **109**, 053002. 106, 111

VITRANT, G., RAIMOND, J.M., GROSS, M. & HAROCHE, S. (1982). Rydberg to plasma evolution in a dense gas of very excited atoms. *Journal of Physics B: Atomic and Molecular Physics*, **15**, L49. 146

VOGT, T., VITEAU, M., ZHAO, J., CHOTIA, A., COMPARAT, D. & PILLET, P. (2006). Dipole blockade at förster resonances in high resolution laser excitation of rydberg states of cesium atoms. *Phys. Rev. Lett.*, **97**, 083003. 41

VOGT, T., VITEAU, M., CHOTIA, A., ZHAO, J., COMPARAT, D. & PILLET, P. (2007). Electric-field induced dipole blockade with rydberg atoms. *Phys. Rev. Lett.*, **99**, 073002. 41

VULETIC, V. (2006). Quantum networks: When superatoms talk photons. *Nature Physics*, **2**, 801–802. 146

WALTHER, H., VARCOE, B.T.H., ENGLERT, B.G. & BECKER, T. (2006). Cavity quantum electrodynamics. *Reports on Progress in Physics*, **69**, 1325. 28

WANG, T., YELIN, S.F., CÔTÉ, R., EYLER, E.E., FAROOQI, S.M., GOULD, P.L., KOŠTRUN, M., TONG, D. & VRINCEANU, D. (2007). Superradiance in ultracold rydberg gases. *Phys. Rev. A*, **75**, 033802. 146

WASILEWSKI, W., JENSEN, K., KRAUTER, H., RENEMA, J.J., BALABAS, M.V. & POLZIK, E.S. (2010). Quantum noise limited and entanglement-assisted magnetometry. *Phys. Rev. Lett.*, **104**, 133601. 82

WEIDEMÜLLER, M. (2013). Atomic interactions at a distance. *Physics*, **6**, 71. 111

WEIMER, H., LÖW, R., PFAU, T. & BÜCHLER, H.P. (2008). Quantum

critical behavior in strongly interacting rydberg gases. *Phys. Rev. Lett.*, **101**, 250601. 111

WESTBROOK, C. (2009). Atom chips: Read the labels. *Nature Physics*, **5**, 538–539. 17

WILK, T., GAËTAN, A., EVELLIN, C., WOLTERS, J., MIROSHNYCHENKO, Y., GRANGIER, P. & BROWAEYS, A. (2010). Entanglement of two individual neutral atoms using rydberg blockade. *Phys. Rev. Lett.*, **104**, 010502. 22, 35, 144

WINELAND, D.J., MONROE, C., ITANO, W.M., LEIBFRIED, D. & B. E. KING, D.M.M. (1998). Experimental issues in coherent quantum-state manipulation of trapped atomic ions. *Journal of Research of the National Institute of Standards and Technology*, **103**, 259. 57

WÜSTER, S., STANOJEVIC, J., ATES, C., POHL, T., DEUAR, P., CORNEY, J.F. & ROST, J.M. (2010). Correlations of rydberg excitations in an ultracold gas after an echo sequence. *Phys. Rev. A*, **81**, 023406. 111

XIA, T., ZHANG, X.L. & SAFFMAN, M. (2013). Analysis of a controlled phase gate using circular rydberg states. *Phys. Rev. A*, **88**, 062337. 36

XU, J.S. & LI, C.F. (2013). Quantum discord under system-environment coupling: the two-qubit case. *International Journal of Modern Physics B*, **27**, 1345054.

YAO, Y., LI, H.W., ZOU, X.B., HUANG, J.Z., ZHANG, C.M., YIN, Z.Q., CHEN, W., GUO, G.C. & HAN, Z.F. (2012). Quantum discord in quantum random access codes and its connection to dimension witnesses. *Phys. Rev. A*, **86**, 062310. 103, 147

YAVUZ, D.D., KULATUNGA, P.B., URBAN, E., JOHNSON, T.A., PROITE, N., HENAGE, T., WALKER, T.G. & SAFFMAN, M. (2006). Fast ground state manipulation of neutral atoms in microscopic optical traps. *Phys. Rev. Lett.*, **96**, 063001. 15

YEAZELL, J.A., MALLALIEU, M., PARKER, J. & STROUD, C.R. (1989). Classical periodic motion of atomic-electron wave packets. *Phys. Rev. A*, **40**, 5040–5043. 32

YOSHIDA, S., REINHOLD, C.O., BURGDÖRFER, J., MESTAYER, J.J., LANCASTER, J.C. & DUNNING, F.B. (2008). Transferring rydberg wave packets between islands across the chaotic sea. *Phys. Rev. A*, **77**, 013411. 32

YOUNGE, K.C., REINHARD, A., POHL, T., BERMAN, P.R. & RAITHEL, G. (2009). Mesoscopic rydberg ensembles: Beyond the pairwise-interaction approximation. *Phys. Rev. A*, **79**, 043420. 112

YU, C.S., ZHANG, J. & FAN, H. (2012). Quantum dissonance is rejected in an overlap measurement scheme. *Phys. Rev. A*, **86**, 052317. 80, 81

YU, C.S., YI, X.X., SONG, H.S. & FAN, H. (2013). Entangling power in deterministic quantum computation with one qubit. *Phys. Rev. A*, **87**, 022322. 80

ZANARDI, P., ZALKA, C. & FAORO, L. (2000). Entangling power of quantum evolutions. *Phys. Rev. A*, **62**, 030301. 79

ZHANG, X.L., ISENHOWER, L., GILL, A.T., WALKER, T.G. & SAFFMAN, M. (2010). Deterministic entanglement of two neutral atoms via rydberg blockade. *Phys. Rev. A*, **82**, 030306. 36

ZHANG, X.L., GILL, A.T., ISENHOWER, L., WALKER, T.G. & SAFFMAN, M. (2012). Fidelity of a rydberg-blockade quantum gate from simulated quantum process tomography. *Phys. Rev. A*, **85**, 042310. 24, 36, 96

ZHAO, W., MESTAYER, J.J., LANCASTER, J.C., DUNNING, F.B., REINHOLD, C.O., YOSHIDA, S. & BURGDÖRFER, J. (2006). Navigating localized wave packets in phase space. *Phys. Rev. Lett.*, **97**, 253003. 32

ZHOU, M.K., HU, Z.K., DUAN, X.C., SUN, B.L., ZHAO, J.B. & LUO, J. (2010). Precisely mapping the magnetic field gradient in vacuum with an atom interferometer. *Phys. Rev. A*, **82**, 061602. 82

ZHOU, M.K., HU, Z.K., DUAN, X.C., SUN, B.L., CHEN, L.L., ZHANG, Q.Z. & LUO, J. (2012). Performance of a cold-atom gravimeter with an active vibration isolator. *Phys. Rev. A*, **86**, 043630. 82

ZHOU, X.Q., RALPH, T.C., KALASUWAN, P., ZHANG, M., PERUZZO, A., LANYON, B.P. & O'BRIEN, J.L. (2011). Adding control to arbitrary quantum operations. *Nature Communications*, **2**, 413. 106

ZU, C., WANG, Y.X., CHANG, X.Y., WEI, Z.H., ZHANG, S.Y. & DUAN, L.M. (2012). Experimental demonstration of quantum gain in a zero-sum game. *New Journal of Physics*, **14**, 033002. 105